81SRC35

SPECTROPHOTOVOLTAIC ORBITAL POWER GENERATION (PHASE II)

FINAL REPORT

APRIL 1, 1981

(NASA-CR-161813) SPECTROPHOTOVOLTAIC ORBITAL POWER GENERATION, PHASE 2 Final Report, Aug. 1980 - Mar. 1981 (Honeywell Systems and Research) 107 p HC A06/MF A01 CSCL 10A G3/44

N81-27620

Unclas 30745

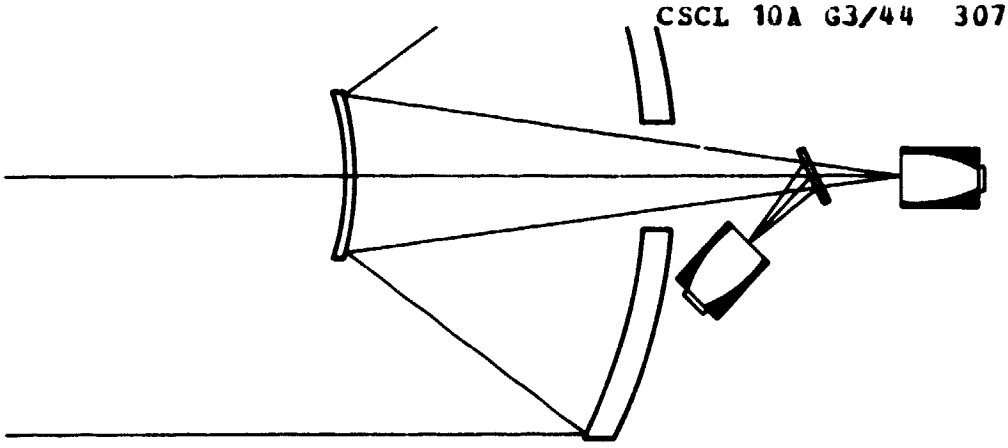

for

GEORGE C. MARSHALL SPACE FLIGHT CENTER

Contract NAS 8-33511

by

Honeywell

Systems and Research Center
2600 Ridgway Parkway
P.O. Box 312
Minneapolis, MN 55440

UNCLASSIFIED

SECURITY CLASSIFICATION OF THIS PAGE (WHEN DATA ENTERED)

REPORT DOCUMENTATION PAGE

READ INSTRUCTIONS BEFORE COMPLETING FORM

1. REPORT NUMBER

2. GOVT ACCESSION NUMBER

3. RECIPIENT'S CATALOG NUMBER

4. TITLE (AND SUBTITLE)
Spectrophotovoltaic Orbital Power Generation
(Phase II)

5. TYPE OF REPORT/PERIOD COVERED
Final Report
August 1980 - March 1981

6. PERFORMING ORG. REPORT NUMBER
81SRC35

7. AUTHOR(S)
Sau Kwan Lo
Ray Lin
Dave Stoltzmann
Gary Knowles

8. CONTRACT OR GRANT NUMBER(S)
NAS 8-33511

9. PERFORMING ORGANIZATIONS NAME/ADDRESS
Honeywell Inc., Systems & Research Center
P.O. Box 312, 2600 Ridgway Parkway
Minneapolis, MN 55440

10. PROGRAM ELEMENT, PROJECT, TASK AREA & WORK UNIT NUMBERS

11. CONTROLLING OFFICE NAME/ADDRESS
NASA/George C. Marshall Space Flight Center
Marshall Space Flight Center, Alabama 35812

12. REPORT DATE
April 1, 1981

13. NUMBER OF PAGES
107

14. MONITORING AGENCY NAME/ADDRESS (IF DIFFERENT FROM CONT. OFF.)

15. SECURITY CLASSIFICATION (OF THIS REPORT)
Unclassified

15a. DECLASSIFICATION DOWNGRADING SCHEDULE
None

16. DISTRIBUTION STATEMENT (OF THIS REPORT)

Unlimited.

17. DISTRIBUTION STATEMENT (OF THE ABSTRACT ENTERED IN BLOCK 20, IF DIFFERENT FROM REPORT)

18. SUPPLEMENTARY NOTES

19. KEY WORDS (CONTINUE ON REVERSE SIDE IF NECESSARY AND IDENTIFY BY BLOCK NUMBER)

Solar Concentrator System
Cassegrain Telescope
Compound Parabolic Concentrators
Dichroic Mirrors
Beamsplitters
Solar Cells
Gallium Arsenide
Silicon

20. ABSTRACT (CONTINUE ON REVERSE SIDE IF NECESSARY AND IDENTIFY BY BLOCK NUMBER)

A subscale model of the spectral splitting concentrator system with 10" aperture is defined and designed. The model is basically a scaled-down version of Phase I design with an effective concentration ratio up to 1000:1. The system performance is predicted to be 21.5% for the 2-cell GaAs/Si system, and 20% for Si/GaAs at AM2 using realistic component efficiencies. Component cost of the model is projected in the $50K range. Component and system test plans are also detailed.

DD FORM 1 JAN 73 1473 EDITION OF 1 NOV 55 IS OBSOLETE

UNCLASSIFIED

SECURITY CLASSIFICATION OF THIS PAGE (WHEN DATA ENTERED)

FOREWORD

This report summarizes the results of the second phase of the Spectrophotovoltaic Orbital Power Generation program for NASA/George C. Marshall Space flight Center. The purpose of the program is to define and assess a concentrator spectrophotovoltaic approach that offers a significant overall improvement over conventional array technology. The objective of the second phase of the program is to define and design a subscale model which will demonstrate the hardware feasibility of selected components of the full-scale spectrophotovoltaic orbital power generation system up to a concentration ratio of 1000:1. The design for ground-based testing is detailed in order to produce a subscale model capable of demonstrating the performance characteristics of the major components and the integrated system.

A subscale model of the spectral splitting concentrator system with 10" aperture is defined and designed. The model is basically a scaled-down version of Phase I design with an effective concentration ratio up to 1000:1. The system performance is predicted to be 21.5% for the 2-cell GaAs/Si system, and 20% for Si/GaAs at AM2 using realistic component efficiencies. Component cost of the model is projected in the $50K range. Component and system test plans are also detailed.

Sau Kwan Lo of Honeywell's Systems and Research Center (SRC) organized this report with contributions from Dave Stoltzmann, Ray Lin, and Gary Knowles. Dave designed the optics, Ray designed the beamsplitter, Gary designed the thermal/mechanical support systems, and Sau obtained information on the solar cells and directed other system level efforts.

The Spectrophotovoltaic Orbital Power Generation Program is under the sponsorship and direction of NASA/George C. Marshall Space Flight Center, Marshall Flight Center, Alabama. Mr. W.L. Crabtree of that agency is the Contract Monitor for this program.

CONTENTS

CONTENTS (concluded)

LIST OF ILLUSTRATIONS

LIST OF ILLUSTRATIONS (continued)

LIST OF ILLUSTRATIONS (concluded)

LIST OF TABLES

SECTION 1

INTRODUCTION AND SUMMARY

SUMMARY OF PHASE I

During the previous phase of the program, a spectral splitting photovoltaic concept was defined. In this concept, the energy spectrum is split into different bands in which photon energy is effectively converted into electrical energy via photovoltaic cells that have matching spectral responses. The efficiency of the system also increases with the concentration ratio if the temperature of the cell is maintained constantly ∿300K. Assuming this condition is met, a system with 1000:1 concentration ratio is defined, using a Cassegrain telescope as the first stage concentration (270 x), and compound parabolic concentrators (CPC) for the second stage concentration of 4.7 x for each spectral band. Using reported state-of-the-art (S.O.A.) solar cells device parameters and considering structural losses due to optics and beamsplitters, the efficiencies of one-to-four-cell systems were calculated with efficiencies varying from ∿22% to ∿30%. Taking into account the cost of optics, beamsplitter, radiator, and that of de oping new cells, the most cost-effective system is the 2-cell GaAs/Si system.

The advantages of the spectrophotovoltaic concept are: 1) the increase in photoelectric conversion efficiency without development of new materials and cells; 2) intrinsic particle radiation hardness, since the cells are not directly exposed to particle radiation; and 3) intrinsic resistance to laser damage, since the acceptance angle of the concentrator system is only $\pm 0.5^{o}$ pointing at the sun. Thus, the spectrophotovoltaic concept is especially suitable for space power generation.

PROGRAM OBJECTIVES FOR PHASE II

For this phase of the program the objective is to define and design a subscale model which will demonstrate the hardware feasibility of selected components of the full-scale spectrophotovoltaic orbital power generation system up to a concentration ratio of 1000:1. The design for ground-based testing will be in sufficient detail to produce a subscale model capable of demonstrating the performance characteristics of the major components and the integrated system.

HIGHLIGHTS AND SUMMARY

The program was carried out under six major task areas:

1. Model Definition
2. Optical Design
3. Beamsplitter Design
4. Thermal/Mechanical Design
5. Model Cost
6. Testing Plan

The subscale model defined was a 10" aperture system with an effective concentration ratio up to 1000:1, similar to that defined in Phase I. The partially concentrated solar spectrum was divided into two bands by a beamsplitter, and then focused onto two selected cells. The chosen cells were well-developed GaAs and Si solar cells. Both reflective and transmitting mode to GaAs (denoted by GaAs/Si and Si/GaAs respectively) will be tested, since each configuration has its own merits. The model to be built is aimed at demonstrating the high conversion efficiency due to both spectrum splitting and high concentration ratio of the defined concept. In addition, thermal

data on various system components will be taken which will shed light on system losses and thus lead to a more optimal design. The ability of the system components to withstand such high concentration will also be tested.

A tradeoff is being considered between outdoor testing in ambient sunlight and testing in a laboratory under a solar simulator. The main areas of tradeoff are between the stability and spectral versatility of a simulator, and the narrow beam collimation from the sun and its variable atmospheric attenuation. However, the optical design that would accommodate a $\pm$ 3.0° incoming beam has much higher secondary obscuration and a much higher number of reflections inside the CPC's, which would be required to handle most of the concentration. The resulting design, both inefficient and little-resembling the space system, was abandoned. With the original design, indoor testing can be carried out, but at reduced intensity.

The optical design for the subscale model is therefore a scaled-down version of the design in Phase I with an increase of the back focal length from 3" to 6" to allow room for thermal measurement of the CPC and solar cell closest to the primary. This causes the secondary obscuration to increase from 7% to 10%. The design was verified by raytracing, which showed that over 95% of the spectral energy was imaged onto the solar cells after one reflection at the CPC's. Three manufacturing methods for the optical components are explored. Among these, electroforming, a version of electroplating, appears to be the most economical for the CPC's. Diamond tuning and conventional glass grinding appear best for the primary and secondary. Optical tolerance analysis of the mirrors has included three other mirror combinations. The most critical alignment is the separation between the primary and secondary mirrors, which has to be maintained within $\pm$ 0.015".

Several beamsplitter designs were completed for the 2-cell GaAs/Si and Si/GaAs configurations. The first set of designs covers a reflection band from 0.3 to 0.9 μm which utilizes 65-layer Ta_2O_5/MgF_2 and a

reflection band from 0.9 to 1.1 μm with 21-layer CaF_2/ThO_2. The dielectric materials chosen are UV transparent, have the proper indices of refraction, show a minimum of thermal stress, and are thermally stable and non-hygroscopic. Inquiries into the S.O.A.[1] spectral response of the solar cells (both GaAs and Si) indicate a very sharp cut-off between 0.4 and 0.5 μm. Thus, the first beamsplitter designed with a reflection band from 0.3 to 0.9 μm onto the GaAs cell would be over-designed. By narrowing the band to 0.43 to 0.90 μm, we could decrease the number of dielectric coatings from 65 to 35 layers. To optimize the system efficiency, the final design before fabrication would be tailored to the measured spectral response, of the actual cells being used.

We have contacted Varian Associates, Hughes Research at Malibu, Rockwell International and Spectrolab for details of their solar cells' characteristics and their supply schedule. Among these suppliers, Varian has the cells most suitable to our needs. We received 2 GaAs cells from Rockwell with specifications of their performance. Varian is willing to supply us with their GaAs and Si cells at nominal cost. Both Rockwell's and Varian's cells are designed for high concentration and have dimensions similar to our design. To optimize performance, the system dimensions should be scaled to the available cell size: 1/3" diameter (Varian). Both companies claim their cells to be high performance cells.

Mechanical support for the system aimed at ground-based laboratory and field testing has been detailed and finalized with technical drawings. Design for thermal testing of the CPC's and cells was completed. Due to the small amount of thermal dissipation in a subscale system, insulation around the measured components is required to obtain accurate data. If loss due to air convection is neglected, then a 5% error in the measurement is foreseen. Thermal analysis on the 10" system based on predicted cell performance shows at AM2 ~23% conversion efficiency (power output/total flux intercepted)

for the GaAs/Si system and ∿21% for the Si/GaAs system. Correction for poor blue response of the cells decreases the efficiencies to 21.5% and 20.1% respectively.

Model cost should include the cost of components, component testing, system integration, system laboratory testing and field testing. However, we are only required to detail component cost in this report. Major components and their suppliers were identified. Potential long lead items could be the mirrors and solar cells, but no problem is foreseen in meeting our need schedule. The estimated component cost is $53.5K, with major costs being fabrication of beamsplitters, telescope body, and fixtures. Most of the cost is for the set-up, so the cost of the full-scale system is not a direct scale-up from this figure.

Our test plan consists of component testing, system performance prediction, system laboratory testing, and field testing. Prior to system integration, the major components (mirrors, CPC, beamsplitters, solar cells, and cooling system) would be tested and calibrated to make sure that they meet specifications. With the integrated system, calibration of the input flux (both intensity and spectral distribution) is a critical step. A standard approach is to use calibrated silicon cells as standards or to use a pyrheliometer, either with standard Schott-glass spectral filters or simply clear aperture. In lab testing a more eleborate spectrophotometer can be used. After calibration, electrical and thermal output of the system would be measured as a function of concentration ratios, cell temperatures, spectral splitting arrangements, input spectral distribution, etc. This would be compared with the performance prediction similar to the one shown in the section on component demonstrations, except the component efficiencies will be that of measured rather than predicted values. For qualitative demonstration of the enhancement of power conversion with the spectrophotovoltaic concept, the electrical output will be compared to that of an equivalent area planar array.

Our plan is to build and test the model both for measuring the efficiency of the defined concept and for optimizing various system parameters so that a practical, high-performance, high-power space system can be designed.

SECTION 2

THE SUBSCALE MODEL

MODEL DEFINITION

The purpose of designing and eventually constructing the subscale model is to demonstrate the enhanced power generation efficiency of the spectrophotovoltaic concept defined in Phase I, and to prove hardware feasibility of the optical components including the beamsplitter and the solar cells. The designed model, therefore, should closely resemble the full-scale space system so that the information obtained could be scaled up to the full system.*

Based on this criterion, drastic redesign of the optical system to make it suitable for full sun simulator testing was rejected. While the basic design is unchanged, the question of how large to make the subscale model remains. In selecting an aperture size, the driving considerations were to make the aperture large enough so that the amount of energy collected would be readily measureable, and to make the concentrator small enough to be reasonably priced and readily portable. Consideration was given to a system with a primary diameter up to 16 inches. Construction methods considered were both conventional glass grinding and diamond turning of a metal mirror. Analysis of the energy conversion processes showed that for a 10-inch aperture system, the thermal and electric output for each cell would

*It is not clear at this point whether the full-scale system would be a direct scale-up to ∿20 m aperture single system or a number of smaller systems with the same total effective aperture area for a power generation of 100 kW.

be in the 0.1 to 6-watt range. Electric power can readily be measured to ±100 micro watt accuracy, and the thermal measurements can be made to approximately ±5 milliwatt accuracy. A 16-inch aperture system would increase the thermal and electric signal output by 2.5 times that of a 10-inch system, with only a small increase in measurement uncertainty.

Fabrication of the primary mirror by diamond turning is currently limited to surfaces less than 14 inches in diameter. Conventional glass grinding for a 16-inch f/0.7 mirror would be very expensive. A third fabrication technique considered was electroforming. This method could produce a very thin (0.20 inch) mirror which would be very portable. For a single unit construction it would be a very expensive fabrication technique, since a high quality master mold must be fabricated on which the metal can be plated. With these considerations in mind, the decision was made to limit the subscale model to the more economically constructed 10-inch aperture. The final size of the model could be fine-tuned to the available solar cell dimension; that is, for a 0.333" cell diameter, the nominal design would be scaled up by a factor of 1.182.

The model should be able to demonstrate qualitatively and quantitatively the enhancement of power conversion with a beamsplitter and with increasing concentration ratio as compared to an equivalent area planar array. Thus the model should be tested with and without the beamsplitter, as well as at variable concentration ratios, by reducing the source intensity or placing neutral density filters in front of the aperture, and comparing the result to a planar array of Si solar cells which have the same aperture area. By monitoring various components of the system before and after integration, information on system losses would be available to aid in optimizing future designs.

SOLAR CELLS

There is no development of solar cells in this program. It is desirable to use the most developed cells for the subscale model for demonstration of the spectrophotovoltaic concept. The ideal size of the solar cells for the subscale model is 0.28" in diameter. All the companies we contacted are willing to custom-make Si and/or GaAs cells at a cost of ~$2000 to $5000. On the other hand, if we can use the available larger size cells, it will be at minimal or no cost to the program. Since the dark current from the cell can either be measured or calculated, and is expected to be much smaller than the photogenerated current, cells of sizes larger than required by the model can be used.

At the end of this phase of the program, we received 2 GaAs cells from Rockwell, whereas Varian promised to supply us with their GaAs and Si cells at a minimal cost. The specifications of their cells are given in Table 1 and Figures 1-7. For performance comparison, we would need a small area Si cell. The specification is given in Table 2.

OPTICAL DESIGN

Background

Power requirements for space missions are expected to be in the several kilowatts of electrical and thermal power for heating/cooling and direct electrical applications. When thermal power is required at high temperatures, concentration of solar energy seems to be a practical way to obtain these desired temperatures. And for directly converting solar flux to electricity, a concentration system allows the size of the solar cells to be reduced by the concentration ratio.

TABLE 1. CONCENTRATOR SOLAR CELLS

Type of Cell	AlGaAs/GaAs	AlGaAs/GaAs	Si
Manufacturer	Rockwell Inst. Thousand Oaks, CA	Varian Assoc. Palo Alto, CA	Varian Assoc. Palo Alto, CA
Cell Size	3/4 cm Diameter Circle	1/3" Diameter Circle	1/3" Diameter Circle
Highest Conc.	1000X	∿500X	∿500X
Efficiency %	22%* (AM2)	14-15% (AM2)	5% (AM2)
Grid Coverage	∿10% See Figure 1	11%	11%
Mounting	None	See Figure 4	See Figure 4
Spectral Resp.	See Figure 2	See Figure 5	See Figure 7
I-V Characteristics	See Figure 3	See Figure 6	

*System/Structure efficiencies assumed to be 1.0

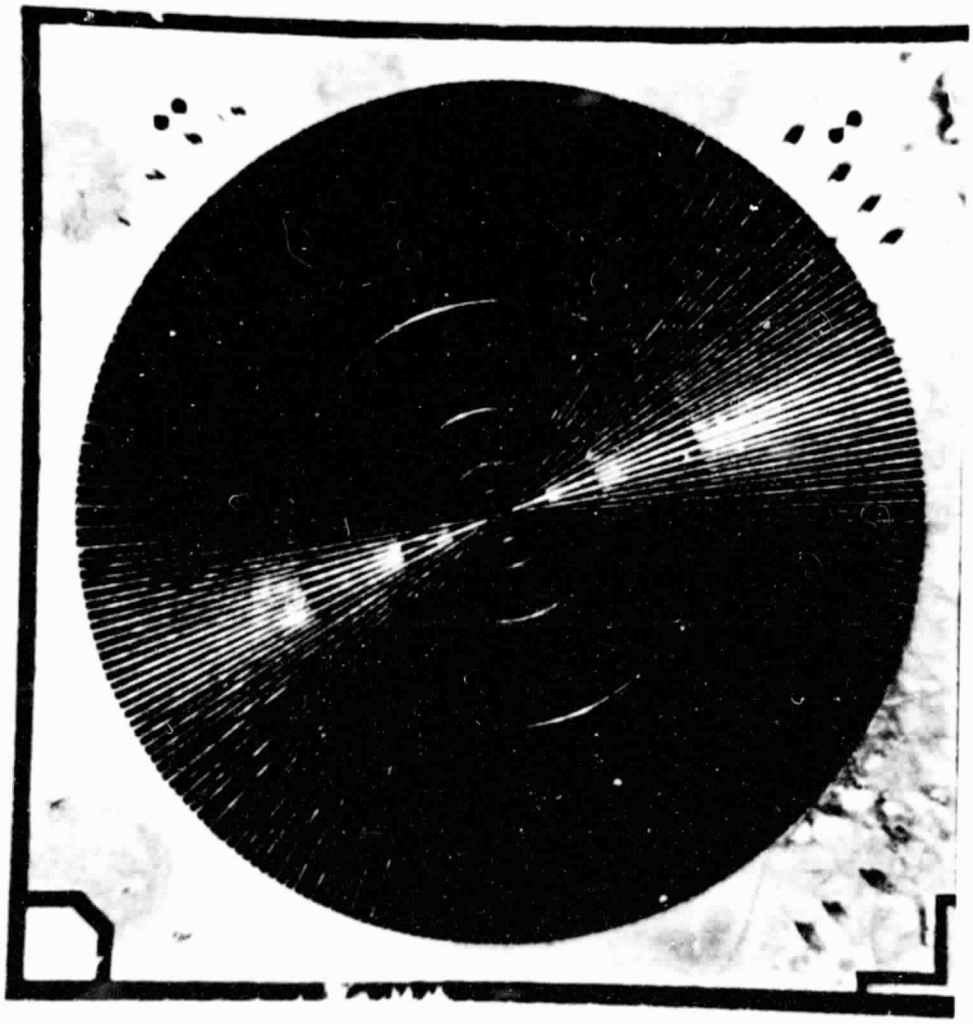

Figure 1. Grid Pattern of a Typical Concentrator Cell

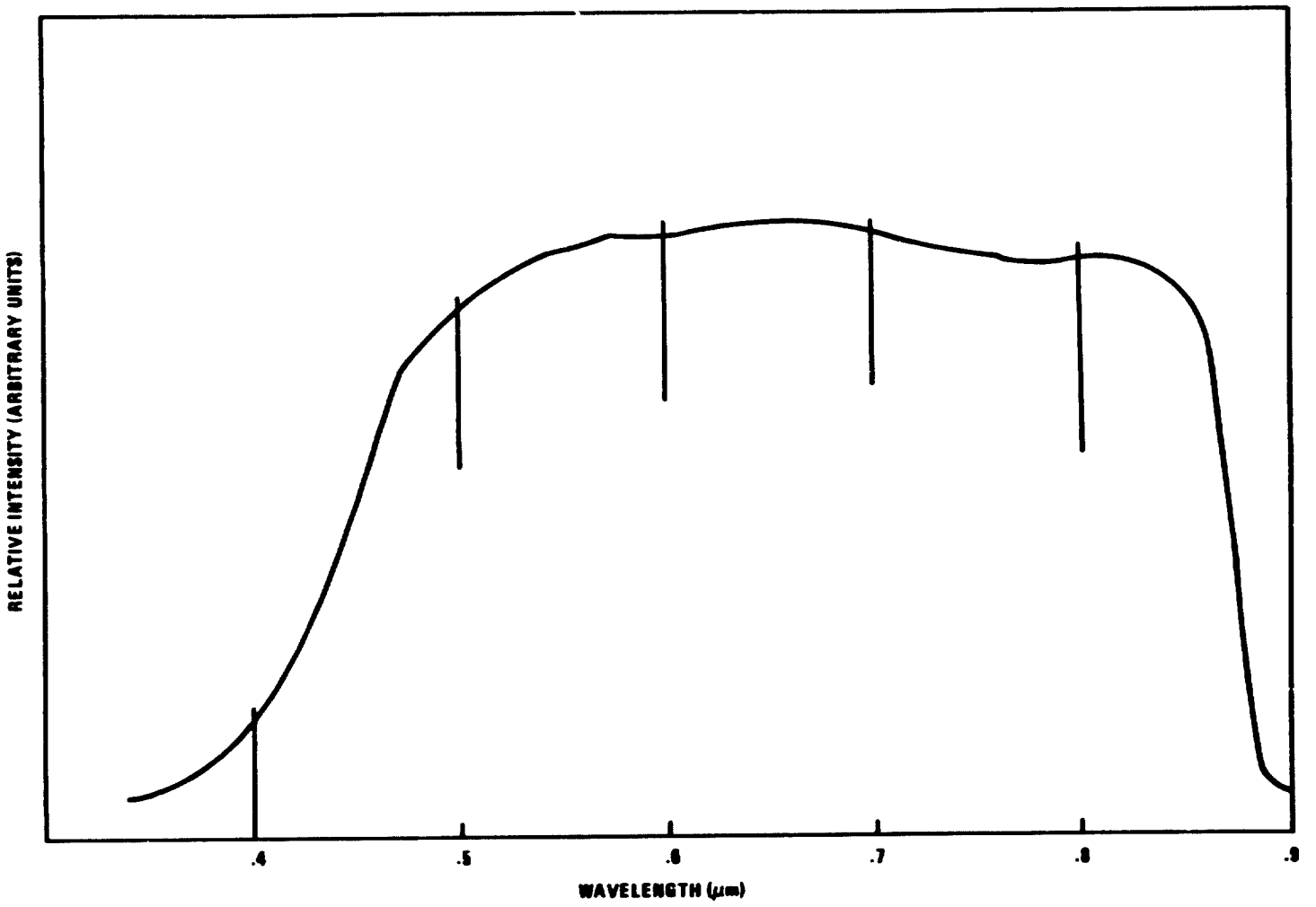

Figure 2. Spectral Response of Rockwell's AlGaAs/GaAs Cells

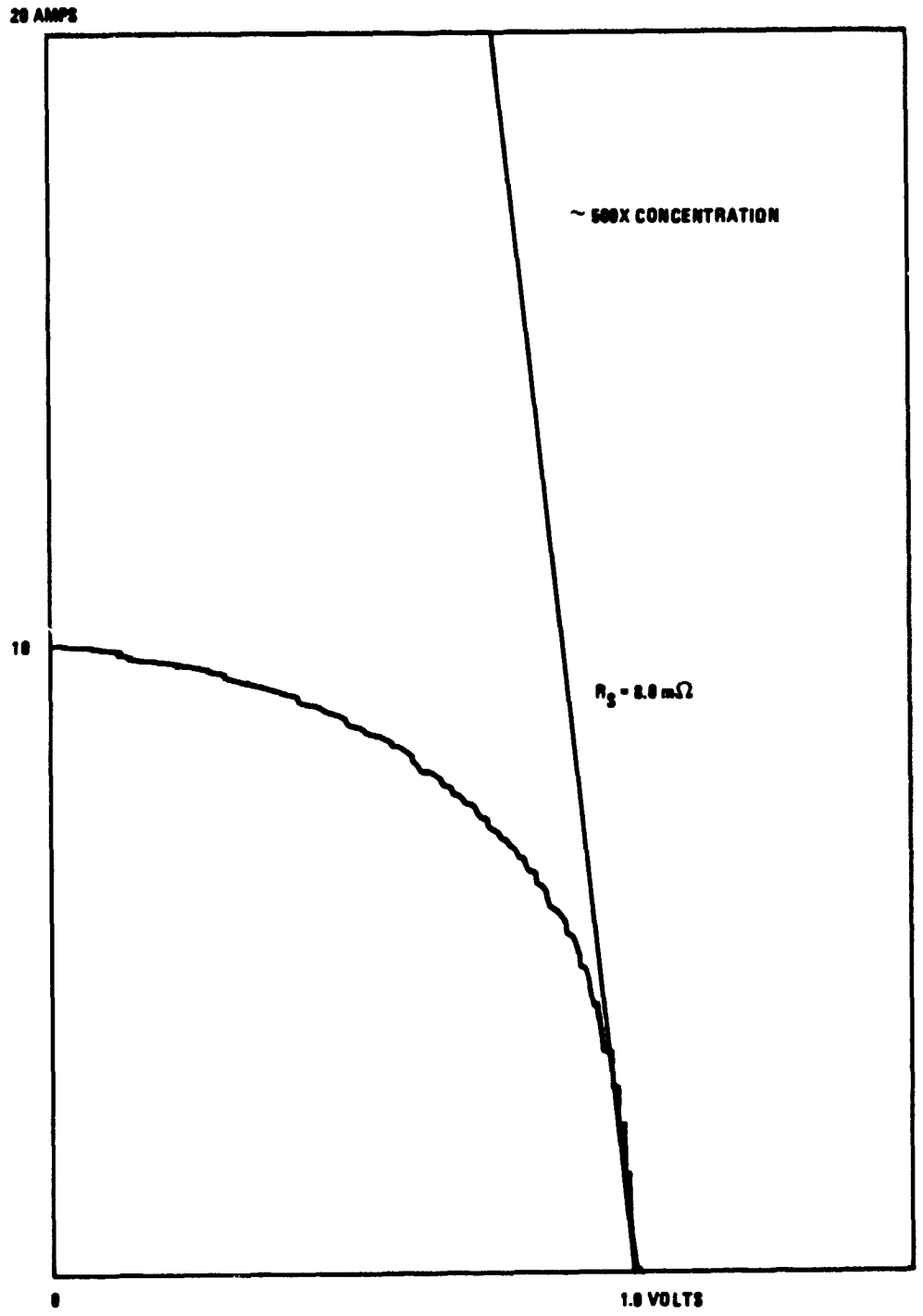

Figure 3. I-V Plots of Rockwell's AlGaAs/GaAs Cells

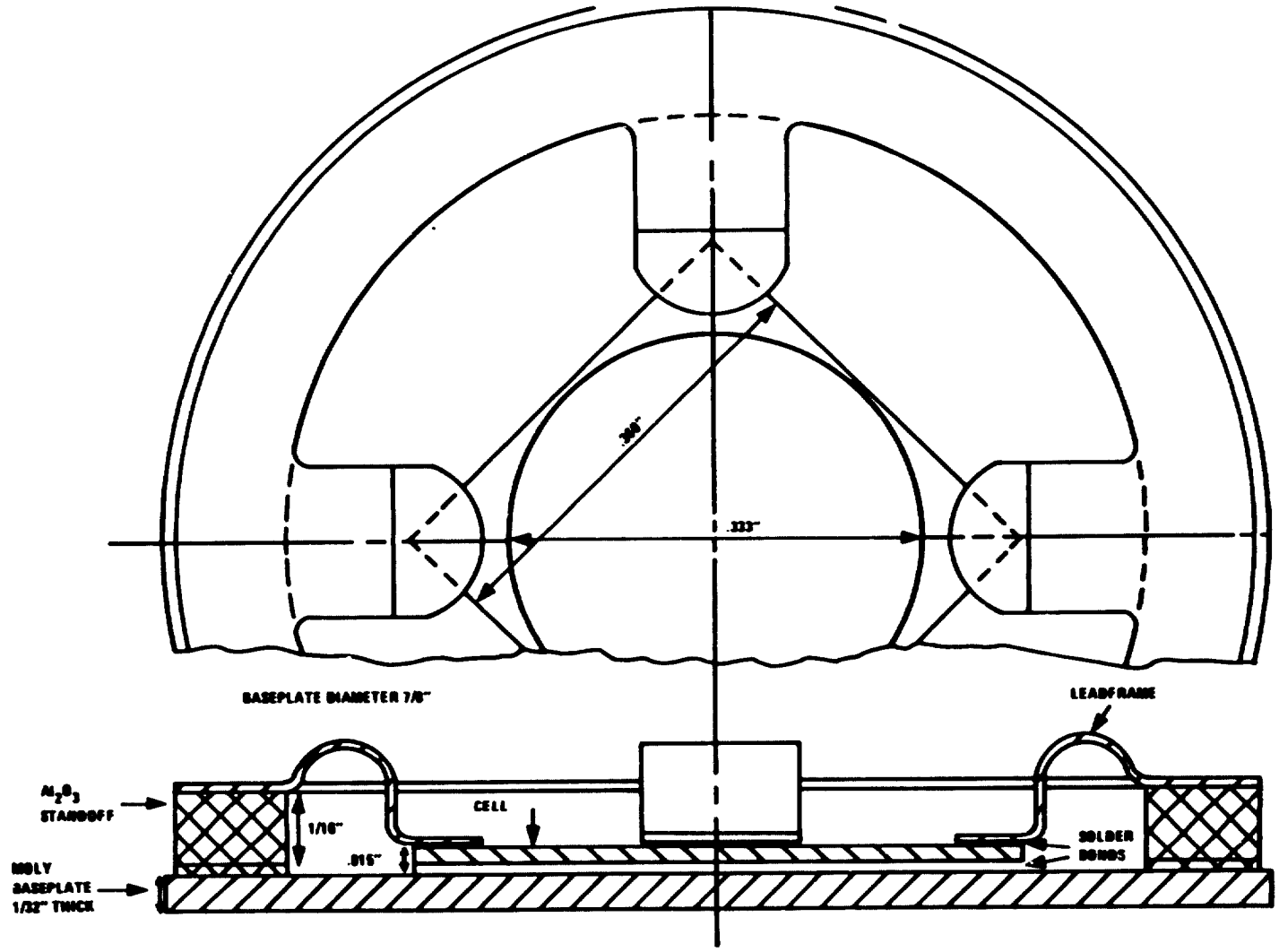

Figure 4. Mounting Configuration of Varian's Solar Cell

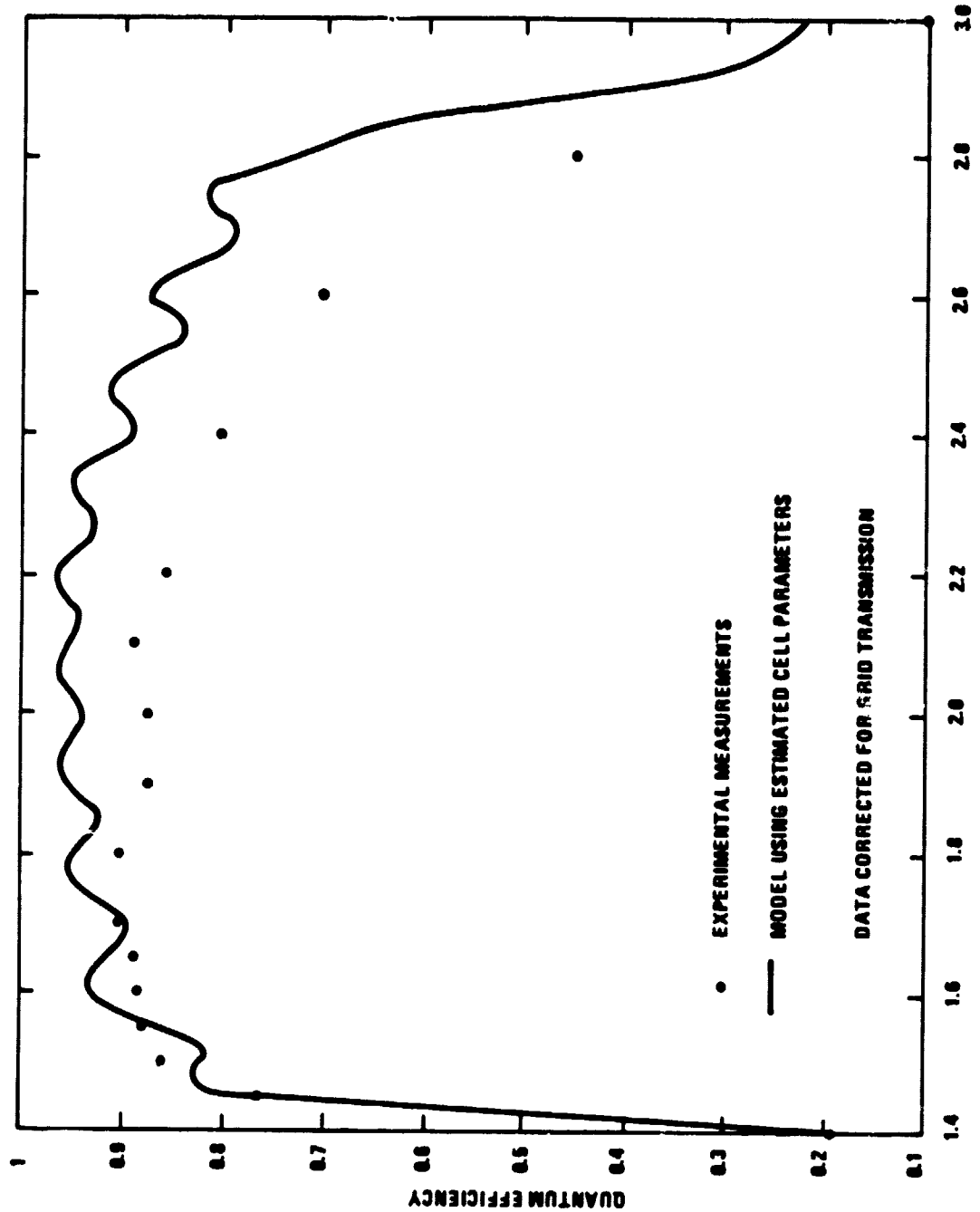

Figure 5. AlGaAs/GaAs Concentrator Solar Cell 9-27-7M RF1

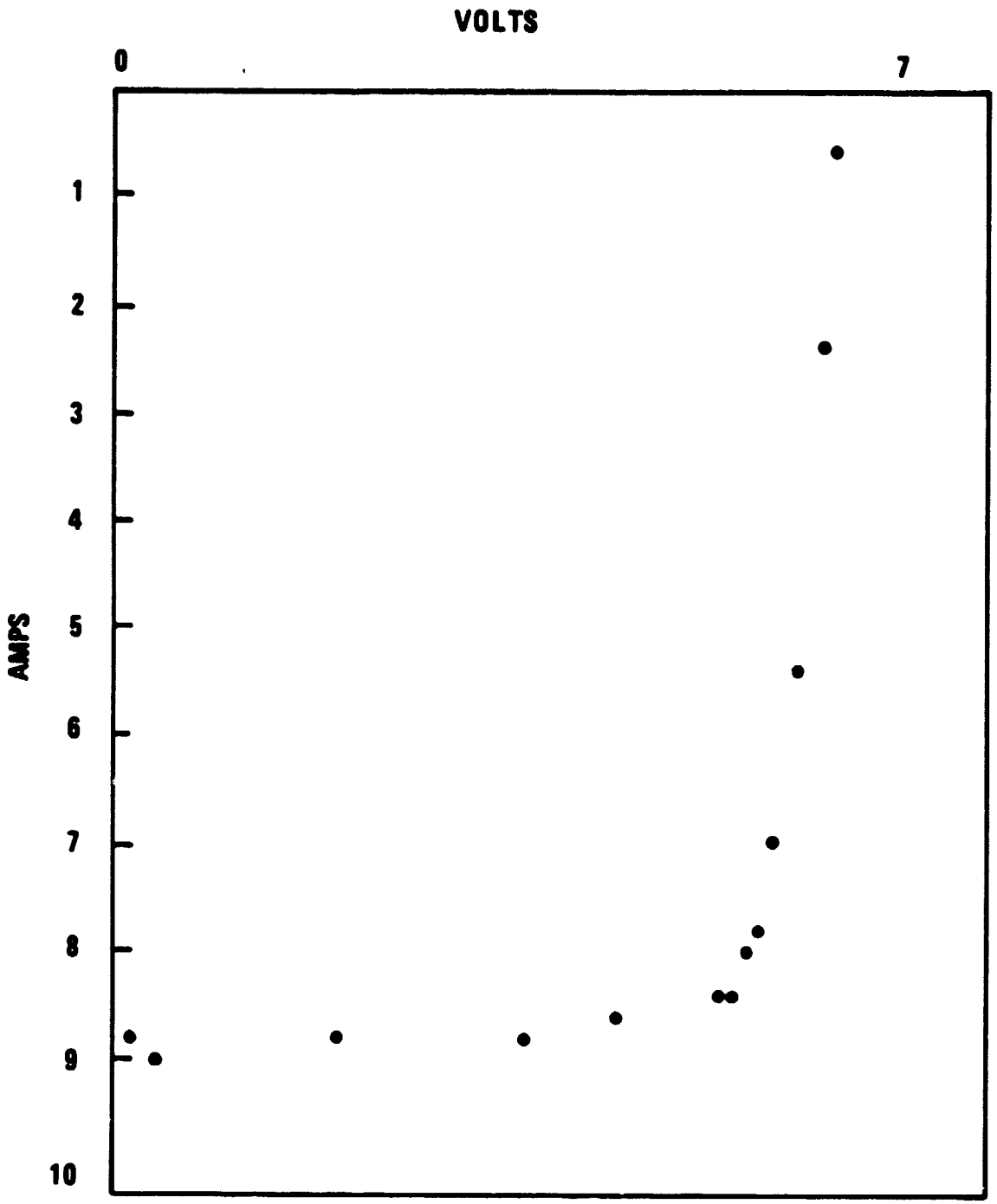

Figure 6. I-V Plot of Varian's AlGaAs/GaAs Cell

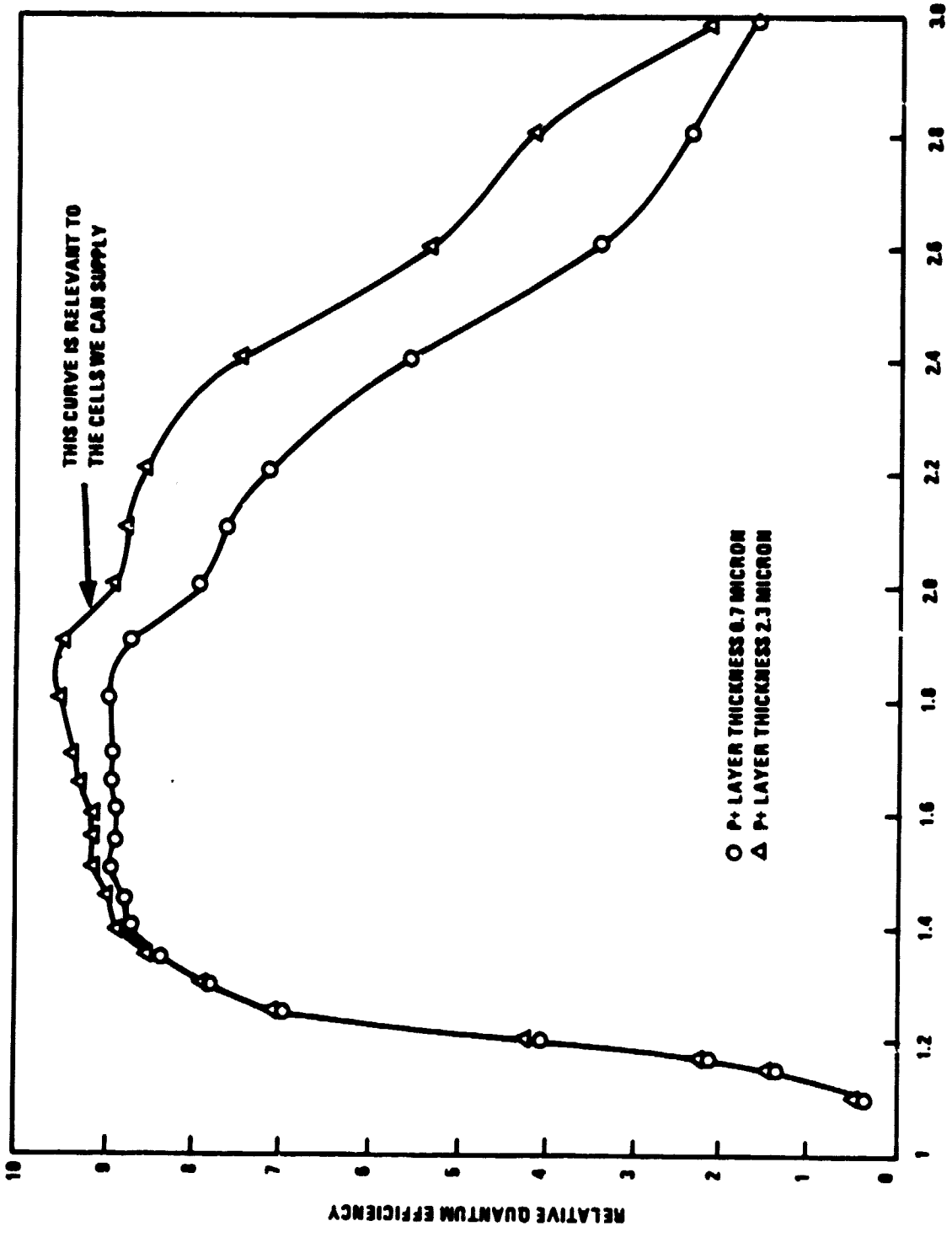

Figure 7. Si Cell Quantum Yield Measurements

TABLE 2. FLAT PANEL Si CELLS

TYPE OF CELL	Si	Si
MANUFACTURER	SOLAREX, ROCKVILLE, MD	APPLIED SOLAR ENERGY, CA
CELL SIZE	2 x 2 cm SQUARE	2 x 2 cm SQUARE
CONC. RATIO	1	1
EFFICIENCY	10%	14-15%
GRID COVERAGE	5%	7%
MOUNTING	ADHESIVELY BONDED TO ALUMINUM	SOLDERABLE TO Ti-Pd-Ag BACKPLATE

Earlier work indicated that the concentration system should be able to produce optical concentrations in the vicinity of 1000:1. To achieve this goal, a survey of collector-concentration concepts was conducted. A two-stage concentration system was found to be optimum, with each stage performing some of the concentration. The first stage was chosen to be a Cassegrain telescope because this type of optics would keep the collector close to the spacecraft. The second stage of concentration employs compound parabolic concentrators. A schematic of this system, for a three-cell configuration, is shown in Figure 8.

The first-stage concentration of the Cassegrain is the ratio of the area of the entering beam to the area of the image; the second-stage concentration of the CPC's is the ratio of the area of the entrance aperture to the area of the exit aperture, assuming the exit aperture is the same as the solar cell array. The resultant optical concentration of the system is the product of the concentration of the telescope and the CPC.

In order to determine the optimum concentration ratio for each stage, a preliminary system's design was performed on two systems with f-numbers of 2 and 5. These two systems are shown in Figures 9 and 10. Some general design considerations resulted from this comparison. In the f/2 system most of the concentration was performed by the Cassegrain, resulting in a very compact system. However, the components have steep curvatures, large concentrated power is incident on the beamsplitters, and a relatively large obscuration is present. In the f/5 system, most of the concentration is performed by the CPC's, resulting in a large system. The components are less steeply curved and less power is incident on the beamsplitters. While the obscuration is reduced in this latter configuration, the system becomes very long.

Since a large number of design parameters are involved in the actual design configuration, a computer program was written using parametric equations for

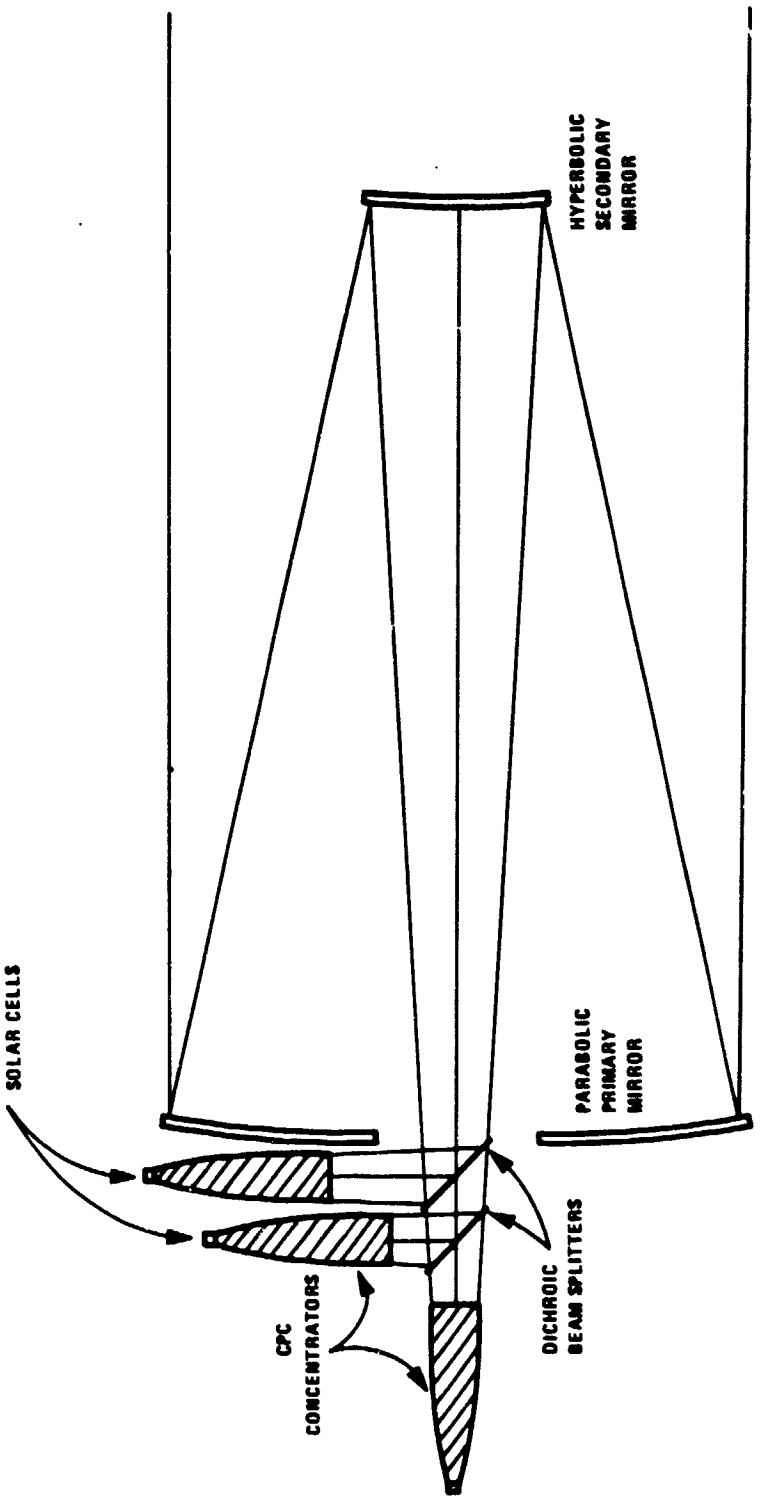

Figure 8. Schematic of Optical System

f/1.0 PRIMARY MIRROR
2.0x SECONDARY MIRROR
SYSTEM EFL = 35.6 m; f/2.0
SECONDARY OBSCURATION = 15%

CPC DIAMETER = 0.62 m
CPC LENGTH = 0.37
CPC CONCENTRATION RATIO = 1.425

BS_1 MAJOR AXIS = 1.4 m
BS_2 MAJOR AXIS = 2.2 m

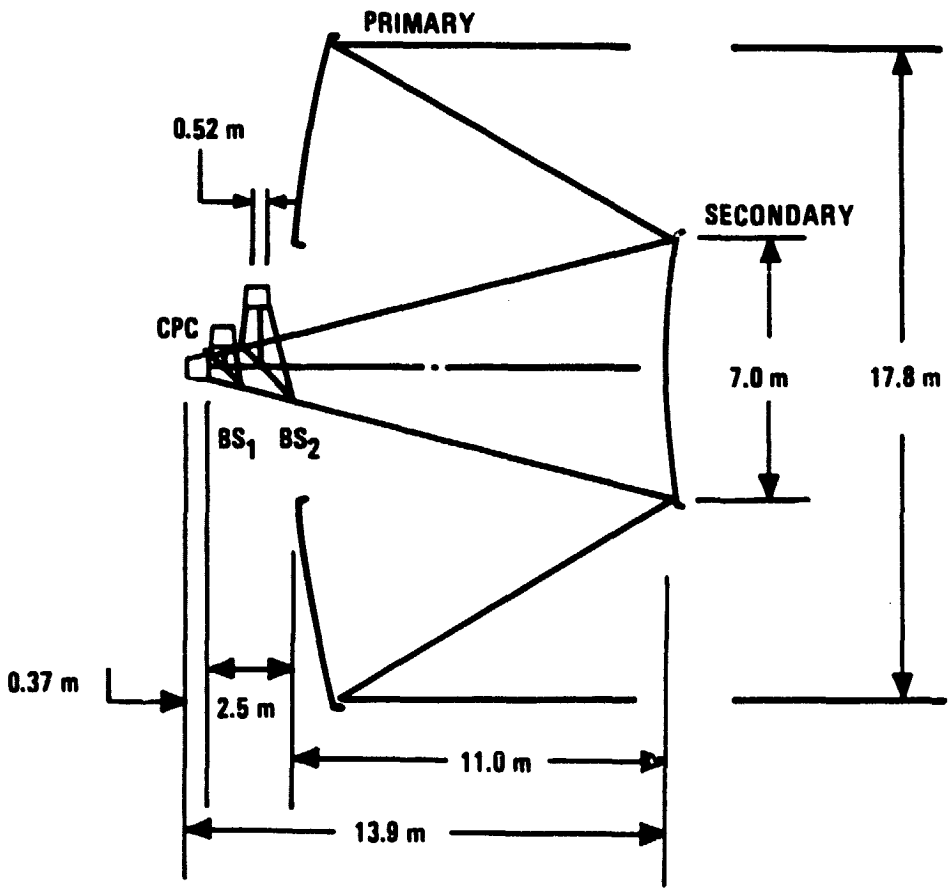

Figure 9. 100 kW f/2.0 Optical System

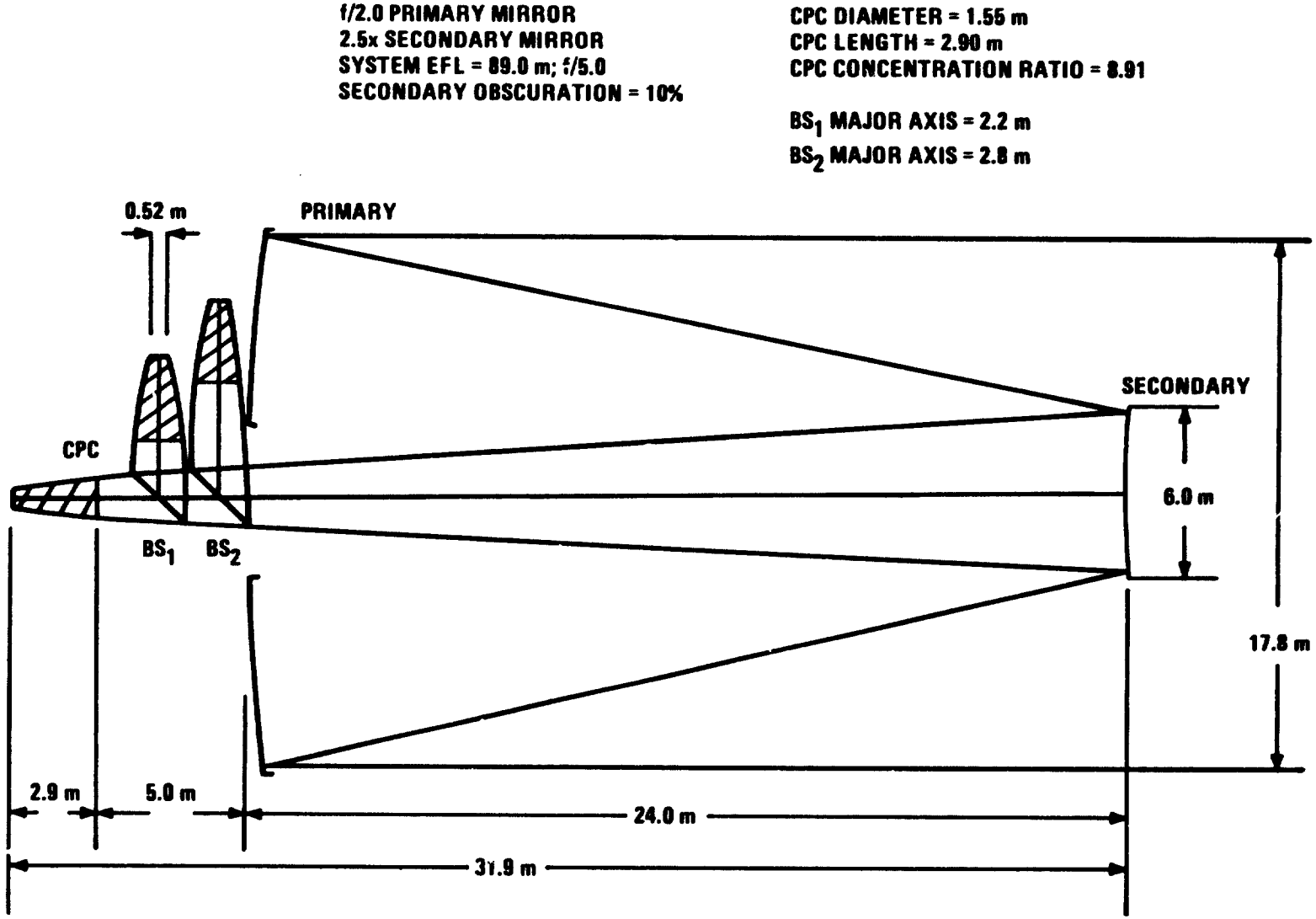

Figure 10. 100 kW f/5.0 Optical System

all the design parameters. This program was used to arrive at the best system. An f/3.5 system having concentration ratios of 270 and 4.7 for the first and second stages respectively, was found to be optimum. A detailed design of this system was then performed, including a complete raytrace of the optical components. A schematic of the system is shown in Figure 11. The optical description of this system scaled to a primary diameter of 1.0 is shown in Figure 12. The system design parameters are detailed in Figure 13.

Optical Design

Having designed an optimum solar concentration system in the previous phase, the final optical system design (Figure 11) could then be scaled down to an appropriate size for field testing as a demonstration model. The actual size of the model would depend on the available sizes of the solar cells, and on the concentration ratio to be demonstrated. In addition, the testing environment (ambient sunlight vs laboratory solar simulator) needed to be considered in the final scale of the model.

Thus, an initial comparison was made between two systems of 10" and 16" apertures, scaled from the final design of the previous phase. The parameter values for these two systems are given in Figure 14. Both of these systems require CPC's whose size is reasonable to fabricate, but the fabrication of the 16" primary mirror appeared to be questionable. At present, diamond machining lathes cannot handle a 16" diameter, while a glass mirror which is ground and polished conventionally would be extremely expensive and heavy in this large size.

Concurrently with the discussions on the size requirements of the subscale model, the possibility of using a laboratory solar simulator was researched. The simulators could produce beam apertures from 5" to 10", although some modification of the simulator optical system would be required

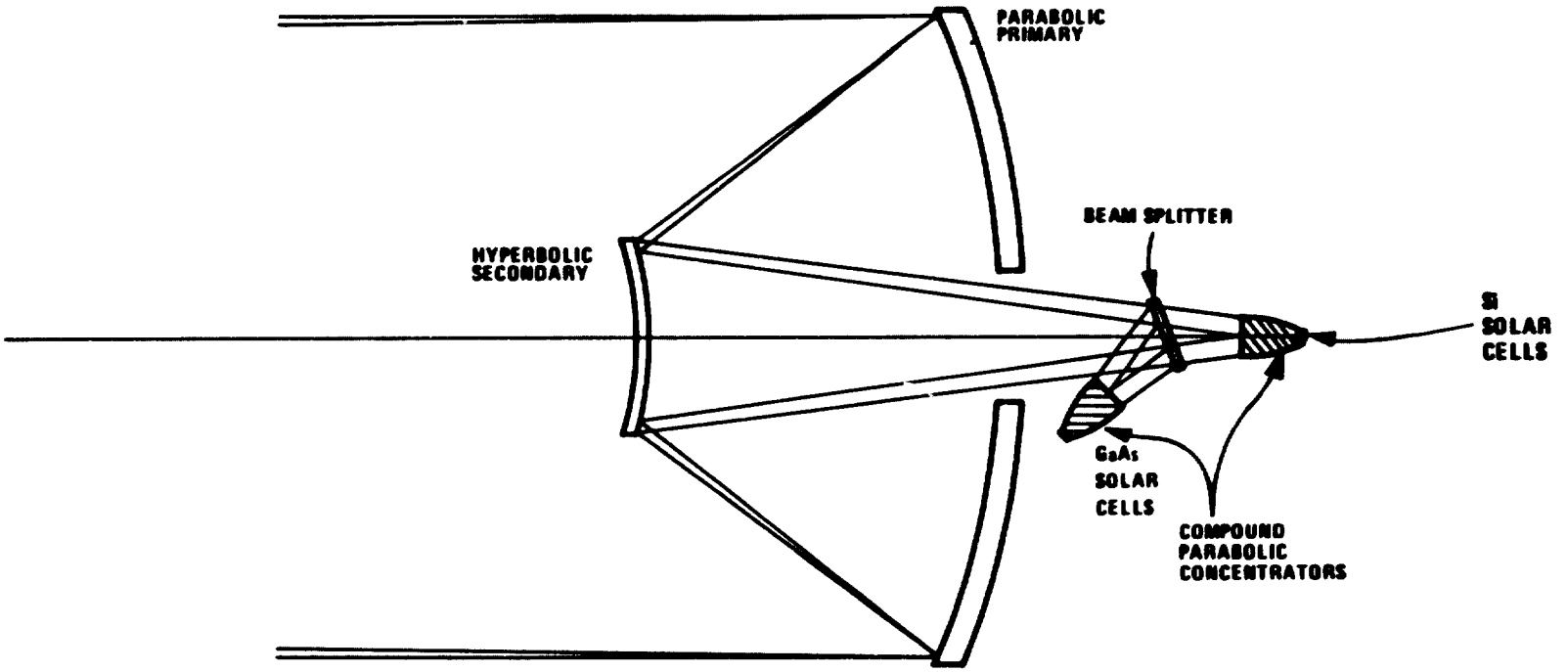

Figure 11. f/3.5 System

```
****************************************

SOLAR CONCENTRATOR - FINAL DESIGN
SYSTEM SCALED TO PRIMARY DIAMETER = 1
CPC REPRESENTED AS ELLIPSE

****************************************


LENS UNITS ARE INCHES

 REF OBJ HT                    REF AP HT    OBJ SURF   REF SURF   IMG SURF
 -.436335E+08 (    .25 DG)       .50000          0          1         17

    EFL           BF          F/NBR        LENGTH          GIH
    3.5000      0.0000          3.50         .4532         .0165

WAVL NBR          1           2           3           4           5
WAVELENGTH     .58756      .48613      .65627      .43584      .70652
SPECTRAL WT    1.0000      1.0000      1.0000      1.0000      1.0000

BASIC LENS DATA

SURF        CV            RD            TH          MEDIUM
  0      0.000000      0.000000  1.000000E+10      AIR
  1      -.714286     -1.400000      -.522000      REFL
  2     -2.247191      -.445000       .490000      REFL
  3      0.000000      0.000000       .085244      AIR
  4      0.000000      0.000000       .010942      AIR
  5   -103.737668      -.009640      -.010942      REFL
  6      0.000000      0.000000       .010942      AIR
  7   -103.737668      -.009640      -.010942      REFL
  8      0.000000      0.000000       .010942      AIR
  9   -103.737668      -.009640      -.010942      REFL
 10      0.000000      0.000000       .010942      AIR
 11   -103.737668      -.009640      -.010942      REFL
 12      0.000000      0.000000       .010942      AIR
 13   -103.737668      -.009640      -.010942      REFL
 14      0.000000      0.000000       .010942      AIR
 15   -103.737668      -.009640      -.010942      REFL
 16      0.000000      0.000000      0.000000      AIR
 17      0.000000      0.000000      0.000000      AIR

CC AND ASPHERIC DATA

SURF        CC
  1   -1.00000E+00
  2   -2.25000E+00
  5   -9.91140E-01
  7   -9.91140E-01
  9   -9.91160E-01
 11   -9.91160E-01
 13   -9.91140E-01
 15   -9.91140E-01
```

Figure 12. Optical Layout for a Solar Concentrator

Parameter	Parameter Value	
	Normalized System	GaAs/Si, 100 kW
Primary diameter	1m	20.43m
Primary focal length	0.7m	14.30m
Primary conic constant	-1	-1
Secondary diameter	0.26m	5.31m
Secondary focal length	0.2225m	4.55m
Secondary conic constant	-2.25	-2.25
Secondary Magnification	5.0	5.0
Obscuration (Area)	7.3σ	7.3σ
Obscuration efficiency	0.927	0.927
CPC diameter	0.061m	1.25m
CPC length	0.085m	1.74m
Cassegrain concentration	269.63	269.63
CPC concentration	4.66	4.66
System concentration (Design)	1256.60	1256.60
System focal length	3.5m	71.51m
System f-number	3.5	3.5
Beam splitter area	$0.0075m^2$	$3.13m^2$
Solar cell array diameter	0.0282m	0.576m

Figure 13. Solar Concentrator Final Design

PARAMETER	PARAMETER VALUE		
	NORMALIZED SYSTEM	10" PRIMARY	16" PRIMARY
PRIMARY DIAMETER	1	10.0 in	16.0 in
PRIMARY FOCAL LENGTH	0.7	7.0 in	11.2 in
PRIMARY CONIC CONSTANT	−1	−1	−1
SECONDARY DIAMETER	0.26	2.6 in	4.16 in
SECONDARY FOCAL LENGTH	0.2225	2.225 in	3.56 in
SECONDARY CONIC CONSTANT	−2.25	−2.25	−2.25
SECONDARY MAGNIFICATION	5.0	5.0	5.0
OBSCURATION (AREA)	7.3%	7.3%	7.3%
OBSCURATION EFFICIENCY	0.927	0.927	0.927
CPC DIAMETER	0.061	0.61 in	0.98 in
CPC LENGTH	0.085	0.85 in	1.36 in
CASSEGRAIN CONCENTRATION	269.63	269.63	269.63
CPC CONCENTRATION	4.66	4.66	4.66
SYSTEM CONCENTRATION (DESIGN)	1256.60	1256.60	1256.60
SYSTEM FOCAL LENGTH	3.5	35.0 in	56.0 in
SYSTEM F-NUMBER	3.5	3.5	3.5
BEAM SPLITTER AREA	0.0075	0.75 in^2	1.92 in^2
SOLAR CELL ARRAY DIAMETER	0.0282	0.282 in	0.451 in

Figure 14. Solar Concentrator Scaled Designs

to produce a 10" aperture. Model designs for these apertures were investigated, and the pertinent design parameters for representative 5" and 10" systems are given in Figure 15. The substantial increase in the source divergence angle for the laboratory simulators was found to place severe demands on the CPC's. Most of the concentration was now being performed by the CPC's instead of the Cassegrain, which resulted in very long CPC's, and much more obscuration by the secondary mirror.

Thus, considering the manufacturability and efficiency of the CPC's for systems designed for large source divergence, we conclude that such designs are not desirable. The solar simulator can be modified to aperture down the source, which decreases the angular divergence, but this also reduces the intensity significantly. We feel, however, that the intensity will still be adequate to allow accurate concentration measurements. The system was, therefore, designed to have a 10" aperture, concentrating a $\pm 0.5^{o}$ or smaller source. The design parameters for this system are listed in Figure 16, and a schematic drawing is given in Figure 17. The optical raytrace computer listing is given in Figure 18.

Essentially, the only change needed in this system, from the scaled system of the last phase, is to scale it to 10" aperture and increase the back focus slightly to allow sufficient clearance for thermal measurements and mechanical mounting of the CPC's. This results in a slightly larger secondary placed slightly closer to the primary, and a 3% increase in the system obscuration.

Optical Analysis

The final optical design presented in the previous phase used a Casegrain telescope as the first stage of concentration, followed by compound parabolic concentrators (CPC) as the second stage. The telescope consists of a parabolodial primary mirror and a hyperboloid for the secondary, as the nominal design. Certainly, with two-mirror telescopes, there are an

PRIMARY DIAMETER =	5.0"	10.0"	10.0"
PRIMARY FOCAL LENGTH =	3.5"	7.0"	7.0"
PRIMARY F/# =	0.7	0.7	0.7
SECONDARY MAGNIFICATION =	5.0	5.0	5.0
SYSTEM BACK FOCAL LENGTH =	4.0	4.0	3.0
SOURCE ANGULAR SUBTENSE =	$\pm 3.0^\circ$	$\pm 1.5^\circ$	$\pm 0.5^\circ$
SYSTEM FOCAL LENGTH =	17.50"	35.00"	35.00"
SYSTEM F/# =	3.50	3.50	3.50
SECONDARY FOCAL LENGTH =	-1.56"	-2.29"	-2.23"
SECONDARY DIAMETER =	1.81"	2.89"	2.80"
PRIMARY-SECONDARY SEPARATION =	2.25"	5.17"	5.33"
SECONDARY OBSCURATION =	0.16	0.08	0.07
OBSCURATION EFFICIENCY =	0.84	0.92	0.93
CPC ENTRANCE APERTURE DIA. =	1.83"	1.83"	0.61"
CONCENTRATION OF CASSEGRAIN =	7.43	29.76	269.63
SOLAR CELL DIAM. =	0.16"	0.31"	0.28"
CONCENTRATION OF CPC =	134.74	33.65	4.66
LENGTH OF CPC =	11.57"	6.23"	0.85"
SYSTEM CONCENTRATION =	1000	1000	1256

Figure 15. System Design Parameters for Different Divergence Sources

PRIMARY DIAMETER =	10.0"
PRIMARY FOCAL LENGTH =	7.0"
PRIMARY F/# =	0.70
SECONDARY MAGNIFICATION =	5.0
SYSTEM BACK FOCAL LENGTH =	6.0"
SOURCE ANGULAR SUBTENSE =	$\pm$ 0.5°
SYSTEM FOCAL LENGTH =	35.00
SYSTEM F/# =	3.50
SECONDARY FOCAL LENGTH =	–2.71"
SECONDARY DIAMETER =	3.18"
PRIMARY-SECONDARY SEPARATION =	4.83"
SECONDARY OBSCURATION =	0.10
OBSCURATION EFFICIENCY =	0.90
CPC ENTRANCE APERTURE DIA. =	0.61"
CONCENTRATION OF CASSEGRAIN =	269.63
SOLAR CELL DIAMETER =	0.28"
CONCENTRATION OF CPC =	4.66
LENGTH OF CPC =	0.85"
SYSTEM CONCENTRATION =	1256

Figure 16. System Design Parameter for Subscale Model

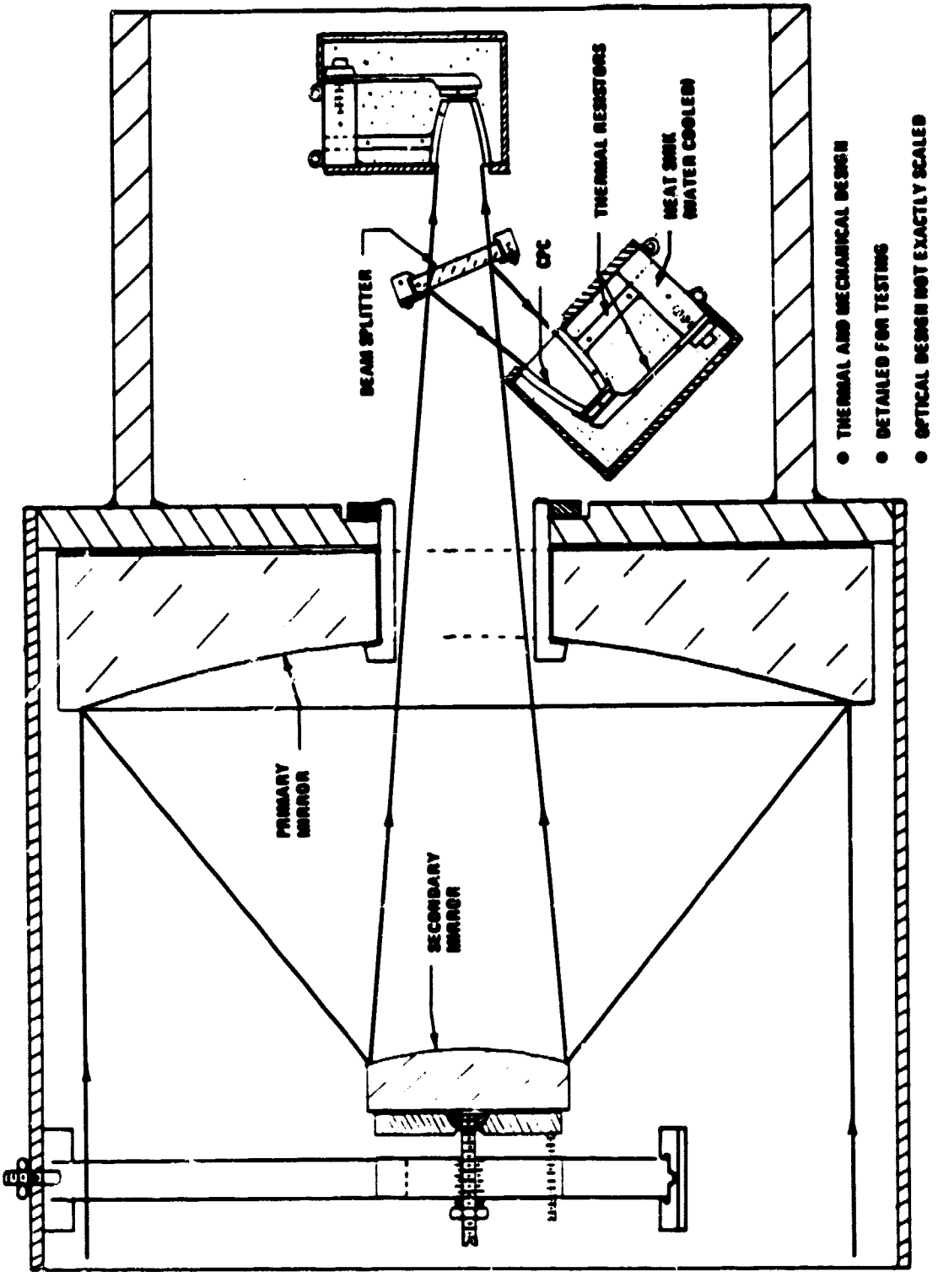

Figure 17. Subscale Model Design

```
**************************************

SOLAR CONCENTRATOR - MOD1
PRIMARY DIAM=10, BFS=0(GRA)
ALPHA=2

**************************************


LENS UNITS ARE INCHES

 REF OBJ HT                    REF AP HT    OBJ SURF   REF SURF   IMG SURF
 -.836335E+08 (    .25 DG)      5.00000         0          1         11

    EFL            BF          F/NBR        LENGTH         GIH
   1.2664         0.0000          .19         6.8524        -.2075

WAVL NBR          1           2           3           4           5
WAVELENGTH      .58756      .48613      .65627      .43584      .70652
SPECTRAL WT     1.0000      1.0000      1.0000      1.0000      1.0000

BASIC LENS DATA

SURF        CV            RD            TH          MEDIUM              RN
  0      0.000000      0.000000  1.000000E+10    AIR

  1      -.071429    -14.000000     -6.833333    REFL

  2      -.184615     -5.416667     10.833333    REFL

  3      0.000000      0.000000       .852640    AIR

  4      0.000000      0.000000       .109420    AIR

  5    -10.373767      -.096397      -.109420    REFL

  6      0.000000      0.000000       .109420    AIR

  7    -10.373767      -.096397      -.109420    REFL

  8      0.000000      0.000000       .109420    AIR

  9    -10.373767      -.096397      -.109420    REFL

 10      0.000000      0.000000      0.000000    AIR

 11      0.000000      0.000000      0.000000    AIR


CC AND ASPHERIC DATA

SURF      CC            AD            AE            AF            AG
  1  -1.000000E+00
  2  -2.250000E+00
  5  -8.997800E-01
  7  -8.997800E-01
  9  -8.997800E-01
```

Figure 18. Raytrace Listing of the 10" Subscale Model

infinite number of combinations of primary/secondary mirror shapes which will perform well as first stage concentrators. The Dall-Kirkham, having a spherical secondary and an elliptical primary, and the Ritchey-Chretien, having two hyperboloids, are but two well-known examples of alternate telescope configurations. In an orbital space environment, where these surface profiles will be approximated by a deployable mechanical super-structure, one design is as easily configured as another. In a subscale model, however, where the surface profiles must be generated by conventional manufacturing methods, the issue of ease-of-manufacture must be considered to keep the model costs as low as possible.

Thus, we considered the following modifications to the nominal design, in an effort to identify a telescope system which maintained adequate concentration performance, but could be fabricated at the lowest cost:

Configuration	Primary	Secondary
Nominal design (Cassegrain)	Paraboloid	Hyperboloid
Dall-Kirkham	Ellipsoid	Sphere
Ritchey-Chretien	Hyperboloid	Hyperboloid
Spherical Primary	Sphere	Oblate Spheroid

Each configuration listed is corrected on-axis for third order spherical aberration, while some are better corrected than others for off-axis aberrations. All of these systems have the same element sizes and spacings, while only the actual surface shapes are changed slightly from one system to another. And while we are not primarily interested in using the telescope for good "imagery," we must still maintain a reasonable level of point-to-point mapping from object-to-image in order to concentrate the energy adequately. In addition, the fabrication of the elements for these systems is understood well in the industry, and would likely not cause any needless confusion.

Currently two manufacturing methods are available for producing the primary and secondary of such systems to the accuracy required. These methods are diamond machining of the surface profiles, and optical grinding/polishing of the surfaces. Because of the steep surface profiles needed for these two surfaces, it is unclear at this time which manufacturing method is the most cost-effective. Clearly, diamond-turning can be used to produce the elements for any of these systems, with the same associated costs irrespective of the system. This is because it is just as easy to diamond turn an asphere as it is turn a sphere. The same cannot be said of conventional grinding and polishing techniques, however, where the fabrication of an asphere is many times more costly than making a sphere. Typically, the cost of fabricating a sphere by conventional grinding and polishing is less than diamond-turning the same sphere, because the tooling and set-up costs are far less.

The costs associated with fabricating each system by conventional grinding and polishing also vary considerably, whereas the diamond-turning costs are about the same for each system. If possible, one would like to use spherical elements to simplify their conventional manufacture. Thus, the Dall-Kirkham and Spherical Primary configurations appear as likely candidates for cost-effective systems. But, the performance of these systems must be checked by raytracing, and the cost of the other aspheric elements determined. If they prove difficult to manufacture, they might offset the reduced cost of the spherical element. Clearly, the Ritchey-Chretien system can be eliminated from consideration if we decide to use grinding and polishing methods. Its improvement over the nominal Cassegrain is minimal, and the cost of making two hyperboloids is much greater than the paraboloid/hyperboloid combination of the Cassegrain.

To investigate the performance of these candidate systems, slightly different surface profile relationships must be used. Only the conic constants of the surfaces are changed from one configuration to another; the basic design equations presented in the previous phase remain the same. The system is shown schematically in Figure 19.

C_1 and C_2 are the curvatures of the primary and secondary, D is their separation, B is the system back focal length, and Y is the semi-aperture of the primary. In addition, there are the conic constants, k_1 and k_2, associated with the surfaces. The curvatures of the system are the direct result of the first-order constructional parameters, and are given by:

$$C_1 = \frac{(B - F)}{2\,DF}$$

$$C_2 = \frac{(B + D - F)}{2\,D\,B}$$

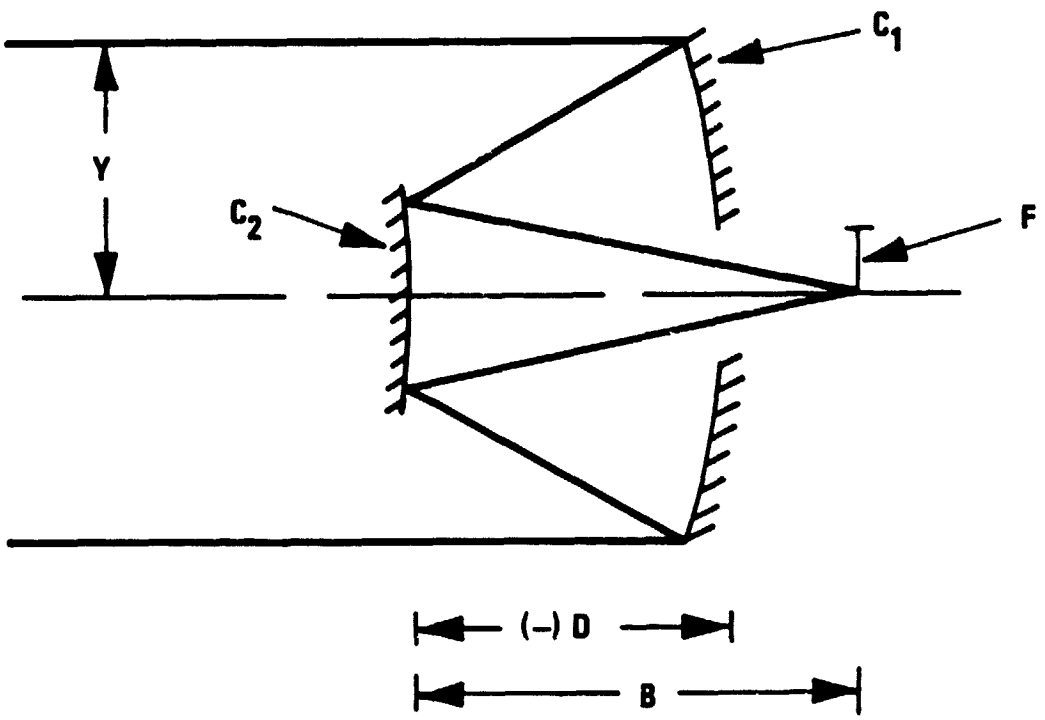

Figure 19. Two-Reflector Optical Schematic

where F is the system focal length. The conic constants can be written in terms of equivalent deformation parameters, K_1 and K_2:

$$K_1 = \frac{k_1 C_1^3}{8}$$

$$K_2 = \frac{k_2 C_2^3}{8}$$

Thus, the surfaces of the various systems can be derived in terms of these deformation parameters:

- Cassegrain

$$C_1 = \frac{(F - B)^3}{64 D^3 F^3}$$

$$K_2 = \frac{(F - D - B)(F + D - B)^2}{64 B^3 D^3}$$

- Dall-Kirkham

$$K_1 = \frac{F (F - B)^3 - B (F - D - B)(F + D - B)^2}{64 D^3 F^4}$$

K_2 = 0.0 (sphere)

- Ritchey-Chretien

$$K_1 = \frac{2 BD^2 - (B - F)^3}{64 D^3 F^3}$$

$$K_2 = \frac{2 F (B - F)^2 + (F - D - B)(F + D - B)(D - F - B)}{64 B^3 D^3}$$

o Spherical Primary

$K_1 = 0.0$ (sphere)

$$K_2 = \frac{F\,(B - F)^3 + B\,(F - D - B)\,(F + D - B)^2}{64\,B^4\,D^3}$$

The resulting conic constants for these systems are tabulated in Table 3.

Note that two values are given for the secondary conic constant in the case of the spherical primary. The value in parenthesis is a value obtained by performing an optimization computer run based on real rays, and not on third-order aberration theory. Basically, the extreme surfaces of these designs produce aberrations of higher-order, which in the case of the spherical primary require a better solution than that given by third-order theory. Third-order theory (and thus the other conic constants of Table 3) is adequate for the other systems.

TABLE 3. SURFACE CONIC CONSTANTS FOR TELESCOPE CONCENTRATOR

SYSTEM	k_1	k_2
CASSEGRAIN	−1.0	−2.25
DALL-KIRKHAM	-- .643429	0.0
RITCHEY-CHRETIEN	−1.035862	−2.476293
SPHERICAL PRIMARY	0.0	+4.060096 (+5.243370)

These alternate configurations were then raytraced to determine the actual system performance, based initially on perfectly manufactured surfaces. The performance is shown in Table 4.

Table 4 shows that all configurations are able to direct the light from one solar diameter to the solar cell, although the efficiency is poorer for systems requiring more reflections from the CPC. (The Cassegrain and Ritchey-Chretien performances are identical.) The nominal system is designed to accept two solar diameters ($\alpha = 2$) to allow for tracking errors, imperfectly manufactured surfaces, and alignment tolerances. Thus, the performance at 1.5 solar diameters (which equates to a tracking error of $\pm 1/8$ degree for "perfect" systems) should be high as well. Except for the spherical primary, the systems efficiently send the energy to the solar cell with a minimum of reflections from the CPC walls. The spherical primary, however, not only requires more than 3 reflections from the CPC for some of the energy, but allows 25 percent of the light to miss the CPC entrance aperture entirely. Thus, the spherical primary system is much more sensitive to tracking errors than any of the other systems.

In addition to tracking sensitivity, one must investigate the sensitivity of these systems to manufacturing and alignment errors. In the previous phase, an analysis was performed to identify the relative sensitivities of the primary and secondary, regarding slope errors occurring at the surface. The relationship derived was:

$$\frac{\text{Secondary Slope Sensitivity}}{\text{Primary Slope Sensitivity}} = 1 + \frac{2\,C_2\,D}{\left[1 - (k_2 + 1)\,C_2^{\,2}\,y_2^{\,2}\right]^{3/2}}$$

TABLE 4. TELESCOPE CONCENTRATION PERFORMANCE (NOMINAL SYSTEM)

SYSTEM	FIELD-OF-VIEW (SUN DIAMETERS)	FRACTIONAL ENERGY REACHING SOLAR CELL (PERCENT)
CASSEGRAIN (RITCHEY-CHRETIEN)	1.0	30 DIRECT 70 1 CPC REFLECTION 100 ON SOLAR CELL
	1.5	2 DIRECT 98 1 CPC REFLECTION 100 ON SOLAR CELL
DALL-KIRKHAM	1.0	29 DIRECT 71 1 CPC REFLECTION 100 ON SOLAR CELL 97 1 CPC REFLECTION 3 2 CPC REFLECTION 100 ON SOLAR CELL
SPHERICAL PRIMARY	1.0	1 DIRECT 99 1 CPC REFLECTION 100 ON SOLAR CELL
	1.5	59 1 CPC REFLECTION 11 2 CPC REFLECTION 3 3 CPC REFLECTION 2 GREATER THAN 3 REFLECTION (25) MISS CPC 75 ON SOLAR CELL

For the nominal Cassegrain design, this results in a secondary having a factor of 2.53 less sensitivity to surface errors than the primary. To expand on this analysis, a more detailed tolerance analysis was performed with respect to radius, separation, and surface conic constant tolerances, as well as the tilt and decentration of the secondary relative to the primary. (Actually the combination of tilt and decenter of the secondary results in an equivalent decentration, somewhat larger in magnitude.) Table 5 lists the relative sensitivities resulting from this analysis.

Table 5 confirms the fact that in all the systems, the primary is a much more sensitive element than the secondary. This result has been emphasized by normalizing the actual sensitivities to those of the secondary (thus producing the values of 1.0 for the secondary sensitivities). The large sensitivity of the separation of the primary-secondary versus that of the separation of the secondary-CPC is chiefly a result of the magnification of

TABLE 5. PRIMARY/SECONDARY RELATIVE TOLERANCE SENSITIVITIES

		RELATIVE SENSITIVITY		
CONFIGURATION		Δ RADIUS	Δ SEPARATION	Δ CONIC CONSTANT
CASSEGRAIN	PRIMARY	1.62	21.43	6.33
(RITCHEY-CHRETIEN)	SECONDARY	1.00	1.00	1.00
		DECENTRATION (SECONDARY) = 0.90		
DALL-KIRKHAM	PRIMARY	1.63	25.54	6.97
	SECONDARY	1.00	1.00	1.00
		DECENTRATION (SECONDARY) = 1.07		
SPHERICAL	PRIMARY	1.71	40.97	8.94
PRIMARY	SECONDARY	1.00	1.00	1.00
		DECENTRATION (SECONDARY) = 1.11		

the secondary mirror. A change in the axial positioning of the secondary by an amount ΔZ results in a displacement of the image position by an amount $m^2 \Delta Z$, or a factor of 25 in our system. The values listed for the decentration of the secondary are relative to the tolerance applied to the primary-secondary separation.

The relative sensitivities shown in Table 5 indicate that the primary is more sensitive than the secondary in the case of the spherical primary. The actual sensitivities of the surfaces for the spherical primary configuration are about one-half of those of the other systems. The Cassegrain, Ritchey-Chretien, and Dall-Kirkham all have about the same actual surface and separation tolerances, while the spherical primary has tolerances about half the other systems'. Thus, even though the spherical primary mirror would be easier to manufacture, the alignment and surface shape tolerances of this system are more stringent by a factor of 2.

To check the tolerance results, the telescope systems were raytraced after shape and positioning parameters were changed slightly to simulate alignment and manufacturing errors. In addition to examining the telescope's performance for the solar disc, tracking errors were simulated by examining the performance at various points in the field of view of the systems up to two solar diameters. A typical example of the raytrace output for a $\alpha = 2$ (twice the diameter of the sun) is shown in Figure 20. Figure 20 also shows the uniform distribution of approximately 2000 rays entering the telescope; the number associated with each ray identifies the progress of that ray during its trajectory according to the following legend:

4 - Ray hits solar cell directly
6 - Ray hits solar cell after 1 reflection from CPC
8 - 2 reflections
A - 3 reflections
• - Greater than 3 reflections
5 - Ray misses CPC entrance aperture

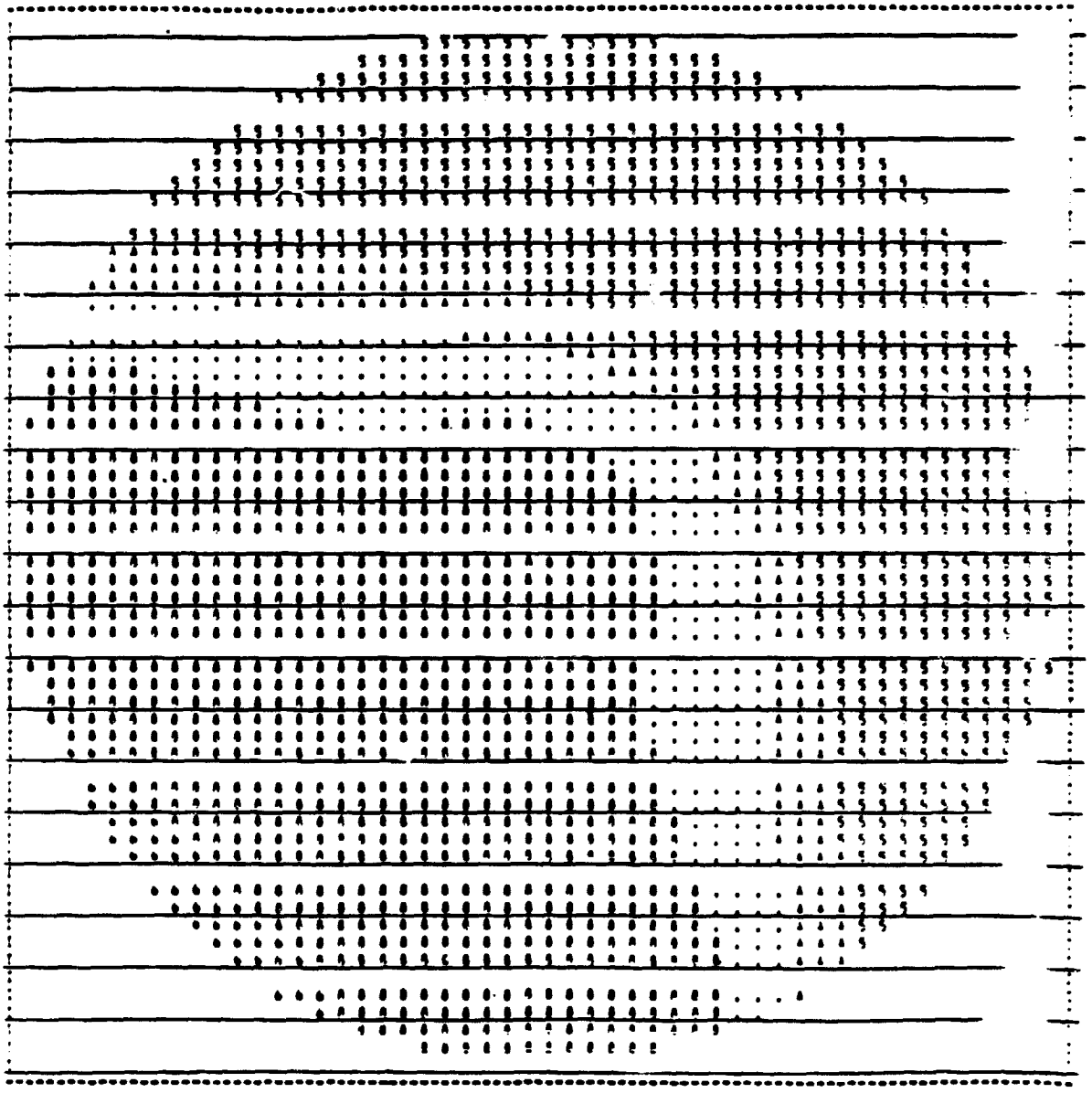

Figure 20. Raytrace Output for Typical Tolerance Analysis Computer Run

Upon completion of the ray trace, a summary is printed identifying the percentages of rays in each of the above categories. The results of the ray traces are that the Cassegrain, Ritchey-Chretien, and Dall-Kirkham perform well, with minor surface and misalignment errors. The spherical primary configuration allows too much energy to miss the CPC with the same magnitude of tolerances. It thus cannot be used as a telescope configuration in our model.

Based on the results from the tolerance analysis, Table 6 lists the nominal sags of the primary and secondary, and the resultant envelopes about the nominal profiles. The envelopes bound the maximum permissible errors in the surface profile, assuming the actual manufactured surface profile is smooth and contacts the nominal profile at the vertex. Thus, any smooth surface profiles having sags within the envelopes given in Table 6 will result in an adequate first stage of concentration. Note that the spherical primary configuration is not listed due to its poor performance and demanding tolerances. Note also that the secondary of the Dall-Kirkham is assumed to be perfect, since this spherical element can be easily fabricated to very precise optical tolerances far exceeding the requirements.

In addition to the surface shape tolerances listed in Table 6, the separation of the primary and secondary for all three systems should be held to $\pm$0.015 inches. This is basically a result of the corresponding shift in location of the CPC's, since the degradation of the concentration performance is minimal. And thus, as we have seen earlier, the decentration of the secondary should also be held to within $\pm$0.015 inches.

The CPC is a very forgiving element in the system in that its surface profile is very insensitive to errors in shape. (In fact, often significant profile changes such as fins or dimples are introduced to help diffuse the light at the exit aperture.) Standard machining tolerances ($\pm$0.003" for example) are adequate for specifying the surface profile envelope of the CPC's.

TABLE 6. SURFACE PROFILE ENVELOPES

SYSTEM CONFIGURATION	PRIMARY ZONE	NOMINAL SAG	SAG ENVELOPE (+/–)	SECONDARY ZONE	NOMINAL SAG	SAG ENVELOPE (+/–)
CASSEGRAIN	1.0	0.03571	0.00013	0.2	0.00269	0.00031
	2.0	0.14286	0.00032	0.6	0.03310	0.00079
	3.0	0.32143	0.00055	1.0	0.09134	0.00108
	4.0	0.57143	0.00087	1.4	0.17730	0.00138
	5.0	0.89286	0.00143	1.6	0.23619	0.00138
RITCHEY-CHRETIEN	1.0	0.03571	0.00013	0.2	0.00369	0.00031
	2.0	0.14283	0.0013	0.2	0.00369	0.00030
	3.0	0.32138	0.00056	1.0	0.09117	0.0110
	4.0	0.57101	0.00089	1.4	0.17667	0.00133
	5.0	0.89184	0.00147	1.6	0.22915	0.00142
DALL-KIRKHAM	1.0	0.03573	0.00010	0.2	0.00369	SPHERICAL
	2.0	0.14312	0.00025	0.6	0.33333	SURFACE
	3.0	0.32276	0.00042	1.0	0.09311	ASSUMED
	4.0	0.57565	0.00069	1.4	0.18405	PERFECT
	5.0	0.90325	0.00130	1.6	0.24170	

Other Feasible Spectrophotovoltaic Concepts

The concept of using tandem solar cells appears to be of some merit once again, since the model will employ only one beamsplitter in a two-cell configuration. While a transmission tandem cell configuration is unavailable at the current time and would present non-negligible losses from grid structures on the surfaces, the possibility of performing some testing of tandem cells in a reflection mode appears feasible. A schematic of the configuration for a two-cell reflection mode is shown in Figure 21. Basically, a highly reflecting coating is directly applied to the backside of a Si cell. This results in a larger Si solar cell with less concentration. The tradeoff to be made is the cost of this larger Si cell with its multilayer coating versus the cost of the beamsplitter plus another CPC and a smaller Si cell.

For our 10" model, the dimensions of the Si cell are a 1" minor axis by 1.13" major axis, if oriented at 22° from the optical axis. This results in an effective concentration ratio at the Si cell of 90, while the CR at the GaAs cell could be either 270 (without CPC) or 1000 (with CPC). This concept also works with Si and GaAs cells interchanged. It would be a relatively easy matter to test both the nominal 2-cell model and a reflective tandem 2-cell arrangement, since most of the model configuration remains unchanged. We plan to investigate this concept further, along with the availability of the larger Si solar cell.

BEAMSPLITTER DESIGN

Design Concept

The air mass zero or extraterrestrial solar spectrum covers from 0.2 μm to about 4.0 μm, with 75% of the energy contained between 0.2 μm to 1.1 μm. The energy between 0.2 μm to 0.3 μm is about 1%.

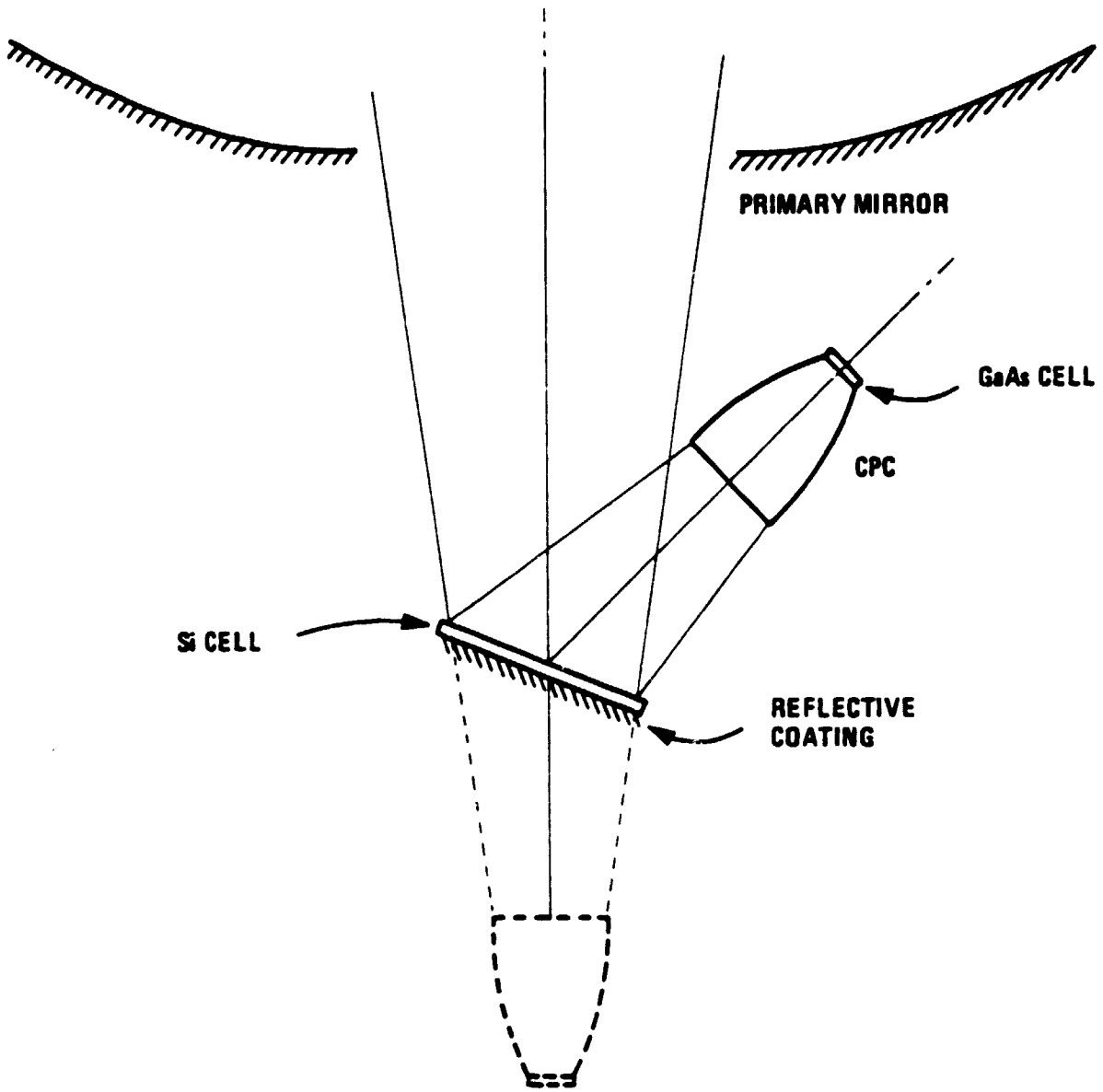

Figure 21. Tandem Cell Concept

In this program, the beamsplitters to be designed are those for the two-cell GaAs/Si and Si/GaAs configurations; that is, both reflection and transmission modes to the GaAs cell will be designed. The beamsplitter for the GaAs/Si configuration reflects 0.3 to 0.9 μm to the ideal GaAs cell while transmitting the longer wavelengths to Si cell, as shown in Figure 22. However, only the 0.9 to 1.1 μm portion of the spectrum is utilized by the Si cell. The beamsplitter for the Si/GaAs configuration reflects 0.9 to 1.1 μm to the Si cell while transmitting the short wavelengths to GaAs, as shown in Figure 23.

To date, the beamsplitters designed in this program were based on the spectral quantum efficiency calculated in the Phase I program, which showed no cut-off in short wavelengths for both GaAs and Si cells. A practical consideration is to use the spectral quantum efficiency cut-off of the state-of-the-art R&D cells. In the above section on solar cells, the GaAs and Si cells' cut-off at short wavelengths is somewhere between 0.4 to 0.5 μm. The final modification of the beamsplitter designs will be made according to the measured spectral quantum efficiency curves of the cells obtained.

Material Selection

The beamsplitter coatings consist of multilayer stacks of transparent dielectric materials. By depositing alternating high and low refractive index dielectric layers on a substrate, very high reflectivity can be achieved over a well-defined spectral range. The spectral width of the reflection band increases with the increase of the ratio of refractive indices used in the stack. Therefore, for the wide reflection spectral range (0.3 to 0.9 μm), one of the important material selection criteria is the high ratio of refractive indices of the material. UV transparency is also a primary concern. A list of the candidate materials is given in Table 7.

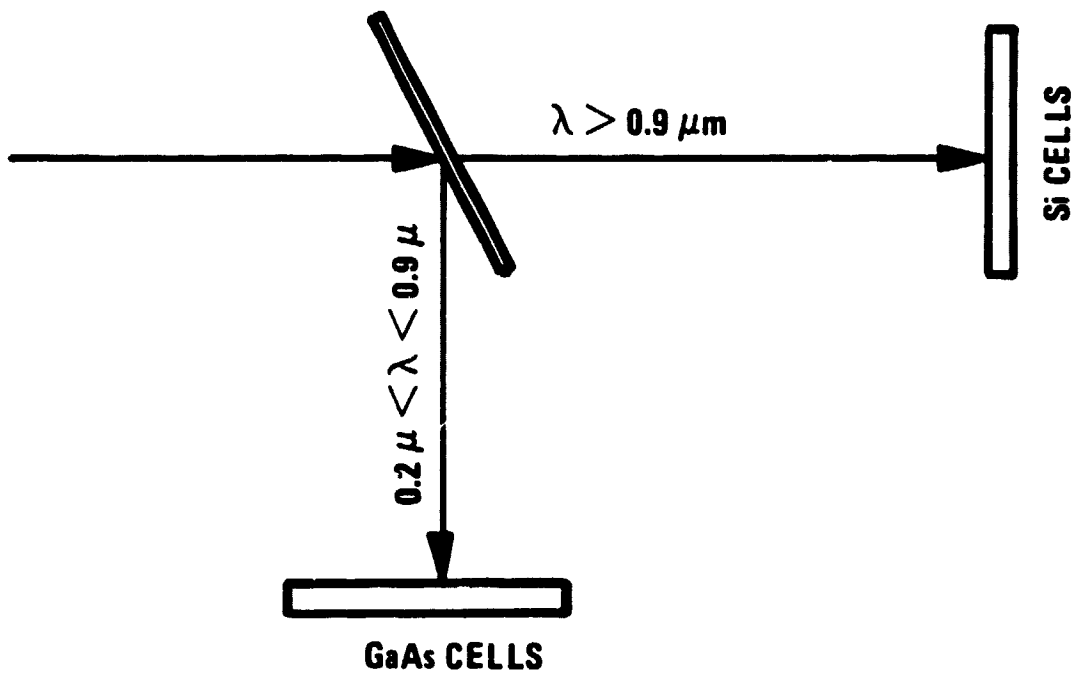

Figure 22. Spectrum Splitting Concept for Two-Cell GaAs/Si Configuration

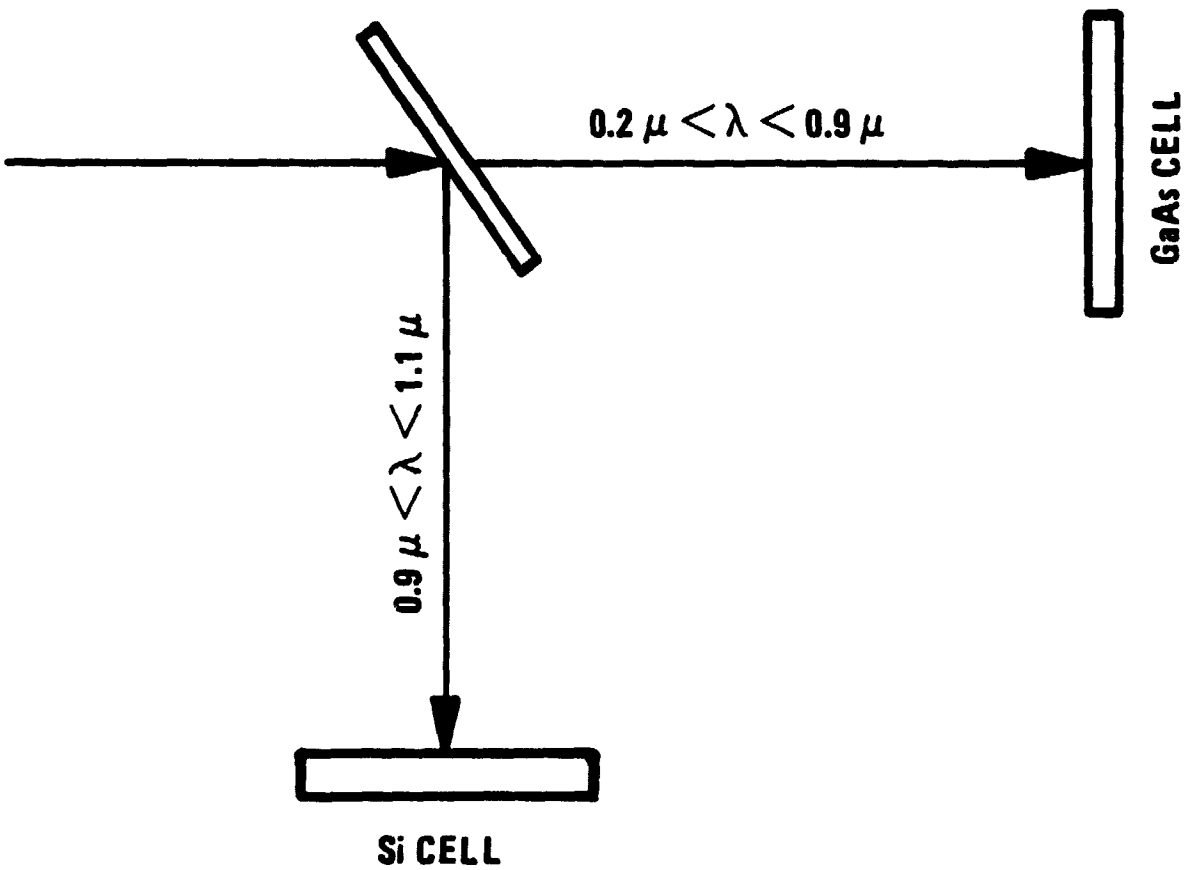

Figure 23. Spectrum-Splitting Concept for Two-Cell Si/GaAs Configuration

TABLE 7. KEY PROPERTIES OF CANDIDATE COATING MATERIAL

	MATERIAL	TRANSMISSION RANGE (μm)	REFRACTIVE INDEX		STRESS ** (Kg/cm^2)	THERMAL EXPANSION COEFFICIENT (10^{-6}/°C)	MELTING POINT (°C)	SOLUBILITY * IN WATER (g/100 $m\ell$)	
			λ (μm)	n				COLD	HOT
HIGH REFRACTIVE INDEXES	ThO_2	0.21–(>5.0)	<1	2.20	950 (T)	9.5	3050	i	i
	Y_2O_3	0.22–(>5.0)	0.4 1.0	1.92 1.83	TBD	6.7 (25°C)	2410	0.00016	–
	Ta_2O_5	0.27–(>5.0)	< 1	2.42	TBD	–	1800	i	i
	ZrO_2	0.3 –7.0	0.55	2.1	TBD	7.5 (00–800°F)	2700	i	i
	TiO_2	0.43–6.0	0.6 0.6	2.20 2.21	200(T), 1000(C)	9.2 (40°C)	1830	i	i
	ZnSe	0.5 –2.0	0.6328 1.1	2.00 2.45	1200 (C)	7.7	>1100	i	–
	ZnS	0.35–14.5	0.578 1.529	2.36 2.20	2000 (C)	6.3 (0°C)	1020	0.000065	–
LOW REFRACTIVE INDEXES	MgF_2	0.11–7.5	0.40 1.00	1.38 1.38	2000 (T)	11.0	1256	0.0076	i
	BaF_2	0.25–15	0.500 1.129	1.48 1.47	1200 (T)	18.4	1280	0.1225	sl.s
	SiO_2	0.35 –4.5	0.6328 1.13	1.42 1.46	2000 (C)	0.5	1610	i	i
	CaF_2	0.13–12	0.5 1.0	1.44 1.43	100 (T)	22.0	1360	0.0016	0.0017

* i -- insoluble
sl.s -- slightly soluble

** T -- tensile stress
C -- compressive stress

The Ta_2O_5/MgF_2 combination is selected for the beamsplitter for the GaAs/Si configuration instead of ThO_2/MgF_2 (which was used in the Phase I program) because Ta_2O_5/MgF_2 has a higher ratio of refractive indices. This makes the total number of layers required for the beamsplitter 65 layers or three stacks, instead of the 86 layers or four stacks of ThO_2/MgF_2. The larger the number of stacks, the more potential fabrication and durability problems are anticipated. The larger number of stacks also tends to have higher, undesirable off-band reflection ripples in the 0.9 to 1.1 μm region.

A combination of CaF_2/ThO_2 is selected for the beamsplitter for the Si/GaAs configuration. CaF_2 is chosen instead of SiO_2 in Phase I, since the transmission range of SiO_2 starts at 0.35 μm and renders it unsuitable for a single beamsplitter system.

Beamsplitter Design

The design details of the beamsplitter with a combination of Ta_2O_5/MgF_2 coatings on a quartz substrate are given in Figure 24. The spectral reflectance of the beamsplitter at incident angles of 0 and 22.5 degrees are shown in Figures 25 and 26, respectively.

The reflection loss from 0.9 to 1.1 μm, which cannot be utilized by either the Si or GaAs cell, is about 5%. The AMO solar energy from 0.2 to 0.3 μm is only about 1%. The Ta_2O_5/MgF_2 beamsplitter design reflects an average of more than 60% in this region. This would degrade the input to the GaAs cell by 0.6% of the total spectral energy. Adding another stack to the coating could extend 100% reflection to 0.2μm, but the trade-offs would be less durability and greater difficulty of fabrication.

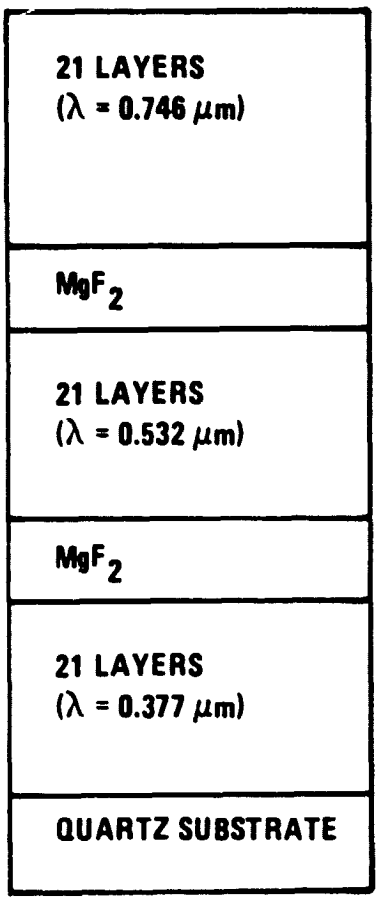

$n_H = 2.42, n_L = 1.38$

LAYERS 45 AND 65: $t = \lambda/8n_N = 0.39\ \mu m$

LAYERS 47, 49, . . 65: $t = \lambda/4n_H = 0.77\ \mu m$

LAYERS 46, 48, . . 64: $t = \lambda/4n_L = 0.135\ \mu m$

LAYER 44: $t = 0.116\ \mu m$

LAYERS 23 AND 43: $t = \lambda/8n_H = 0.028\ \mu m$

LAYERS 25, 27, . . 41: $t = \lambda/4n_H = 0.055\ \mu m$

LAYERS 24, 26, . . 42: $t = \lambda/4n_L = 0.096\ \mu m$

LAYER 22: $t = 0.082\ \mu m$

LAYERS 1 AND 21: $t = \lambda/8n_H = 0.019\ \mu m$

LAYERS 3, 5, . . 19: $t = \lambda/4n_H = 0.039\ \mu m$

LAYERS 2, 4, . . 20: $t = \lambda/4n_L = 0.068\ \mu m$

$n_s = 1.46$

Figure 24. Details of the 65-Layer Ta_2O_5/MgF_2 Beamsplitter Coating Design (t = Physical Thickness)

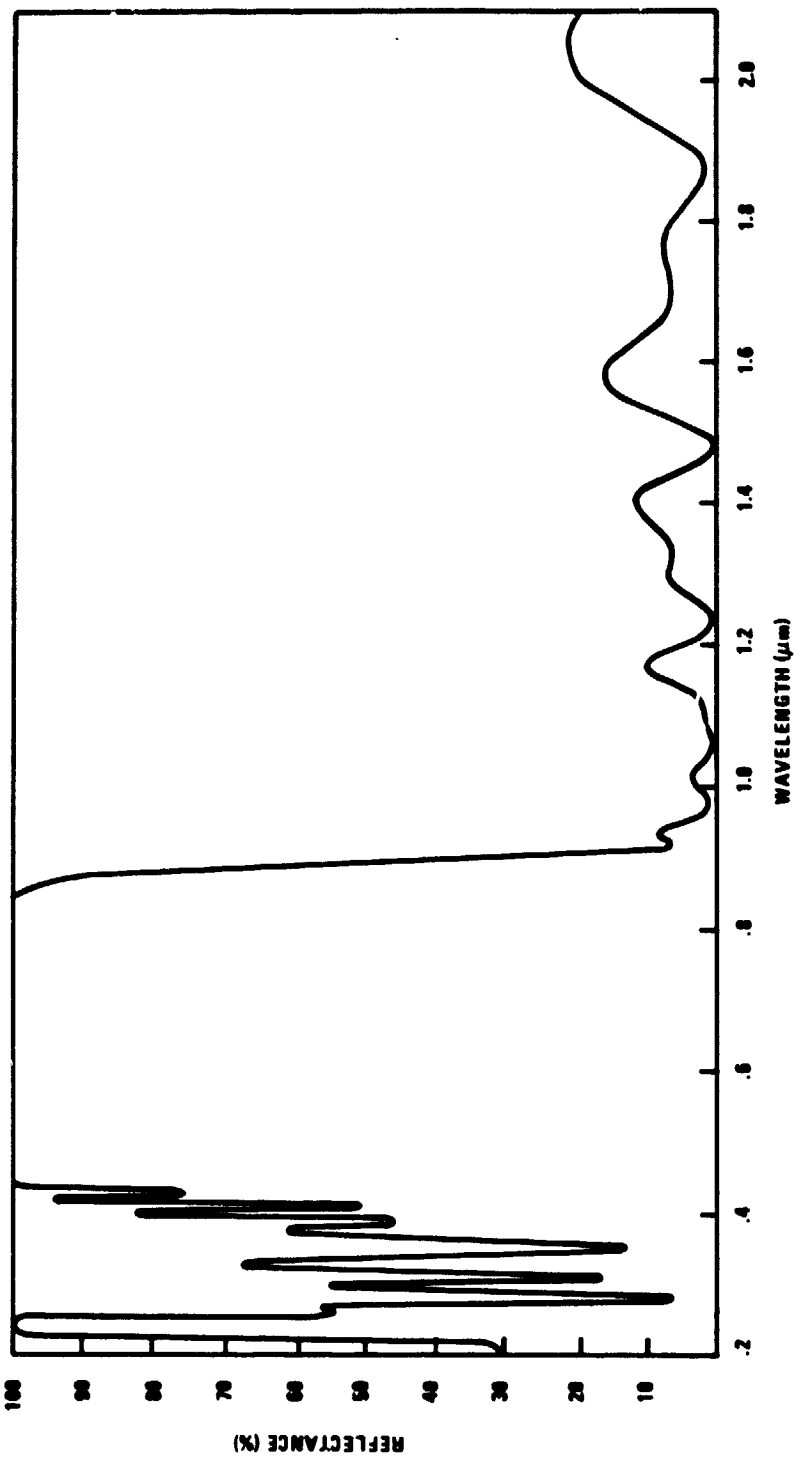

Figure 25. Computed Spectral Reflectance of a 0.3 to 0.9 μm Reflective Ta_2O_5/MgF_2 Beamsplitter (65-Layer)

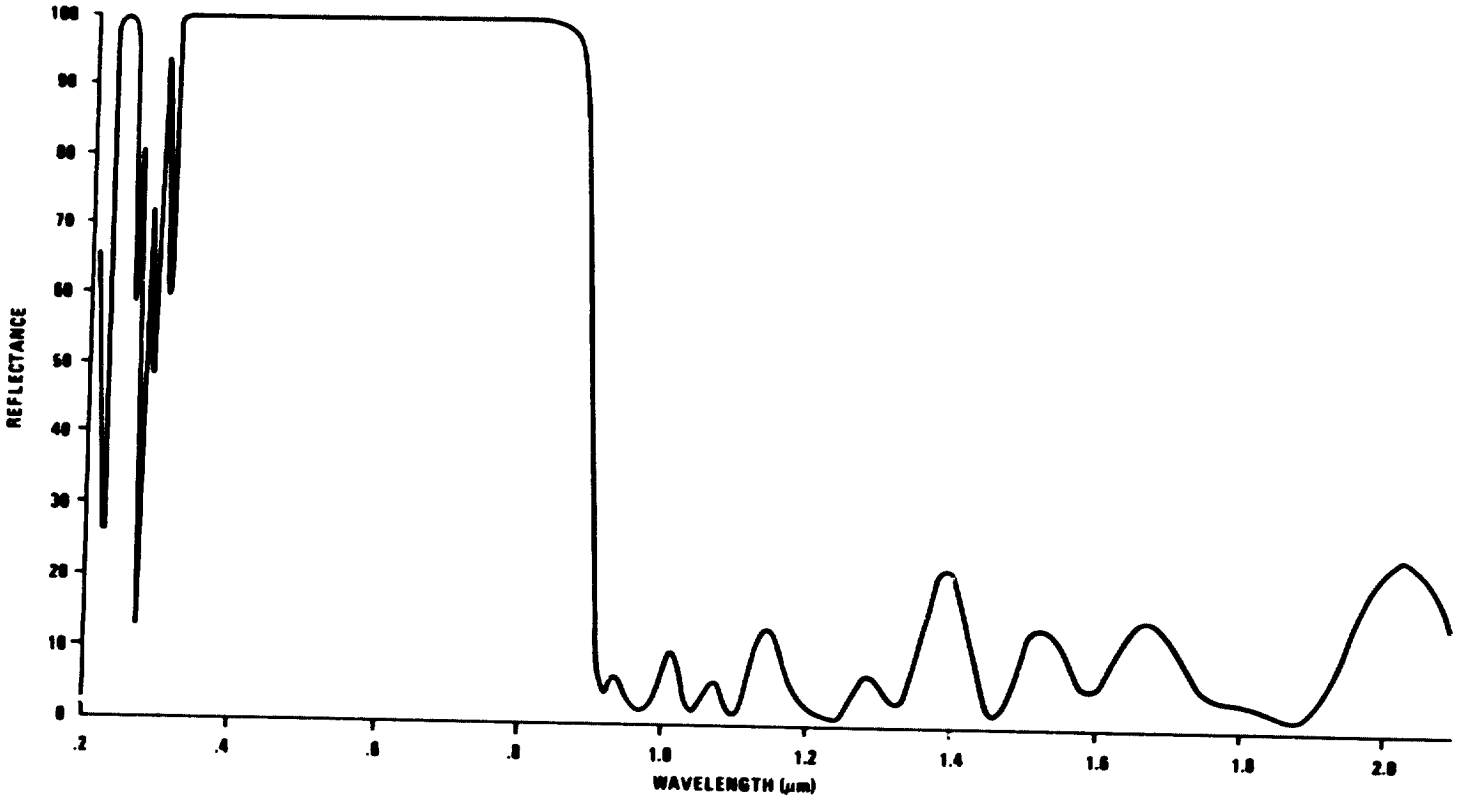

Figure 26. Computed Spectral Reflectance of a 0.3 to 0.9 μm Reflective Ta_2O_5/MgF_2 Beamsplitter (65-Layer)

The above designs were based on the spectral quantum efficiencies of the cells calculated in Phase I of this program, which show no roll-offs in the short wavelengths. Recent inquiries[1 - 9] into the performance of the S.O.A. GaAs and Si cells that would be used in the subscale model pointed out that the blue response of the GaAs cell usually cuts off around 0.43 μm, with exceptionally good cell tailing off shortly beyond 0.40 μm. The Si cells, on the other hand, seem to have better blue response than GaAs. These findings have significant impact on the beamsplitter designs which should be tailored to the actual cells that would be used. From Figure 25 the spectral response of GaAs cuts off around 0.43 μm; therefore the reflection band of the beamsplitter in the GaAs/Si configuration can be conceivably narrowed from (0.3 to 0.9 μm) to (0.43 to 0.89 μm). This would relax the number of dielectric stacks from 3 to 2 and thus favorably influence cost, manufacturability and durability of the beamsplitter without sacrificing the performance of the system. With this major modification, a 43-layer and a 35-layer Ta_2O_5/MgF_2 beamsplitter were designed. The computed spectral reflectance is shown in Figures 27 and 28, with design details given in Figures 29 and 30, respectively. The two designs are given to illustrate the tradeoffs between decreasing number of dielectric layers and system efficiency.

As the number of dielectric layers increases, the width of the reflection band increases, while the edges have increasingly sharp cut-offs. The sharp cut-off is more efficient, since more energy will be reflected to GaAs, a more efficient cell than Si. On comparison, the 35-layer beamsplitter has about 1% less reflectance from 0.8 to 0.84 μm than the 43-layer, and both have approximately the same reflection loss outside of the 0.43 to 0.89 μm reflection band. The 1% decrease in reflectance from 0.8 to 0.84 μm may not be significant, assuming a corresponding increase in transmission of the spectral energy which would be picked up by the Si cell. Thus, the 35-layer beamsplitter design may be more desirable considering lower cost, ease of fabrication, and durability.

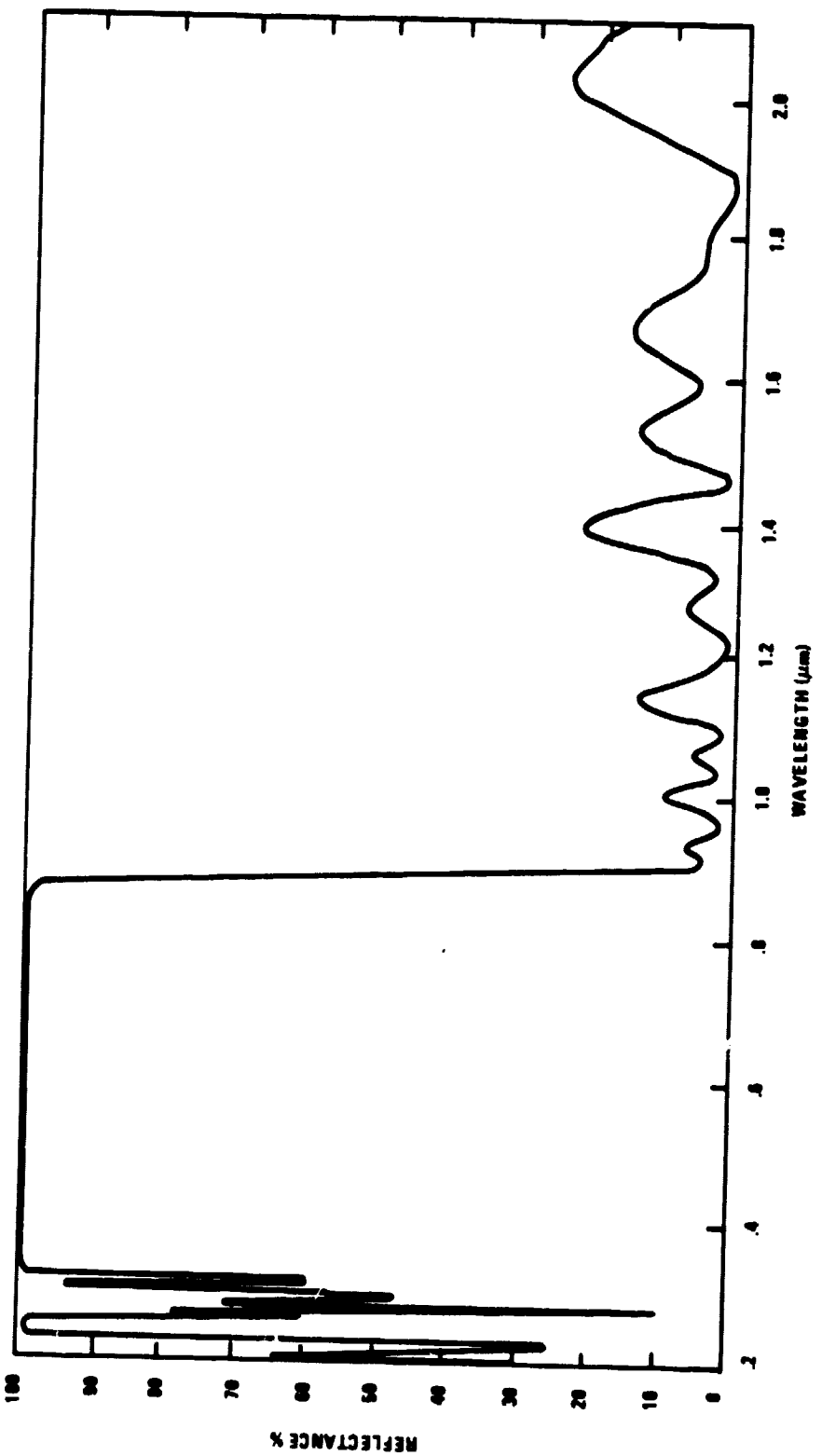

Figure 27. Computed Spectral Reflectance of a 0.43 to 0.89 μm Reflective Ta_2O_5/MgF_2 Beamsplitter (43-Layers, $\theta = 22.5^0$)

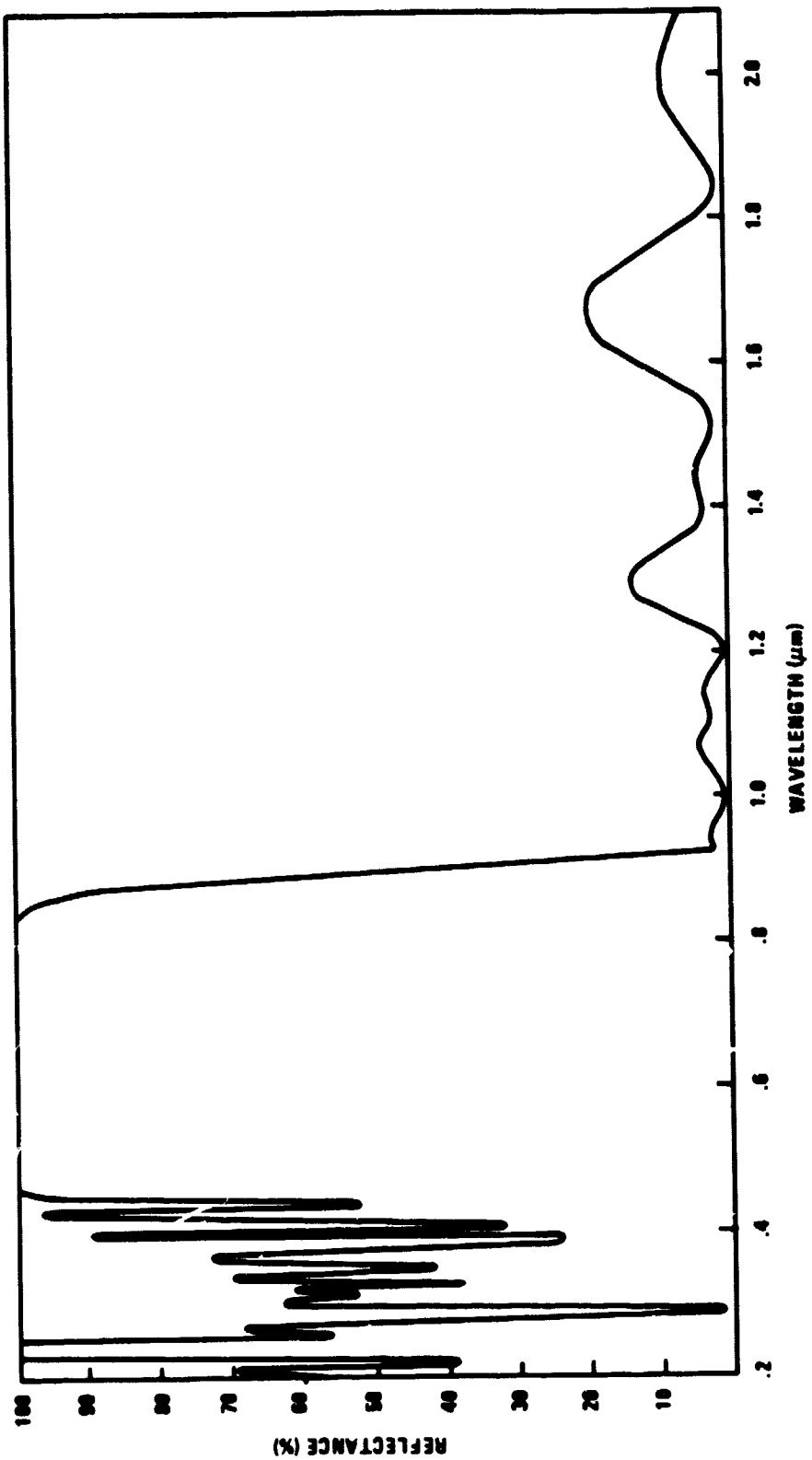

Figure 28. Computed Spectral Reflectance of a 0.43 to 0.89 μm Reflective Ta_2O_5/MgF_2 Beamsplitter (35-Layers, $\theta = 22.5°$)

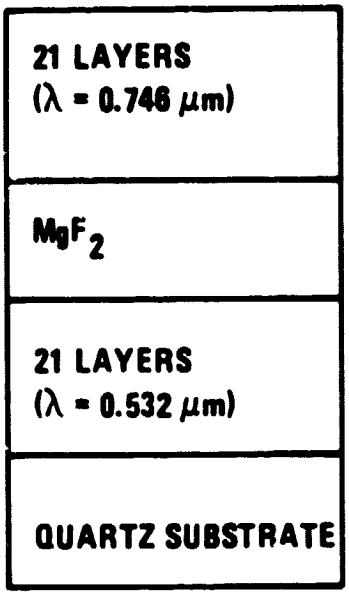

LAYERS 23 & 43: t = $\lambda/8n_H$ = 0.039 μm

LAYERS 25, 27 . . ., 41: t = $\lambda/4n_H$ = 0.077 μm

LAYERS 24, 26 . . ., 42: t = $\lambda/4n_L$ = 0.135

LAYER 22: t = 0.116 μm

LAYERS 1 & 21: t = $\lambda/8n_H$ = 0.0275 μm

LAYERS 3, 5, . . ., 19: t = $\lambda/4n_H$ = 0.055 μm

LAYERS 2, 4, . . ., 20: t = $\lambda/4n_L$ = 0.096 μm

n_s = 1.46

Figure 29. Details of the 43-Layer Ta_2O_5/MgF_2 Beamsplitter Coating Design (t = Physical thickness)

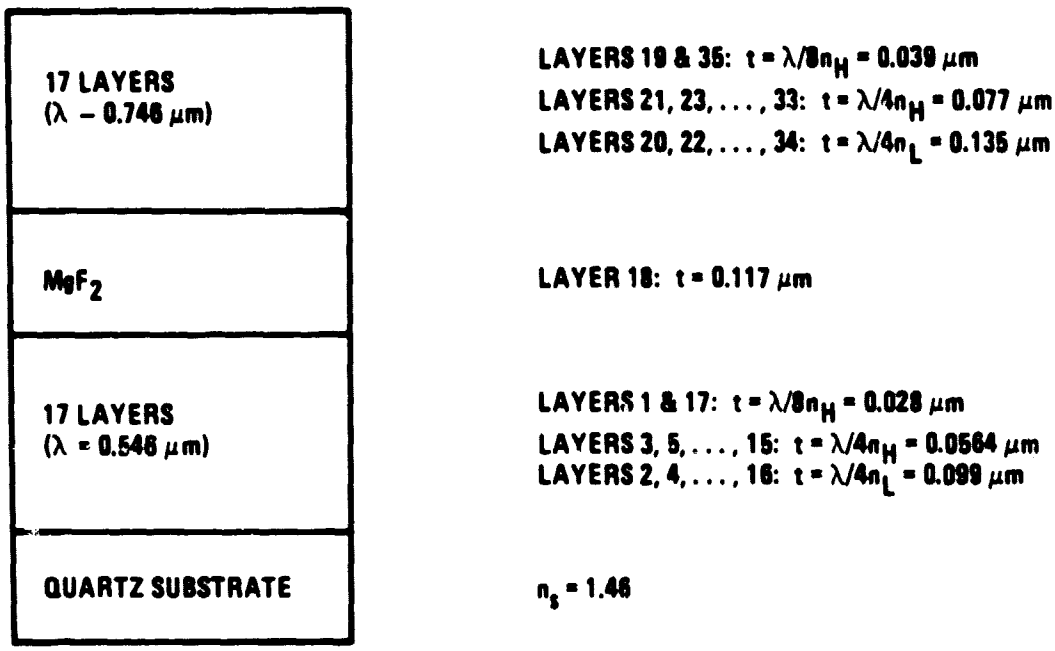

Figure 30. Details of the 35-Layer Ta_2O_5/MgF_2 Beamsplitter Coating design (t = Physical Thickness)

In the Si/GaAs configuration, our recent findings lead us to relax our requirement for wavelengths less than 0.43 μm and optimize our design near the 0.89 μm, where the sensitivity of the two cells crosses over. The beamsplitter is therefore modified accordingly. The predicted spectral reflectance of the modified 24-layer CaF_2/ThO_2 is shown in Figure 31, with design details given in Figure 32. This is compared with the previous 21-layer CaF_2/ThO_2 beamsplitter design shown in Figure 33. The 24-layer design has reduced reflection between 0.75 μm and 0.89 μm, but it has more ripples and spikes <0.43 μm.

In conclusion, in order to optimize the electrical output from the cells, the spectral response of the cells should be first measured, and then the beamsplitter be tailor-designed to maximize the system efficiency. In this phase of the program, we have designed five beamsplitters with different numbers of dielectric layers for the two different configurations of GaAs/Si and Si/GaAs--first assuming no short wavelength roll-off response of the cells, then assuming GaAs roll-offs at 0.43 μm. The final design before fabrication should depend on the cells' spectral response, especially that of GaAs, in order to maximize the efficiency of the feasibility model.

THERMAL/MECHANICAL DESIGN

Thermal Analysis and Design

Spectral energy distribution and solar cell conversion efficiencies have been calculated for the two beamsplitter and solar cell configurations. These results are shown in Table 8.

The convention adopted for calculating energy conversion efficiency for the spectrophotovoltaic concentrator system was to base the efficiency on the total flux intercepted by the primary mirror, including the central

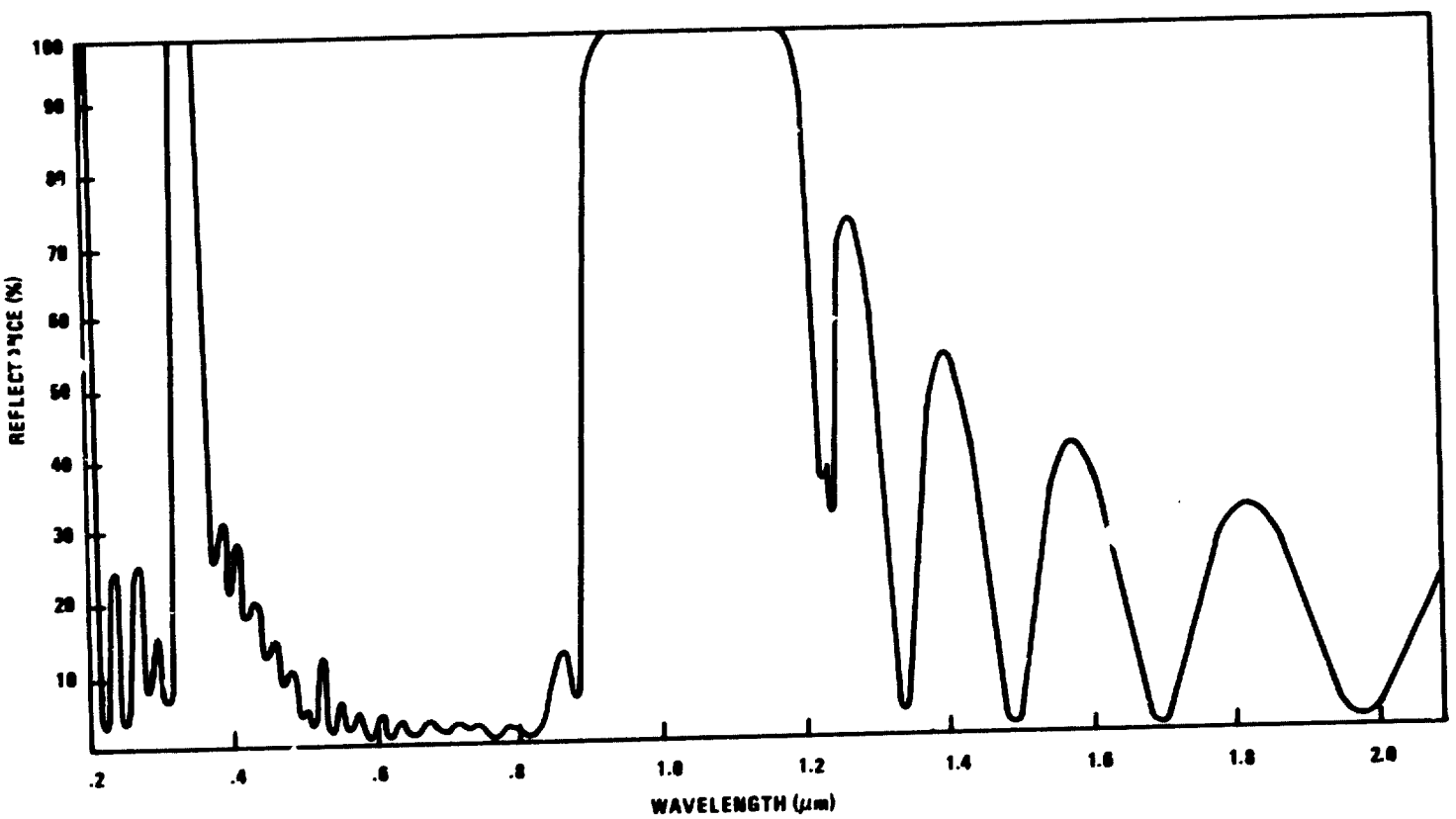

Figure 31. Computed Spectral Reflectance of a 0.89 to 1.1 μm Reflective CaF_2/ThO_2 Beamsplitter (24-Layers, $\theta = 22.5^{o}$)

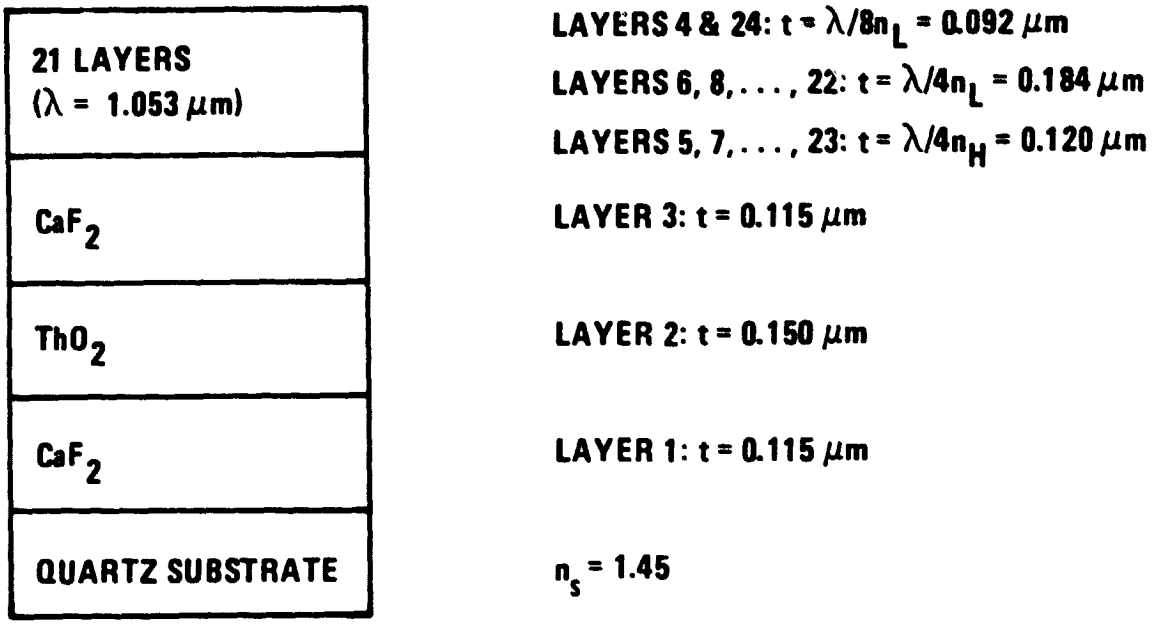

Figure 32. Details of the 24-Layer CaF_2/ThO_2 Beamsplitter Coating Design (t = Physical Thickness)

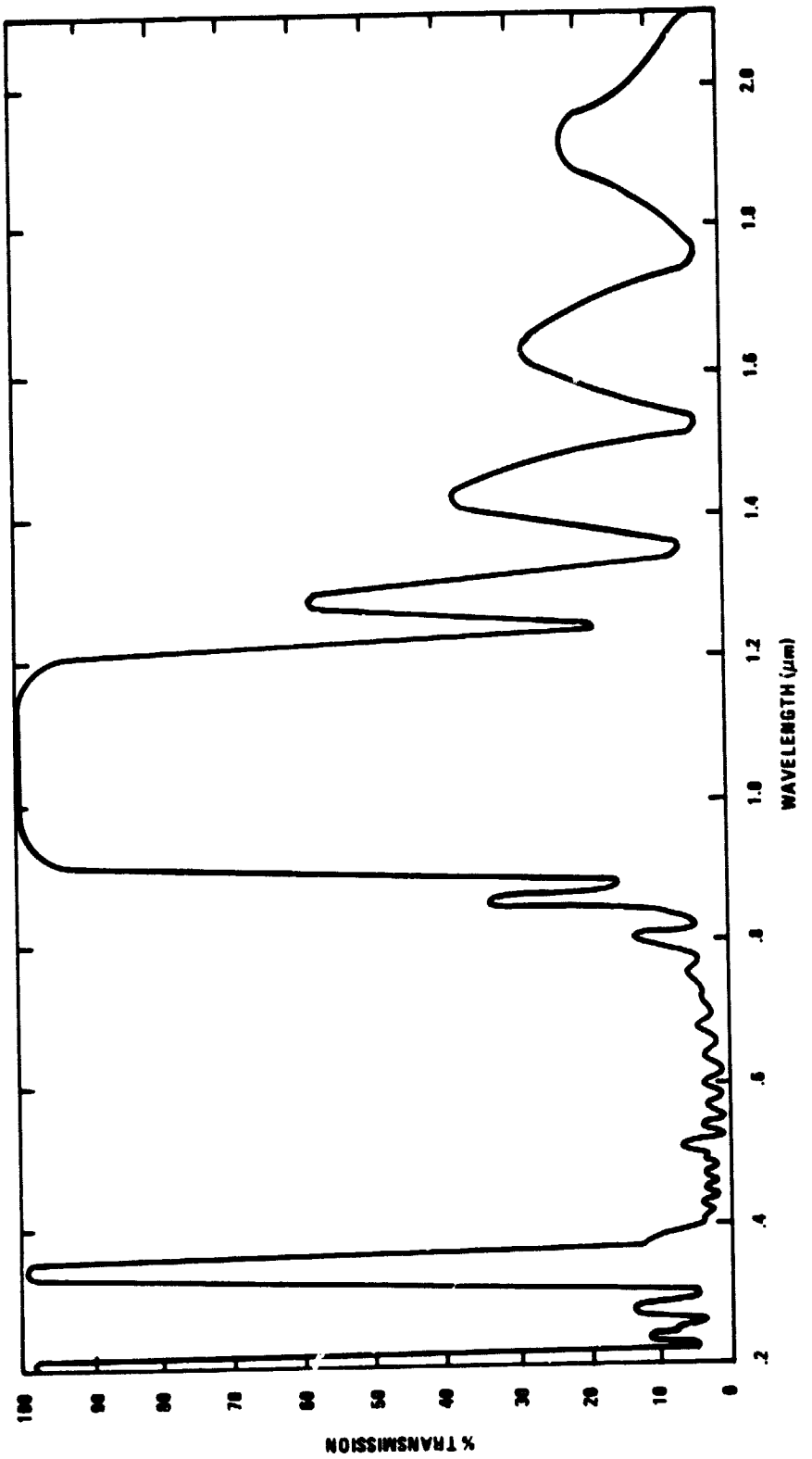

Figure 33. Computed Spectral Reflectance of a 0.89 to 1.1 μ Reflective CaF_2ThO_2 Beamsplitter (21 Layers, $\theta = 22.5^{o}$)

TABLE 8. SOLAR CONCENTRATOR COMPONENT THERMAL FLUXES

APERTURE AREA (10.0 IN DIA)		0.0507 m^2
AM2 SOLAR FLUX (0.3 TO 4.0 μm)		798.10 W/cm^2
INTERCEPTED FLUX		40.46 W
OBSCURATION LOSS	(10.1%)	4.09 W
PRIMARY MIRROR LOSS	(5.0%)	1.82 W
SECONDARY MIRROR LOSS	(5.0%)	1.73 W
NET FLUX TO BEAMSPLITTER		32.83 W

		SYSTEM #1		SYSTEM #2	
	UNITS	GaAs	Si	GaAs	Si
REFLECTED BAND	μm	0.3 TO 0.9			0.9 TO 1.1
TRANSMITTED BAND	μm		0.9 TO 2.5	0.3 TO 0.9 1.1 TO 2.5	
REFLECTION COEFFICIENT	–	0.99			0.99
TRANSMISSION COEFFICIENT	–		0.90	0.90	
REFLECTED ENERGY	W	21.95			3.70
TRANSMITTED ENERGY	W		9.26	25.85	
ABSORBED + SCATTER AT BEAMSPLITTER	W		1.62	3.28	
FLUX TO SOLAR CELLS	W	20.85	8.80	23.27	3.52
GRID REFLECTION (10%)	W	2.09	0.88	2.33	0.35
AR COATING LOSS (5%)	W	0.94	0.40	1.05	0.16
NET FLUX ON CELLS	W	17.83	7.52	19.90	3.01
NET IN-BAND FLUX	W	17.83	2.73	15.36	3.01
CELL ABSORPTION COEFFICIENT		0.957	0.614	0.957	0.614
ABSORBED ENERGY	W	17.06	1.68	14.70	1.85
THERMAL CONVERSION COEFFICIENT		0.346	0.057	0.346	0.057
HEAT GENERATED	W	5.90	0.096	5.09	0.11
ELECTRIC ENERGY OUTPUT	W	8.60	0.94	7.41	1.03
RERADIATED ENERGY	W	2.56	0.64	2.20	0.71
REFLECTED + RERADIATED ENERGY	W	6.36	7.76	10.77	2.38
ENERGY ABSORBED AT CPC (5%)	W	1.42	0.85	1.83	0.30
CONVERSION EFFICIENCY	%	21.3	2.3	18.3	2.6
TOTAL ELECTRIC CONVERSION EFF.	%	23.6		20.9	

obscuration. This results in conversion efficiencies which are lower than expected if compared to single cell performance, but more realistically include concentrator optical losses.

The cutoff wavelength for GaAs is 0.9 microns. Shorter wavelengths are directed to the GaAs cell, while longer wavelengths are directed to the Si solar cell. The spectral energy distribution tabulated was calculated assuming a beamsplitter spectral reflectance of 99% and a 90% spectral transmission. The remaining energy was absorbed in the beamsplitter coatings or scattered out of the concentrated beam.

The conversion efficiency of the GaAs and Si cells are calculated values using the models and equations provided in the Phase I final report. Included in the efficiency calculations are all of the concentrator reflection losses (α = 0.95), beamsplitter losses, grid shadowing and anti-reflection coating losses. The calculations indicate a system conversion efficiency of 23.6% can be obtained for GaAs/Si, and 20.9% for Si/GaAs configurations. Correction for short wavelength cutoff for the solar cells at 0.43 μm has lowered the respective efficiencies to 21.48% and 20.11%. For AMO conditions, the efficiencies are 17.41% and 16.21% respectively.

Concentrating photovoltaic systems produce high thermal fluxes which must be accounted for in the system design. The primary mirror has concentration of unity and therefore requires no cooling. The secondary mirror sees a concentration of approximately 10:1, but its absorptance is only 5%. By increasing its long wavelength emittance with selective coatings or blackening the back side and shading it from direct sunlight, its temperature can be controlled. Table 9 tabulates the heat absorption associated with each of the critical components in the concentrator system.

TABLE 9. COMPONENT THERMAL REJECTION REQUIREMENTS

POWER AT BEAM SPLITTER	**32.8 W**
POWER DENSITY	**8.0 W/cm^2**

	THERMAL ENERGY ABSORBED (GaAs/Si CONFIGURATION)	THERMAL ENERGY ABSORBED (Si/GaAs CONFIGURATION)
GaAs CELL	**5.90 W**	**5.09 W**
CPC	**1.42 W**	**1.83 W**
Si CELL	**0.10 W**	**0.11 W**
CPC	**0.85 W**	**0.30 W**
TOTAL	**8.27 W**	**8.33 W**

The absorption of the beamsplitter directly affects its equilibrium temperature. If the absoprtance is 1% and the long-wave emittance is 0.5 for each surface, the equilibrium temperature would reach 390K. A 2% absorptance coating would result in a 440K beamsplitter temperature. During terrestrial testing, convection will limit the temperature rise to a very small amount.

Thermal energy absorbed by the solar cells and CPC's requires auxiliary cooling and is of sufficient magnitude to be measured. The heat fluxes are tabulated in Table 9 for the two configurations. The results show that cooling of the GaAs cell is far more critical than any other component in the system.

The measurement of CPC and solar cell temperature and heat flux will be performed using the insulated support shown in Figure 34. The CPC and solar cell will be supported in a metal-jacketed, polyurethane foam-insulated box. Cooling will be provided by conduction through 1/4 diameter copper rods attached to a water-cooled heat sink. Heat flux will be inferred from the measured temperature gradient in the cooling rods.

The table included in Figure 34 provides the conductivity data, the sensitivity, and an estimate of the heat loss through the insulation. A major uncertainty will be the amount of convective cooling that will occur. This effect can be minimized by operating the system with the CPC and solar cell temperature at, or slightly below, ambient air temperature

Mechanical Design

The basic system layout and all mechanical shop drawings are completed.

The system optical layout is shown in Figure 35. This drawing provides the critical dimensions of all optical components and their relative placement.

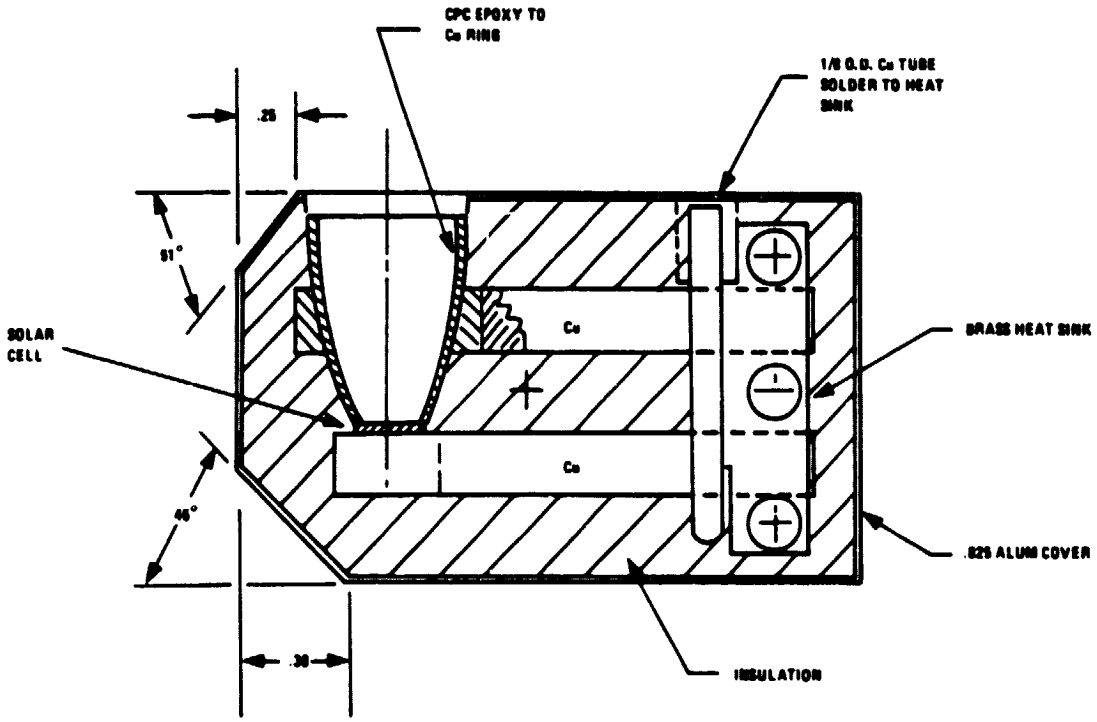

HEAT FLUX	**1 TO 6 W**
CONDUCTANCE	**0.17 W/°C**
SENSITIVITY (Cu/CONST THERMOCOUPLES)	**240 μ V/W**
CONDUCTIVE HEAT LOSS	**~ 3 mW/°C**

Figure 34. Thermal Measurements Sensitivity

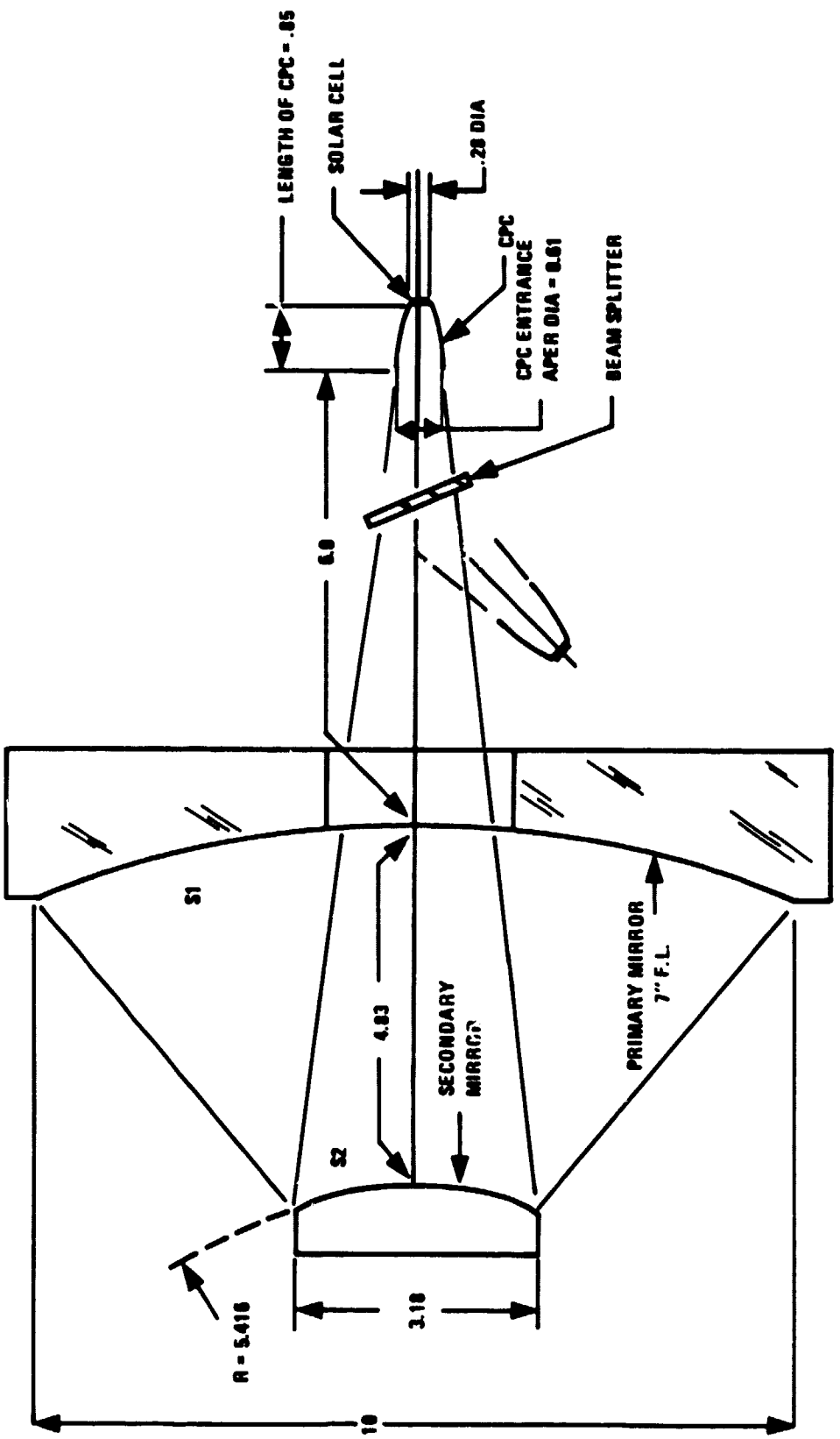

Figure 35. Solar Concentrator Optical Layout

The mechanical support of these components is shown in Figure 36 The mainframe for the telescope is a half-inch-thick aluminum plate. The primary mirror is supported by a collar and sleeve passing through the central hole and attached to the mainframe. Resilient spacers compensate for differences in thermal expansion while maintaining alignment accuracy. This type of mount will work equally well for either glass or metal mirrors.

The secondary mirror is bonded to a metal block suspended by a conventional three-armed spider mount. Radial, axial and tilt adjustment of the secondary mirror is performed with adjustable blocks located at the ends of each spider arm.

The beamsplitter and the CPC's are mounted in an enclosure attached to the back of the mainframe. The bottom and sides of the enclosure are aluminum plate, and the top and back sides are plexiglas. The enclosure will reduce dust contamination of the optics as well as convective heat loss effects from the CPC's and solar cells. The plexiglas covers will permit visual inspections of the tracking accuracy and inspection of internal electrical and coolant connections.

A front dust cover will be provided to protect the optical surfaces when the system is not in use.

Figure 37 shows a rear view of the telescope. The CPC enclosures are mounted on stand-off collars bolted to the bottom plate. Sufficient clearance is provided to allow $\pm$0.25 inches of horizontal movement. Vertical adjustment and tilt will be provided with shims placed between the collar and the CPC mounts.

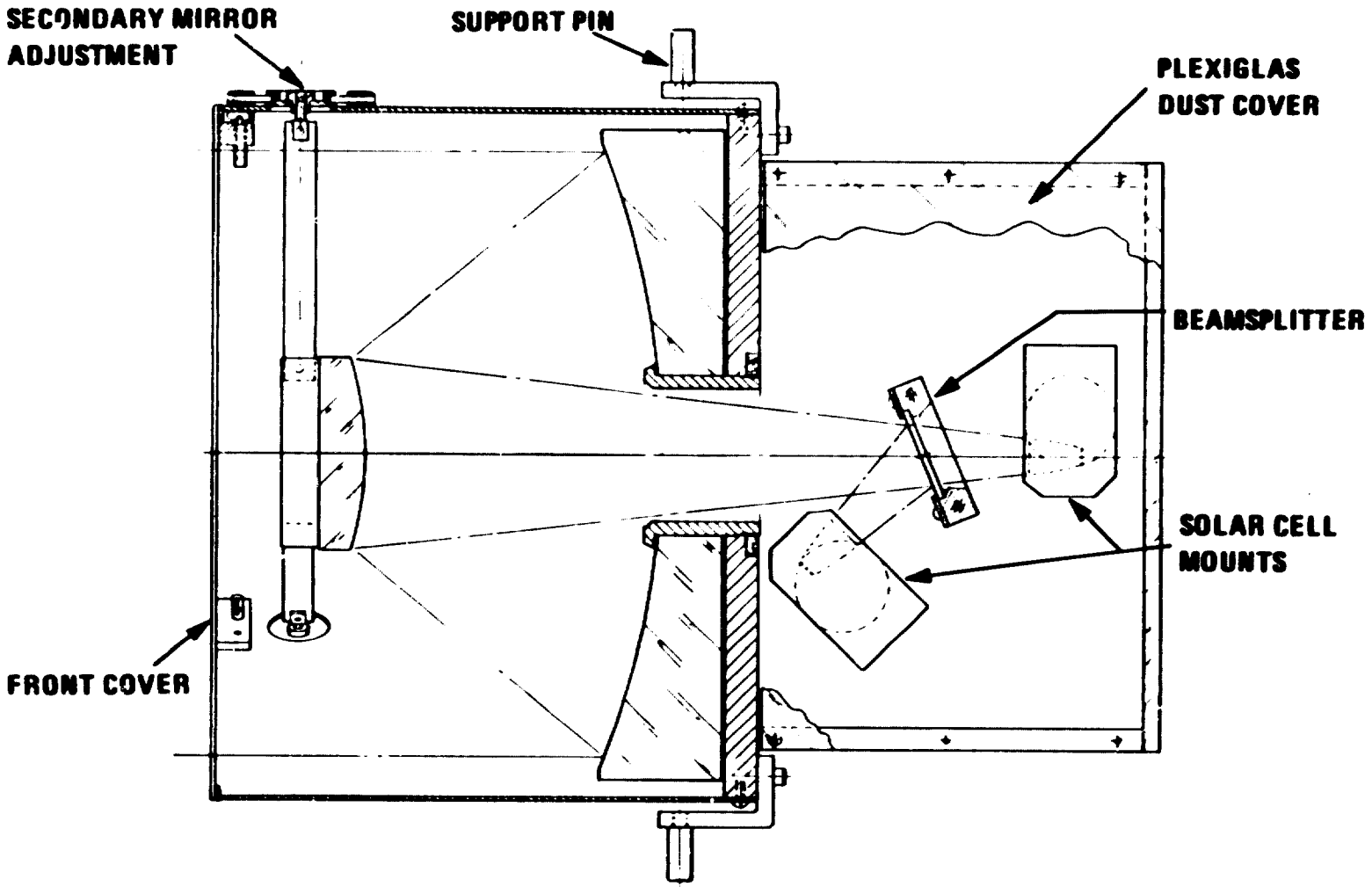

Figure 36. Mechanical Support Cross Section

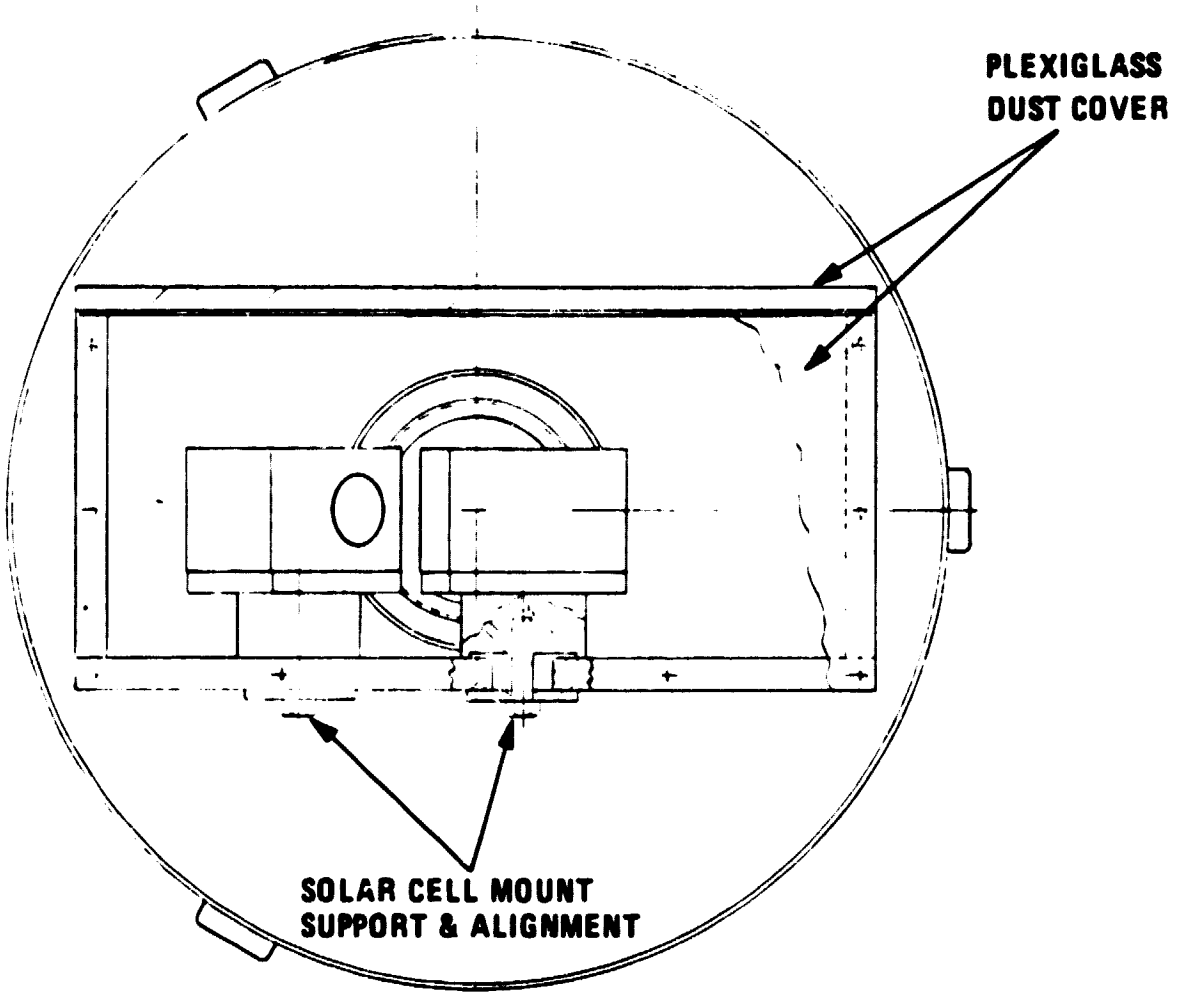

Figure 37. Solar Concentrator Rear View

Figure 38 shows a front aperture view of the solar concentrating telescope. The secondary mirror and spider provide approximately 10% obstruction of the primary mirror. Not shown in this view or in Figure 37 are the mounting pins which will be placed on each side of the telescope so that their axis passes through the system's center of gravity. Their exact location will be calculated when the final bid is received from the mirror fabricators. The weights and mass locations of all of the metal and plastic components are readily calculated, but the final thickness and material for the two mirrors may vary considerably.

The subscale test model can easily be accommodated by an amateur telescope mount. The weight of the telescope may be slightly greater than most mounts are designed to accommodate, but the compact design has a very low radius of gyration. This, coupled with the low tracking precision requirements compared to astronomical measurements, makes an amateur telescope mount and drive an ideal support system. Figure 39 is an artist's conception of the subscale test model on a pedestal mount with a clock motor drive system.

MODEL COST

Only the component cost is detailed in this section. The suppliers for the components are identified and listed in Table 10. Budgeting quotes from vendors and in-house fabrication cost through price is summarized in Table 11.

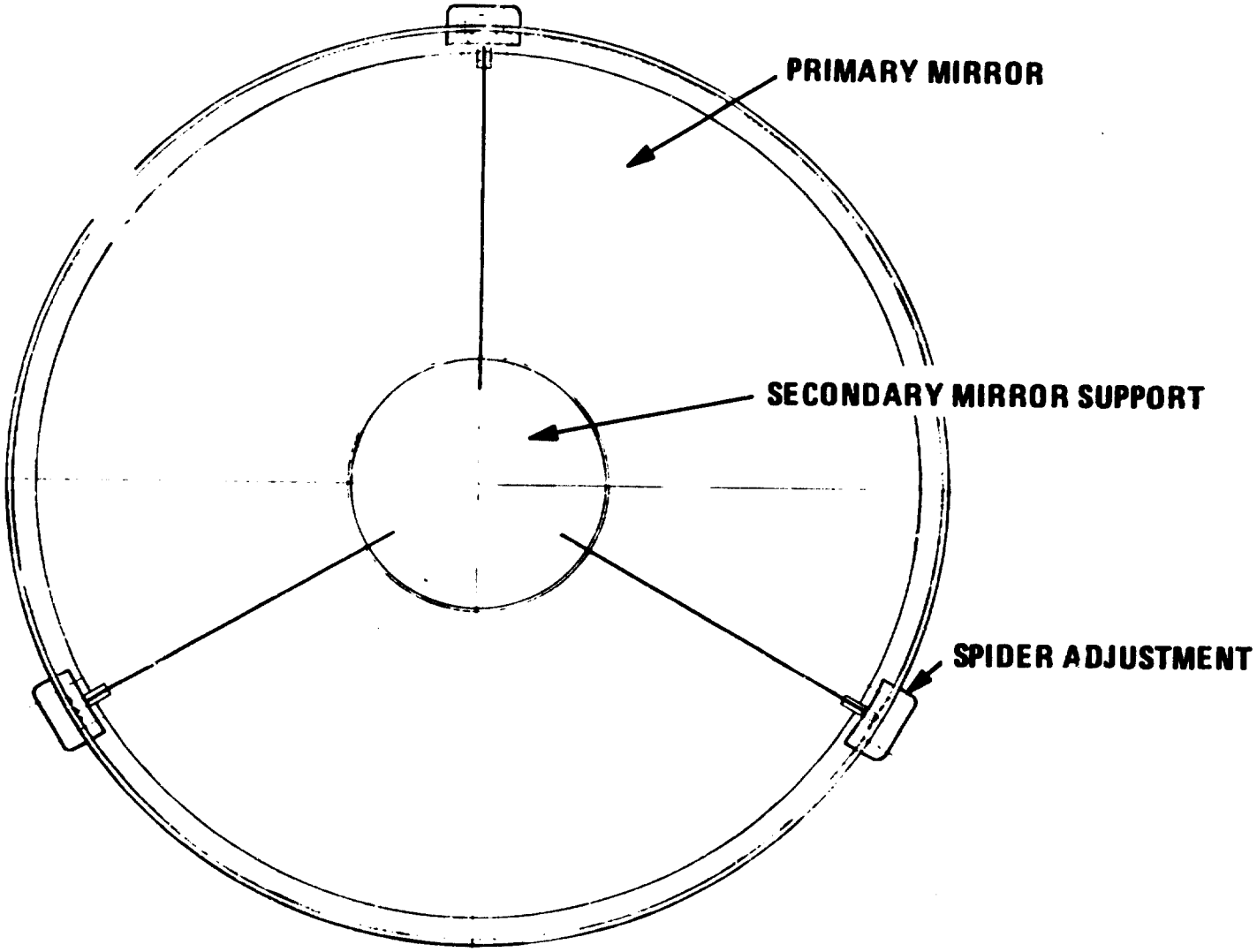

Figure 38. Solar Concentrator Front View

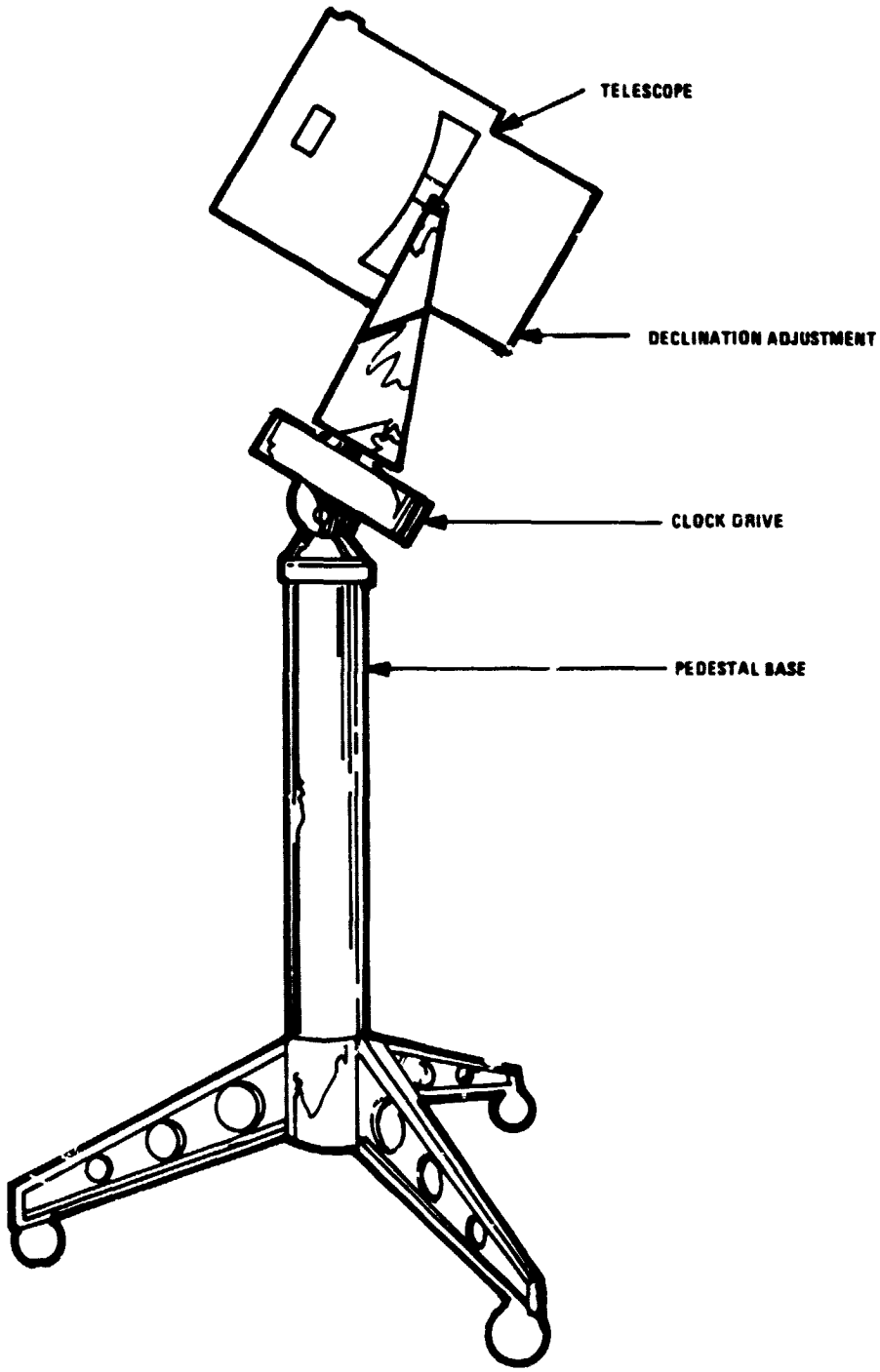

Figure 39. Telescope Drive and Support

TABLE 10. SUPPLIERS FOR MODEL COMPONENTS

1. SOLAR CELLS	
GaAs (CONCENTRATOR CELL)	• VARIAN ASSOCIATES • ROCKWELL INTERNATIONAL
Si (CONCENTRATOR CELL)	• VARIAN ASSOCIATES
2. OPTICS	
PRIMARY MIRROR	• PNEUMO PRECISION INC./ BELL & HOWELL (DIAMOND TURNING)
SECONDARY	• PNEUMO PRECISION INC./ BELL & HOWELL (DIAMOND TURNING) • SPECIAL OPTICS CO. (CONVENTIONAL)
CPC	• OPTICAL RADIATION CORP. (ELECTROFORM)
BEAM SPLITTER	• OPTICAL COATING LAB INC./ IN-HOUSE
3. THERMAL/MECHANICAL	
TELESCOPE SUPPORT STRUCTURE	• IN-HOUSE
COOLING FIXTURES	• IN-HOUSE
MOUNT AND TRACK STRUCTURE	• EDMUND SCIENTIFIC

TABLE 11. COMPONENT COSTS OF SUBSCALE MODEL

COST ITEMS	COST THROUGH PRICE $K
1. SOLAR CELLS	
4 CONCENTRATOR CELLS (VARIAN)	2.8
2" x 2" PLANAR Si CELL	0.1
2. OPTICS	
PRIMARY MIRROR SECONDARY MIRROR	7.0
CPC'S	2.3
BEAMSPLITTER	19.9
3. THERMAL/MECHANICAL	
TELESCOPE MAIN FRAME AND FIXTURES	15.0
MOUNT AND TRACK STRUCTURE	1.1
TOTAL COST	48.2

SECTION 3

MODEL TESTING PLAN

The test plan consists of a component feasibility demonstration and a system performance demonstration. The objective of component testing is to ascertain that each component does meet the performance goals specified in the design so that the overall system efficiency of ~20% can be achieved under AM2 conditions (Table 12). The uncertain component performances are the solar cells' spectral quantum efficiency, the properties of the beamsplitter, and the efficiency of the cooling system in maintaining the cells at a constant temperature. These quantities can be easily measured in the laboratory, where the system performance can be more accurately predicted. The measured spectral efficiency of the solar cells will also serve as a final design specification for the custom-made beamsplitters. The objective of system testing is to show the high conversion efficiency of the concept and the hardware feasibility of the design.

It is planned that testing will be done first in the laboratory, then in the field. The advantage of laboratory simulator testing is having a reproducible and spectrally agile source; that is, AM0 and AM2 spectra can be simulated. However, the disadvantages are having to modify and reactivate a simulator presently in storage, as well as being unable to produce a $\pm 1/2^{o}$ divergence beam with full sun intensity. Thus, to maintain the divergence within the acceptance angle, the system could only be tested at a reduced intensity (~1/10 sun). The consequences would be insufficient stress to really test the hardware feasibility of the system components and the even less reliable thermal data to project to the full-scale system. Therefore, laboratory testing of the system should be followed by field testing to overcome these difficulties. The advantage of field testing is in the availability of the source; however, the terrestrial solar spectrum varies widely in both spectral distribution

TABLE 12. PERFORMANCE GOALS OF COMPONENTS AND SYSTEM

SYSTEMS COMPONENTS		EFFICIENCY GOAL
OPTICS	OBSCURATION	90%
	REFLECTION PER SURFACE	> 95%
BEAMSPLITTER	REFLECTION BAND	99%
	TRANSMISSION BAND	95%
	ABSORPTION	< 1% (LOSS)
SOLAR CELLS	AlGaAs (1.65 eV – 2.8 eV)	> 50%
	Si (1.2 eV – 1.65 eV)	> 50%
HEAT REJECTION	AlGaAs CELL	> 95%
	Si CELL	> 95%
GaAs/Si	AM0	17.4%+
	AM2	21.5%+
Si/GaAs	AM0	16.2%+
	AM2	20.1%+

+ OVERALL SYSTEM EFFICIENCY NORMALIZED TO INTERCEPTED FLUX AT THE PRIMARY MIRROR

and energy content. These variations require close monitoring of the solar spectrum simultaneously with measuring the electrical output of the concentrator cells. A summary of the test plan is displayed in Table 13, while details of the test plan are given below.

COMPONENT DEMONSTRATION

Solar Cell Test Plan

The parameters of interest are the maximum power output and the spectral efficiency of the cell as a function of spectral flux density and cell temperature.

From the I-V plot, the open circuit voltage, short circuit current, and maximum power output, fill factor can be obtained. An electrical circuit is designed which will directly measure the maximum power output, as shown in Figure 40. Another approach is to manually trace the I-V characteristic using a 577 curve tracer to drive load 2N3055, and compute the maximum power from the I-V trace. The latter is more laborious, but will yield more information on the cells. The spectral flux density should be known or calibrated. The standard source is a Xenon lamp or a tungsten-halogen lamp. The spectral distribution of these lamps can easily be measured by a spectrometer. The flash Xenon lamp is known to produce up to ~400 suns' intensity, and a special cavity tungsten lamp up to 50 suns is available.

Absolute spectral efficiency of the cells is crucial for the optimum design of the beamsplitter and for predicting system performance. This information can be obtained by illuminating the cells with a calibrated continuous scanning monochromatic source.

The temperature at which the concentrator cell will be operating will determine the efficiency of the cell. It is important that the temperature be stable and kept as low as possible. For low intensity testing, a 300^{o}K

TABLE 13. TESTING PLAN

COMPONENTS	INFORMATION
OPTICAL, MIRRORS CPC	• REFLECTANCE, • SURFACE PROFILES • C.R. (EACH STAGE)
BEAM SPLITTER	• REFLECTION CHARACTERISTICS • THERMAL ENDURANCE (TEMP. CYCLING AND THERMAL SHOCKS) • UV RESISTANCE • TRANSMISSION
SOLAR CELLS	• SPECTRAL QUANTUM EFFICIENCY • I-V CHARACTERISTICS vs. INTENSITY • I-V CHARACTERISTICS vs. CELL TEMP.
THERMAL MONITOR	• CALIBRATION
INTEGRATED SYSTEM	• ELECTRICAL OUTPUT vs. INPUT FLUX (INTENSITY, SPECTRUM) • THERMAL OUTPUT vs. INPUT FLUX

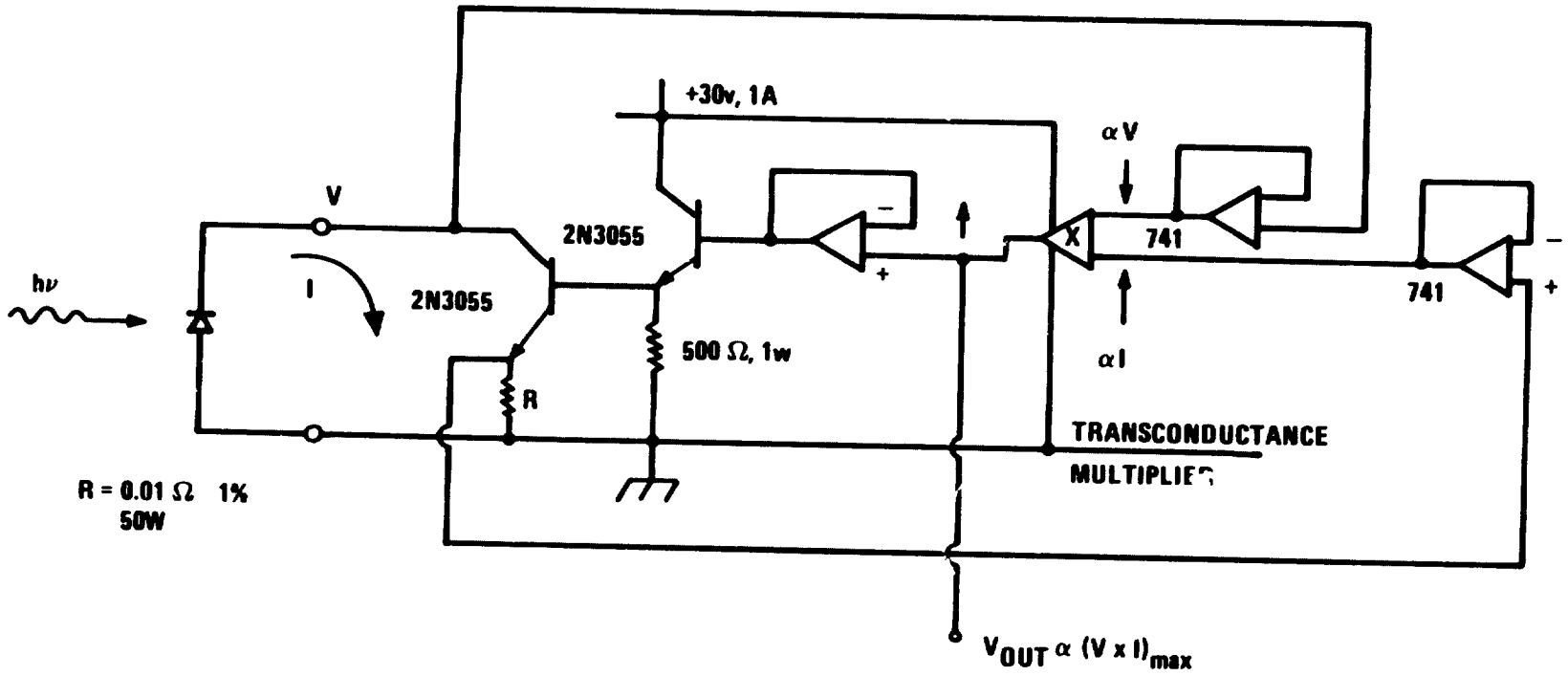

Figure 40. Circuit Design for Directly Measuring Maximum Power Output from a Solar Cell

cell temperature will not be a problem; however, in the concentrator the cooling system has to remove 15-30 watts continuously in order to maintain room temperature operation of the cells.

Optical Component Test Plan

This test plan details the specific tests to be performed on each optical component for the subscale model solar concentration system. These components consist of the primary and secondary mirrors of the Cassegrain telescope, and the compound parabolic concentrators. Each component's performance will be tested and characterized before system integration to ensure proper manufacture and performance of the element. Upon completion of the component tests, the system will be assembled and tested in a laboratory environment to ensure proper alignment and performance of the entire system. Once the preliminary system testing is completed and demonstrates adequate concentration performance, then actual laboratory solar simulation testing and/or field testing can be performed. The detailed component tests are given below.

Primary Mirror--The standard optical surface tests usually applied to concave mirrors are knife-edge shape measurements or interferometric profile measurements. Examples of these testing configurations are shown in Figure 41. The knife-edge testing of Figure 41(a) can take many forms, but all measure the slope errors of the surface under test. These slope errors are then used to determine the corresponding zonal profile surface errors. Surface profile errors are measured directly with an interferometer, as shown in Figure 41(b). Interference of the returning aberrated wavefront and a reference sphere within the interferometer produce characteristic interference fringes. In the double-pass arrangement of Figure 41(b), each interference fringe would measure a surface departure of $\lambda/4$ of the test surface.

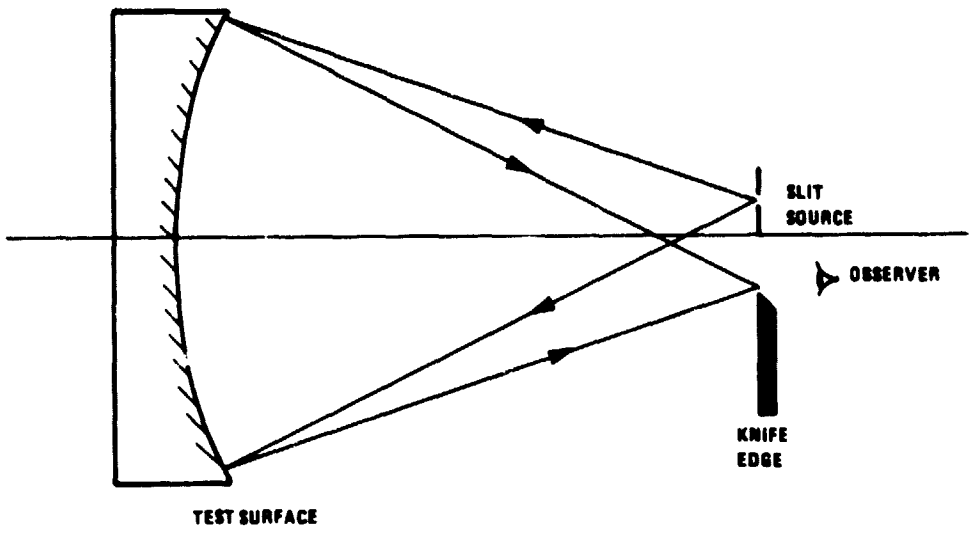

(A) KNIFE-EDGE SLOPE TESTING

a. Knife-Edge Slope Testing

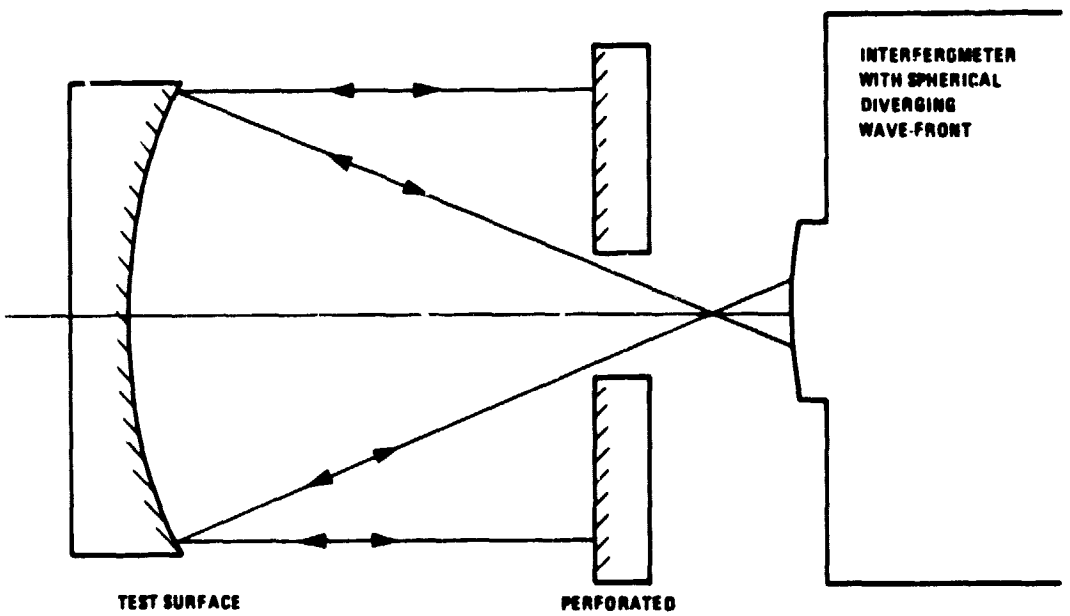

(B) INTERFEROMETRIC PROFILE TESTING

b. Interferometric Profile Testing

Figure 41. Standard Optical Surface Tests for Primary Mirror

The strongly curved primary mirror (f/0.7) will require some modifications to both of the Figure 41 tests. The knife-edge test will need a parallax-free beamsplitter arrangement to place the source and return image (at the knife-edge) coincident, or else a severe off-axis testing arrangement will result. If the primary is paraboloidal, then a double-pass test at the focus of the paraboloid, using a reference flat, will need to be used for a null test. A spherical primary would use a test at the radius of curvature, as depicted in Figure 41(a). Ellipsoidal primaries can be tested by positioning the source at one foci and the knife-edge at the other. Since the slope errors are likely to be substantial (since the allowable surface profile errors are many waves, based on the tolerance analysis), the test can be desensitized to advantage by the use of multiple knife-edge coarse frequency Ronchi rulings as replacements for the knife-edge. The Moire fringes produced by beating the master grating with the return aberrated image of the master grating allow gross slope errors to be measured more easily than a standard knife-edge. This test would be especially useful during the actual fabrication of the element.

Interferometric testing might prove to be too sensitive a test if the surface shape is not paraboloidal or departs too far from a paraboloid. It is likely that too many finely spaced interference fringes will be produced to adequately characterize the shape of the element. Certainly this will be the case if conventional grinding and polishing methods are used to generate the f/0.7 paraboloid. If the nominal surface profile of the primary is not paraboloidal, then the testing arrangement of Figure 41(b) cannot be used, and tests other than interferometry must be used.

A test method likely to be used is a relatively simple profilometer scanned across a diameter, thus producing a direct mechanical measurement of the surface sag. This is typically done in diamond-turning such surface profiles (although non-contact laser profilometers are also used to measure the surface profile and control the cutting). This test is also adaptable

to conventional grinding and polishing operations. Since a sag envelope was developed in the tolerance analysis task of this program, it is a simple matter to compare the nominal sags with those measured to determine if the, lie within the envelope. In addition, a simple qualitative knife-edge test could also be used to ensure that a smooth profile exists on the actual surface. The combination of a smooth surface profile and sags within the tolerance envelope will adequately characterize the surface of the primary.

One advantage of a profilometer measurement scheme is that the measured sag values are easily analyzed with an advanced profile-fitting algorithm we have developed in other programs. This computer program would be used to find the best-fit aspheric profile for the measured surface, and output the curvature, conic constant, and fourth-to-tenth-order deformation coefficients in the standard raytrace format. Thus, subsequent raytracing could be performed on the actual measured profile to determine optimum alignment characteristics and overall system performance.

In addition to the quantitative tests described above, a simple qualitative test can be performed by looking at the image blur for either a collimated bundle or an extended source. For example, in the case of an ext ed source such as the sun (or moon), the blur diameter can be easily measured at the focus of the mirror. Knowing that the secondary (if made perfect) will magnify this image by a factor of 5, we can quickly determine if the blur is too large to eventually be fielded by the CPC in the actual system.

Secondary Mirror--The standard tests for the secondary mirror are shown in Figure 42. Basically, one matches the foci of the particular secondary with the source and center of curvature of the sphere to produce a null wavefront. Depending on the conic to be tested, the arrangement could require the of an auxiliary focusing/collimating lens of good quality. Either a knife-edge test or standard interferometry can be used to analyze the return wavefront from any of the configurations shown in Figure 42.

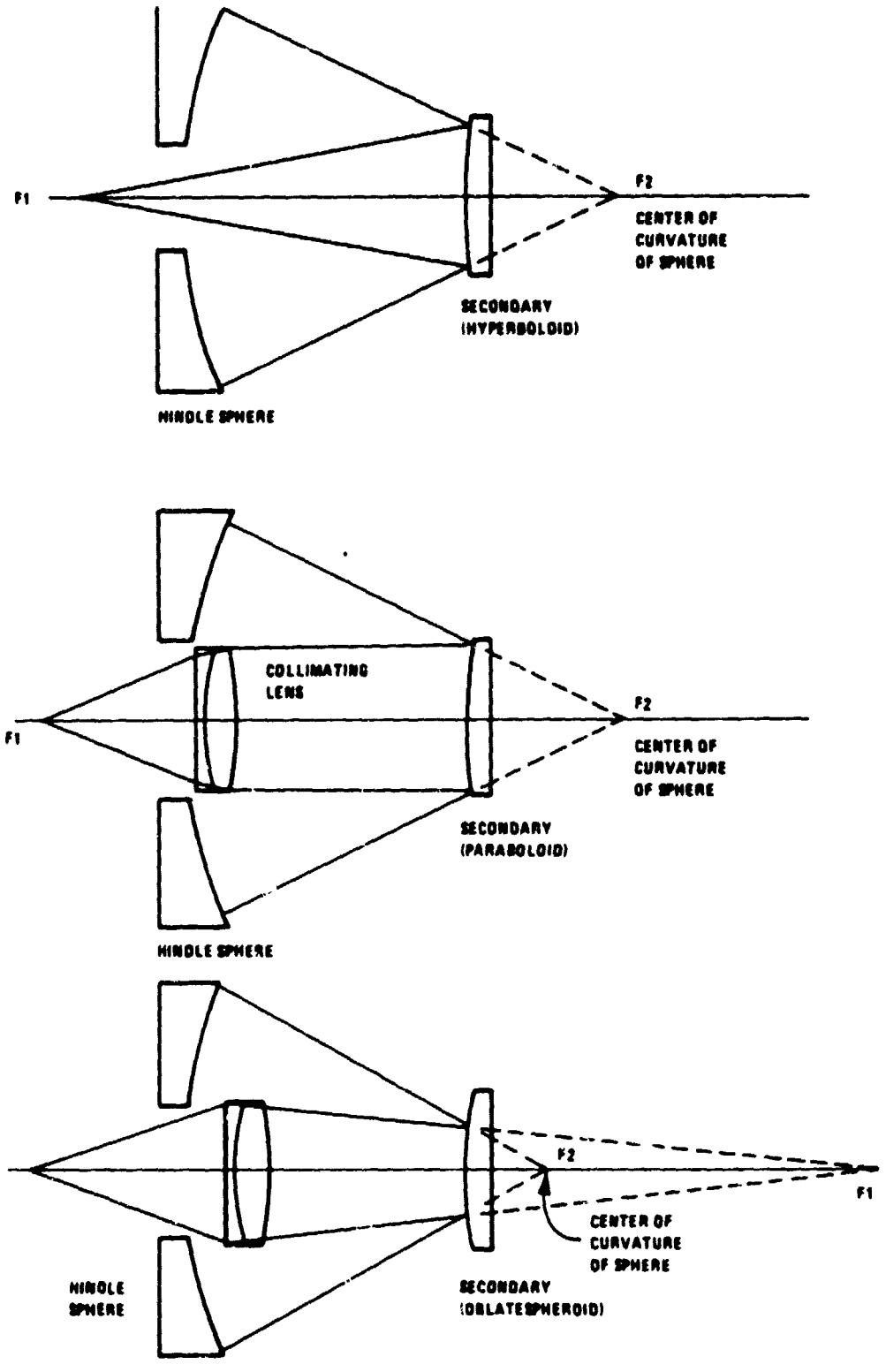

Figure 42. Hindle Sphere Tests for Secondary Mirrors

Quite likely, a coarse Ronchi grating will be used to desensitize the test, since the secondary tolerance envelope will allow substantial departures from the nominal profile.

Should the secondary be diamond-machined, its surface profile could then be measured automatically, or perhaps with the aid of a profilometer as previously described. The same profile-fitting algorithm can then be applied to the measured sags of the secondary, and a best-fit profile calculated. Both actual primary and secondary profiles can then be input to the raytrace program for subsequent analysis.

The primary and secondary mirrors together form the first stage of concentration and would be tested as a unit by examining the extent of the solar blur in the telescope's image plane. The alignment and spacing of the mirrors would be adjusted to produce a solar blur which is entirely accepted by the entrance apertures of the CPC's. The ratio of the primary diameter to the measured diameter of the solar blur is the actual first-stage concentration ratio (uncorrected for optical losses), which would be compared to the nominal value.

CPC--The acceptance of the CPC's would be verified by collimated laser beam measurements made at various entrance angles and at various entrance aperture coordinates. The concentrators would be tested for radiation escaping through the entrance aperture after multiple reflections, thereby reducing the concentration ratio of the CPC's. The surfaces would be reworked by the vendor should such a condition exist for the CPC's. In addition, optical and mechanical profilometer measurements would be performed on the surface to determine the surface accuracy. The ratio of the CPC entrance aperture to exit aperture, which determines the concentration ratio of the CPC, would be measured and compared to the nominal design value.

System--The first and second stages of the concentration would be assembled and tested together as a unit by measuring the solar blur at the exit aperture of the CPC's. A dummy beamsplitter could be used during this testing, since only the blur diameter is of importance. Alingment sensitivity would also be analyzed by monitoring the output from the CPC's while misaligning the two stages. Both laboratory artificial solar sources and the sun would be used to perform this stage of testing. In addition, a laboratory source having an angular subtense of the sun would be used to test the uniformity of the concentrated energy exiting the CPC's. A pinhole detector device which scans the exit aperture of the CPC could be used to map the energy intensity as a function of position. Such uniformity testing will aid the design of CPC baffling or surface-stippling concepts to increase energy uniformity on the solar cells, although we do not anticipate that a nonuniformity will degrade the performance of the single element solar cells.

System Efficiency--Prior to testing the actual model, each optical surface would be individually tested to determine the optical efficiency of the surface for transmission or reflection. This information, combined with the system obscuration caused by the secondary mirror and any mounting hardware, would result in an accurate prediction of the system's actual concentration at the solar cells. This would then be compared with the measured concentration ratio found during lab and field tests. To simulate a variable source intensity, a series of full aperture neutral density filters or a series of aperture masks would be used at the entrance pupil of the concentration system.

Beamsplitter Test Plan

The design goals for the beamsplitter are >99% reflectance in the reflection band, >95% transmittance in the spectral range of interest, and less than 1% absorption so that the temperature rise in the beamsplitter is

moderate. The beamsplitters are also designed for durability in a space environment. Thus, optional test for adhesion, abrasion resistance, thermal breakdown, thermal cycling, thermal shock, UV degradation, weathering and humidity can be carried out. However, at this phase of the program, these properties are of lesser importance than the optical characteristics of the beamsplitter.

Reflectance and transmittance measurement of the beamsplitter can easily be done with a Beckman spectrophotometer, which automatically scans from 0.3 to 2.5 μm. Assuming minimal scattering, the absorptance is just one minus the reflectance and transmittance.

To carry out the environmental tests which are often destructive to the sample, at least 2-3 samples will be required for each test. This will add to the cost of the program. Details of each test are given below:

Adhesion Test--Coating adhesion will be tested by scribing two intersecting sets of parallel lines into the coating and substrate with a sharp knife, applying a strip of tape (3M No. 240 tape), and then snapping the tape from the surface at 90^{0} to the substrate.

Abrasion Test--This test will be carried out using a mechanical device that moves a weighted block back and forth across the surface of the substrate. The block will be fitted with neoprene rubber with an A65 Durometer hardness shore on the flocked side. An abrasive film of 12-micron Al_2O_3 grit and water will be used. The sample will be subjected to 3000 cycles with a shore pressure of one psi.

Humidity Test--The test will be conducted according to MIL-STD-810B, Method 507, Procedure 1.

Thermal Shock test--Samples will be surface-heated using a hot air gun for 1 hour and then dropping the sample into ice water.

Thermal Cycling Test--Samples will be cycled from -50°F to 160° F at a rate of 20°F per hour for 2 days.

Thermal Breakdown Tests--Samples will be heated using a hot air gun until film breakdown occurs; its temperature will then be noted.

UV Reistance Test--A BH 6 mercury vaprous lamp will be used which has high output in the 0.2 to 0.4 μm region. The lamp is positioned in a chamber (as shown in Figure 43) which is equivalent to 100-200 suns' irradiation. The test chamber, as shown, can be used for other tests as well.

Thermal Measurements

Thermal measurements are important for two reasons in characterizing system performance. Solar cell power output decreases with increasing temperature, and a heat-rejected system must be provided to dissipate the absorbed thermal energy. For solar concentrator systems, the heat problem grows with system size and concentration ratio.

To measure the heat absorbed by the solar cells, the CPC and solar cells will be attached to a water-cooled heat sink with copper conducting bars. Heat flux can be determined by measuring the temperature gradient in the conduction bars with thermocouples and knowing the thermal conductivity of the copper. Figure 34 shows the design of the cell and CPC holder and the insulated box surrounding it. The illustration shows 0.25 inch diameter 5.36° C/W copper conduction bars having a conductance 0.187 W/°C per inch of length. To maximize the sensitivity of the measurement, it is desirable to maintain a low conductance. To maximize cell output requires minimizing cell temperature by using a shorter or larger diameter copper support rod, which decreases heat flux measurement sensitivity.

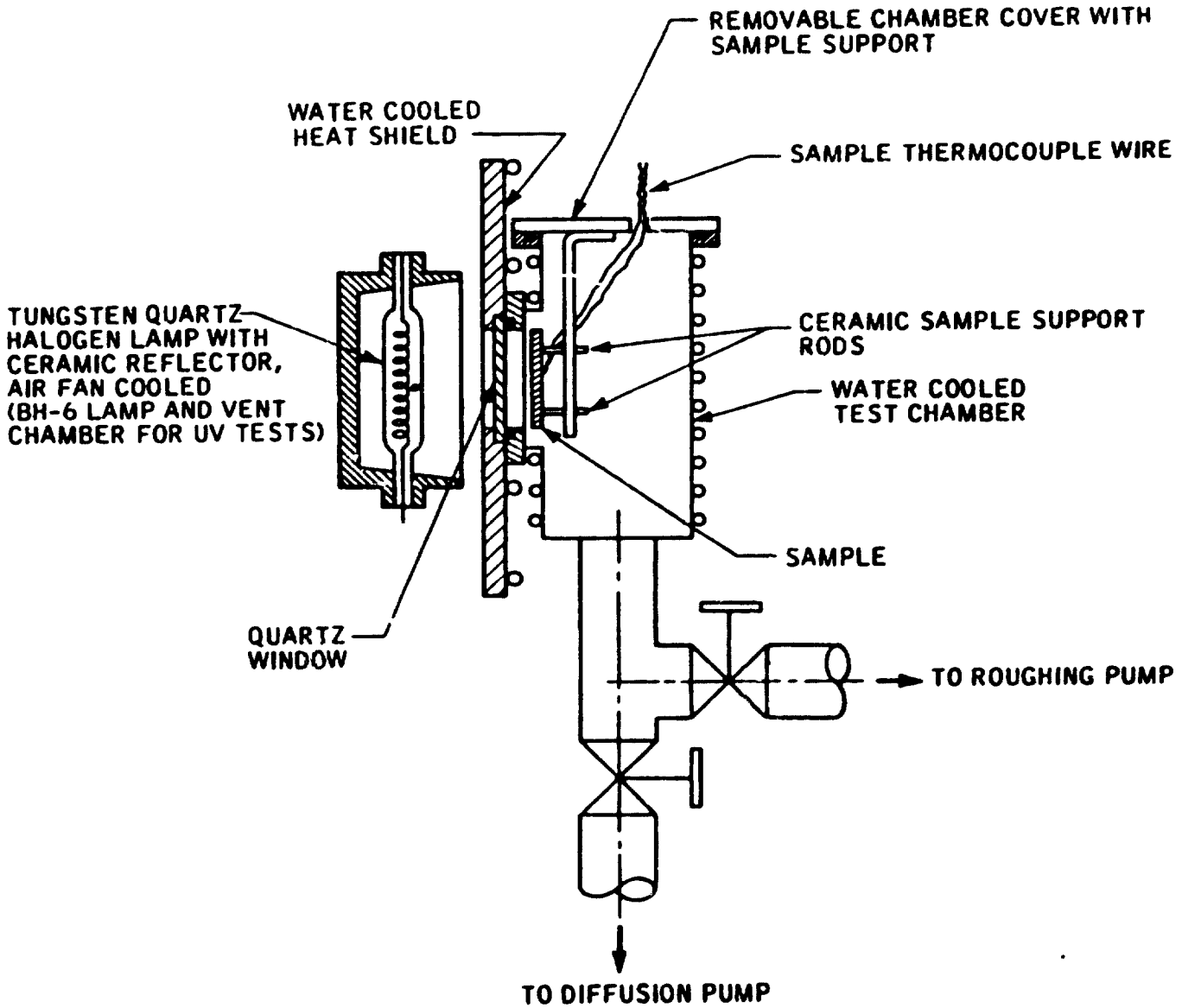

Figure 43. Chamber for Thermal and Ultraviolet Tests

No calibration of the heat flux measurement is required. Thermal properties of pure copper are well known, and by using rods of an inch or more in length, the thermocouple placement becomes insensitive to small errors in separation. Near-ambient temperature thermocouples are generally quite accurate.

SYSTEM PERFORMANCE DEMONSTRATION

Laboratory Testing

Since the concentrator system is designed with $\pm 1/2^{0}$ acceptance angle, in order to test the system in the laboratory, a source with comparable divergence is required. Available simulators have at least $\pm 3^{0}$ divergence, which means the Xenon source has to be apertured down and the beam must be collimated with external optics. This in turn will mean less than full sun intensity for testing, and so added cost to the testing program. However, useful information can be obtained in laboratory testing. Since the source is more stable, by inserting filters in front of the Xenon lamp, solar spectrum from AM0 to AM^{2} can be simulated. It is estimated that the highest intensity we can produce with our simulator is ~1/10 sun at the entrance aperture of the concentrator.

With the modified simulator, the following tests will be carried out:

Optical Efficiency Test--The energy collected and energy density at each stage of concentration will be measured using a radiometer at respective foci. The measured value will be compared to the irradiance without concentration and thus obtain the effective concentration ratio at each stage. The optical throughput of the system has been shown to be very sensitive to the alignment ($\pm 1/4^{0}$) and separation of the mirrors (± 0.015"). Therefore, by optimizing the throughput in this measurement, the optical system will also be critically aligned.

A pin hold detector can be placed at the CPC's exit to monitor the uniformity of the irradiance in the focal plane. A uniform irradiance is theoretically desirable to avoid nonlinear output of the cell due to high injection.

Spectral Splitting Test--The electrical output of the GaAs and Si cells will be monitored without the beamsplitter as the baseline performance of the cells. These values will be compared with the predicted value--a convolution of the spectral efficiencies of the cells and the spectral density of the irradiance.

The proper beamsplitter is then inserted and adjusted to record maximum power output from both cell positions with a radiometer. The cell will then be inserted, and the sum of outputs will be compared to previous measurements without inserting the beamsplitter. An enhancement is predicted with a 2-cell system. The cell efficiencies and system efficiencies can then be deduced by normalizing the cell output to cell irradiance measurements and total intercepted flux.

Variable Concentration Ratio Test--Neutral density filters will be inserted in front of the system aperture to decrease the effective concentration ratio of the system. A radiometer at the exit aperture of the CPC will measure the effective decrease in concentration ratio. Electrical output from the cells as a function of concentration ratio will be recorded. The cell temperature should be constant throughout all the measurement so that the efficiencies of the system calculated are comparable.

Variable Spectral Density Test--Filters with known transmission charcteristics will be used in front of the source aperture to simulate different air mass conditions. The maximum power output from the cells will be measured for different simulated spectral distribution and flux. The result will be compared with predictions.

System Field Testing

Field tests will be conducted to verify solar spectral photovoltaic concentrator system performance in an actual solar environment. The conditions of half-degree collimation, true solar spectral distribution, and one sun intensity cannot easily be met in any laboratory.

Field testing requires frequent measurements of solar intensity and spectral content, along with careful attention to the transient nature of the solar day. Since the concentrator has a very narrow field of view, only direct normal solar flux is concentrated. To measure direct normal solar flux, a tracking pyrheliometer is used. Spectral content can be determined with filters placed in front of the wide band absorbing pyrheliometer. The use of standard or calibrated solar cells and references must be performed carefully to ensure that only the direct normal radiation is contributing to the output reading.

The information that is expected to be obtained from field testing is tabulated in Table 14.

To obtain I, V, and P as functions of solar intensity (I_{solar}), a series of neutral density filters will be placed over the aperture to decrease the intensity. For a large aperture, these filters can easily be approximated by punching a series of holes into a sheet of metal at predetermined spacings. This technique preserves the precise spectral distribution and has little effect upon the areal distribution of flux at the solar cell.

The equipment required to perform the field tests is listed in Table 15.

TABLE 14. FIELD TEST DATA GOALS

I max at AM2 Conditions
V max at AM 2 Conditions
P max at AM2 Conditions
I max as a Function of I_{solar}
V max as a Function of I_{solar}
P max as a Function of I_{solar}

TABLE 15. FIELD TEST EQUIPMENT LIST

Solar Photovoltaic Concentrator with Clock Drive
Pyrheliometer with Filters and Clock Drive
Data Logger
I-V Characteristic Plotter
Filters
Cooling Water
Electric Power

REFERENCES

1. Private communications with Dr. Peter Borden at Varian, Dr. Sanjeeb Kamath at Hughes Research, and Dr. Stan Zehr at Rockwell International, January 1981.

2. Walker, G.H.; Conway, E.J.; Hong, K.H.; and Heinbockel, J.H., "High Temperature Properties of GaAlAs/GaAs Heteroface Solar Cells," Proceedings of the 14th IEEE Photovoltaic Specialists' Conference, San Diego, CA, January 1980, pp. 1098-1101.

3. Fan, J.C.C.; Turner, C.W.; Gale, R.P.; and Bozler, C.O., "GaAs Shallow-Homojunction Solar Cells," Proceedings of the 14th IEEE Photovoltaic Specialists' Conference, San Diego, CA, January 1980, pp. 1102-1105.

4. Bennett, A. and Olsen, L.C., "Analysis of Multiple-Cell Concentrator/Photovoltaic Systems," Proceedings of the 13th IEEE Photovoltaic Specialists' Conference, Washington, DC, 1978, pp. 868-873.

5. Moon, R.L.; James, L.W.; Vander Plas, H.A.; Yep, T.O.; Antypas, G.A.; and Chai, Y., "Multigap Solar Cell Requirements and the Performance of AlGaAs and Si Cells in Concentrated Sunlight," Proceedings of the 13th IEEE Photovoltaic Specialists' Conference, Washington, DC, 1978, pp. 859-867.

6. Meulenberg, A. Jr., Allison, J.F., and Arndt, R.A., "Thin N-I-P Silicon Solar Cells," Proceedings of the 14th IEEE Photovoltaic Specialists' Conference, San Diego, CA, January 1980, pp. 161-165.

7. Young, R.T. and Wood, R.F., "Solar Cells from Ion-Implanted Laser-Annealed Cast Polycrystalline Silicon," Proceedings of the 14th IEEE Photovoltaic Specialists' Conference, San Diego, CA, January 1980, pp. 214-217.

8. del Valle, J.L., Flores, C., and Duenas, F., "Hydrogenation Effects in Cast Polycrystalline Silicon P-N Junction Solar Cells," Proceedings of the 14th IEEE Photovoltaic Specialists' Conference, San Diego, CA, January 1980, pp. 202-207.

9. Loo, R., Kamath, G.S., and Knechtli, R.C., "Radiation Damage in GaAs Solar Cells," Proceedings of the 14th IEEE Photovoltaic Specialists' Conference, San Diego, CA, January 1980, pp. 1090-1097.